2014

Catalytic Mechanism and Maturation of the Metalloenzyme Nitrile Hydratase

Natalie I. Gumataotao
Loyola University Chicago

LOYOLA UNIVERSITY CHICAGO

CATALYTIC MECHANISM AND MATURATION OF THE METALLOENZYME NITRILE HYDRATASE

A DISSERTATION SUBMITTED TO

THE FACULTY OF THE GRADUATE SCHOOL

IN CANDIDACY FOR THE DEGREE OF

DOCTOR OF PHILOSOPHY

PROGRAM IN CHEMISTRY

BY

NATALIE GUMATAOTAO

CHICAGO, IL

DECEMBER 2014

ACKNOWLEDGMENTS

I would like to thank my advisor, Dr. Richard C. Holz, for his guidance and support in my research. Despite his extremely busy schedule, he always made time for project discussion and general merriment. I could not have asked for an advisor so compatible with my personality and working style.

The expertise of Dr. Kenneth Olsen, Dr. Dali Liu, and Dr. Miguel Ballicora allowed me to explore new theories, techniques, and approaches. At different points during my graduate work, I have consulted with each of them and received valuable feedback on my research direction. I would also like to thank Dr. Brian Bennett for his collaboration on a large part of this dissertation. I was always entertained by the ways that his cynicism and humor would sneak into emails and meetings about my project.

It was certainly easier and more fun doing research in the Holz group with Salette Martinez and Ania Starus. Additional thanks to Dr. Misty Kuhn for training a chemist in the ways of a biochemist.

I'd like to thank my roommates from my first years in Chicago, Dr. Tripthi Pillai and Dr. Matthew Clarke, in helping with my transition into Chicago and relative poverty.

Lastly, I'd like to thank my husband Karl Takabayashi for not being upset when I brought a dog home without any notice.

TABLE OF CONTENTS

LIST OF FIGURES

LIST OF TABLES

LIST OF ABBREVIATIONS

Abbreviation	
ATP	ATP
BBA	1-Butaneboronic acid
BSA	Bovine Serum Albumin
CD	Circular Dichroism
CP-SCF	Coupled-Perturbed Self Consistent Field
*Ct*NHase	*Comamonas testosteroni* Ni1 NHase
DEAE	Diethylaminoethanol
DFT	Density Functional Theory
DLS	Dynamic Light Scattering
DTNB	5,5′-dithio-bis-(2-nitrobenzoic acid)
DTT	Dithiothreitol
EDTA	Ethylenediaminetetraacetic Acid
ENDOR	Electron Nuclear Double Resonance
EPR	Electron Paramagnetic Resonance
ESEEM	Electron Spin Echo Envelope Modulation
FPLC	Fast Protein Liquid Chromatography
GDP	Guanosine Diphosphate
GTP	Guanosine Triphosphate

ICP-AES	Inductively Coupled Plasma-Atomic Emission Spectroscopy
IMAC	Immobilized Metal Affinity Chromatography
LMCT	Ligand to Metal Charge Transfer
NHase	Nitrile Hydratase
Ni-NTA	Nickel Nitrilotriacetic Acid
NTP	Nucleotide Triphosphate
MCD	Magnetic Circular Dichroism
MeACN	Methacrylonitrile
NTCB	2-Nitro-5-thiocyanatobenzoic acid
PAN	Polyacrylonitrile
PBA	Phenylboronic acid
*Pc*NHase-23	*Pseudomonas chloraphis* 23 NHase
PDB	Protein Database
*Pt*NHase	*Pseudonocardia thermophila* JCM-3095 NHase
PQQ	Pyrroloquinoline quinone
*Re*NHase-R312	*Rhodococcus* R312 NHase
*Re*NHase TG328-2	*Rhodococcus equi* TG328-2 NHase
RR	Resonance Raman
SCNase	Thiocyanate Hydrolase
SDS-PAGE	Sodium Dodecyl Sulfate-Polyacrylamide Gel Electrophoresis
TCEP	Tris(2-carboxyethyl)phosphine
TEV	Tobacco Etch Virus

TNB	2-nitro-5-thiobenzoate
*Tt*SCNase	*Tt*SCNase from *Thiobacillus thioparus*
UTP	Uridine Triphosphate
UV-vis	Ultraviolet-visible
XAS	X-ray Absorption Spectroscopy

ABSTRACT

Nitrile hydratases are metalloenzymes that catalyze the hydration of nitriles to their corresponding amides in a specific manner at ambient pressures and temperatures at neutral pH. Traditional industrial methods require high temperature and pressure, extreme pH, and heavy metals. NHases are used as biocatalysts in the large scale industrial production of amide precursors to textiles, animal feedstock, and polymers. Notably, NHase is used in the production of ~100,000 tons of acrylamide annually by the Mitsubishi Corporation.

Despite being used extensively in industry, questions remain about NHase. The catalytic mechanism is not defined. Understanding the way in which the nitrile is converted to amide will be useful for engineering a more efficient, specific, and stable enzyme. The improved enzyme will shift industry towards green chemistry. Additionally, the enzyme has a unique metallocenter. Understanding the chemistry of the enzyme will give new information on this rare enzyme configuration.

The maturation mechanism is not understood for NHase. It is understood that activator proteins may act as metallochaperones, bringing the metal to the active site. Metallochaperones regulate potentially toxic, but essential metals in cells. By understanding NHase's maturation, we can not only apply the knowledge to NHase understanding and engineering, but also to similar metallochaperones that may be responsible for causing Alzheimer's disease and the like.

The goal of the dissertation is to answer these questions. The catalytic mechanism will be investigated by studying reaction intermediates using spectroscopic techniques. The activator protein and NHase maturation will be studied with biophysical methods to probe its metal binding and protein-protein interactions.

CHAPTER 1

INTRODUCTION

The Proliferance and Degradation of Nitriles

Nitriles (RCN) are widespread and diverse in nature. They are found mainly as cyanogenic glycosides, which are used in self-defense mechanisms during plant injury.[1] Cyanolipids (reduced nitrogen sources), β-cyanoalanine (cyanide detoxification), and mandelonitrile (chemical defense mechanism in insects) are other examples of naturally occurring nitriles.

Synthetic nitriles are also numerous with a wide array of applications. Acetonitrile is a common organic solvent that is produced as a byproduct in the synthesis of acrylonitrile, a nitrile used to produce polymers like polyacrylonitrile (known as PAN or acrylic).[2] Nitriles are also commonly found in pharmaceutical intermediates and products, such as the antidepressant citalopram, due to the biocompatibility of the cyano group. In fact, there are over 30 nitrile-containing drugs, with 20 nitrile leads, in production.[3] Bromoxynil and ioxynil are two examples of synthetic nitriles that are common pesticides used in agriculture. Generally, nitriles are toxic, carcinogenic, and mutagenic and limited exposure is recommended.[4]

In bacteria, nitriles are metabolized by an assortment of enzymes. The hydration of nitriles is the most common metabolic route and is accomplished with three enzymes. Nitrilase converts nitriles to carboxylic acids and ammonia in a single step. Nitrile

hydratase (NHase) and amidase work in tandem, where NHase first hydrolyzes a nitrile into its corresponding amide after which, amidase reacts with the amide product of NHase to form a carboxylic acid and ammonia. The three nitrile metabolism pathways accomplished by enzymes are shown in Figure 1. Of particular commercial interest is the hydration of a nitrile to its corresponding amide by NHase, due to the commercial value of amides.

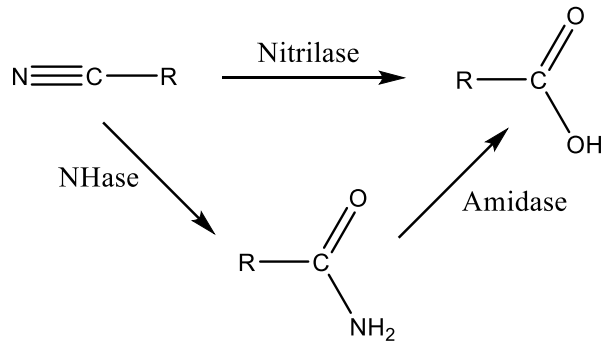

Figure 1. Nitrile hydrolysis pathway in microbes.

Industrial Manufacturing of Amides

Amides are profitable precursors to rubbers, polymers (Nylon), paper fibers, animal feedstock, cosmetics, and textiles.[4] The high demand for amides, particularly polyacrylamide and nicotinamide, traditionally is met through industrial scale manufacturing. The original manufacturing processes require conditions of high acidity, high pressures, high temperatures (200 – 400°C), and/or metal catalysts, such as Raney copper.[5] These extreme conditions result in high levels of chemical waste and require significant energy expenditures. The reaction does not yield 100% amide product due to the formation of an unwanted acrylic acid side product, decreasing the reaction efficiency. The discovery of NHase as a biocatalyst opens up a new potential route for the synthesis of amides from nitriles under very mild reaction conditions.

A Green Alternative to Amide Synthesis

Nitrile hydratase was first isolated from nitrile-degrading bacteria found in wastewater in 1980 by scientists at the University of Kyoto.[6] Collaboration between the University of Kyoto and Nitto Chemical Industrial Company (now Mitsubishi Rayon) enabled the enzyme to be recognized, researched, and applied as a biocatalyst in the production of commodity chemicals, such as acrylamide.[5] The enzyme proved to be an efficient catalyst for acrylamide production from acrylonitrile by eliminating the formation of acrylic acid and performing the reaction in a single step, as opposed to the multi-step reactions required in traditional amide syntheses. The NHase reaction takes place at physiological pH, ambient temperature, and eliminates chemical and heavy metal waste. It exhibits high selectivity for substrates and hydrates nitriles in a regio-, -enantio, and chemoselective manner, something traditional amide synthesis was unable to accomplish easily. The general reaction is shown in Figure 2.

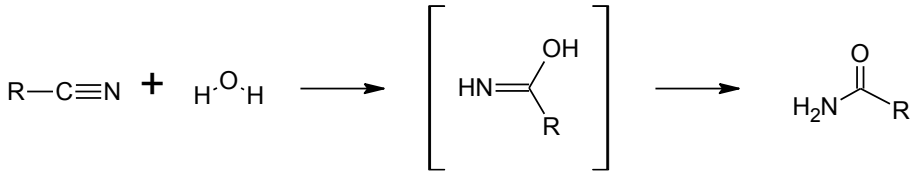

Figure 2. General reaction catalyzed by nitrile hydratase.

The industrial use of NHase, however, has been mostly confined to the use of whole cells, due to the relative instability of the enzyme. A disadvantage to using whole cells is that they also contain amidase, an enzyme that catalyzes the hydrolysis of amides to carboxylic acid, an unwanted side product. Another disadvantage to using whole cells is that some industrially important nitriles do not easily permeate the cell membrane, causing less substrate to be hydrated. Recent advances in enzyme immobilization

methods have provided more stable NHase systems that are gaining popularity in industrial settings.

Despite the stability issues related to NHase, industry has successfully adopted the biocatalytic method. As of 2008, Mitsubishi Corporation produced up to 200,000 tons of acrylamide from acrylonitrile per year using whole cells containing NHase.[7] BASF in Germany and Lonza in Switzerland are two companies who are also using the bioprocess in the production of nicotinamide.[8] CLEA Technologies uses an immobilized form of NHase to make the process more robust and contracts the technology out to make a number of different amides.[9]

Other Applications of Nitrile Hydratase

NHases are not only used for the production of amide intermediates and starting materials for commodity chemicals, but have also been proven to be useful in the bioremediation of chemical wastewater and runoff.[10] Unfortunately, due to the formerly lax regulations of nitrile-based chemicals, this type of waste is extensive. For example, nitrile-based pesticides like bromoxynil linger in soil up to five months after administration of the chemical.[11] NHase has been shown to successfully hydrolyze bromoxynil to the less harmful amide, which is then flocculated and collected.[10] High concentrations of acetonitrile waste have also been treated in a tandem process with NHase and amidase, something that could not be accomplished with just nitrilase alone.[12] This favorable impact on the environment provides a green method for the biological treatment and the removal an environmental toxin.

More recently, NHase has been successfully used in the surface modification of polymers.[13] When NHase was applied to the surface of polyacrylonitrile (PAN) fibers,

the enzyme selectively hydrolyzed the surface nitriles of the fibers.[14,13] This was a significant improvement from earlier procedures using alkaline or acid treatment, which also resulted in less control of the surface modifications and had a negative environmental impact. The NHase process enabled the PAN fibers to retain their bulk properties while making their surface more hydrophilic. In textiles, this is especially important for breathability and the binding of color to synthetic fabrics.

Despite the relatively successful use of NHase in manufacturing, bioremediation, and polymer modifications, the current processes can all be improved. From the stability of the enzyme to understanding the interactions of NHases with a wide variety of substrates, the use of NHase enzymes in industrially processes still requires additional research. This research begins with gaining a fundamental knowledge of NHase enzymes, particularly their mechanism of action.

Nitrile Hydratase Structure

Crystal structures for both types of NHases have been solved to high resolution.[15,16,17] NHases are $\alpha_2\beta_2$ heterotetramers where the α and β subunits are approximately 28 kDa with some variation between bacterial sources.[4] Nitrile hydratases contain either a non-heme Fe(III) or non-corrin Co(III) ion in their active site. The α subunit of NHase contains a homologous cysteine-rich amino acid sequence CXLCSCX (X = T,Y for Co type; S,T for Fe-type) that is the site of metal binding.[18] The metal ion is coordinated to six ligands and the geometry is conserved among all NHases.[19]

Crystal structures for both Fe and Co-type NHase show that the metal ion is coordinated equatorially to two imido-nitrogen atoms from peptide backbone amides and two sulfurs from cysteine, axially by another cysteine sulfur and either water for Co-type

or NO for Fe-type NHase, where the equatorial ligands are in 6-5-5 metallocycles and arranged asymmetrically.[20] The structure of the Co-type NHase active site is shown in Figure 3. The equatorial cysteines in the active site are post-translationally modified to Cys-SOH (sulfenic acid) and Cys-SO_2H (sulfinic acid), which results in a metalloenzyme active site geometry called a "claw setting", which is unique in comparison to other metalloenzymes.[20] The cysteines in the active site must be oxidized for the enzyme to be active for both Fe-type and Co-type NHases.[21]

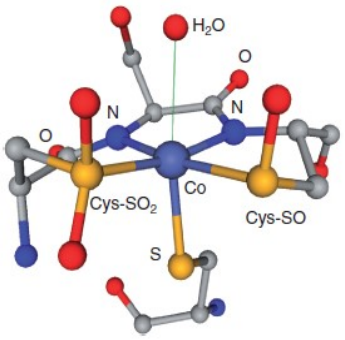

Figure 3. Active site structure of Co-type nitrile hydratase.[20]

The axial thiolate ligand in the active site is strictly conserved in NHases. It is thought that the thiolate increases the axial ligand exchange rate of the metal center which has been proposed as a possible substrate binding site.[22] Both the Co(III) and Fe(III) ions are low spin (S=0 for Co and S=½ for Fe) resulting in both being classified as kinetically inert. The *trans*-thiolate ligand enhances the lability of the axial position by "pushing" electrons toward the metal ion, making it a Lewis acid. This in turn increases the bond length between the *trans* ligand, causing increased dissociativity.[19] The axial Cys sulfur atom is 3.1 to 3.2 Å away from the oxygen of an equatorial cysteine sulfinic acid, indicating a potential hydrogen bonding interaction, which would decrease the

anionic character of the Cys sulfur.[19] This, combined with the oxidized equatorial cysteine ligands required for catalytic activity, modulates and boosts the Lewis acidity of the of the active site metal ion. The metal ion is therefore kinetically able to bind and activate nitriles or to make the bound water a better nucleophile, depending on the catalytic mechanism.

Catalytic Mechanism

Molecular characterization of both Fe-type and Co-type NHase enzymes has provided insight into how the molecular structure controls enzyme function. Based on these data and several elegant studies on active site NHase model complexes, several possible reaction mechanisms have been proposed (Figure 4). In each, imidate is produced as a reaction intermediate, which then isomerizes to the corresponding amide. The formation of imidate is the result of nucleophilic attack by a hydroxide moiety, however, the source of this nucleophile has not been identified.

The most accepted catalytic mechanism for NHases, involves the binding of the nitrogen of the nitrile substrate to the metal center and is called the "activated substrate" mechanism (Figure 4).[23] The nitrile group of the substrate displaces the hydroxide/water group at the metal center, making it more electrophilic and subject to nucleophilic attack by a base-activated water molecule.[24,25] The identity of the base was suggested to be the strictly conserved βTyr72, αSer113, or αCys-SOH.[24,25,26] However, no direct evidence exists supporting the direct coordination of a nitrile nitrogen atom to the active site metal ion of an NHase.[19]

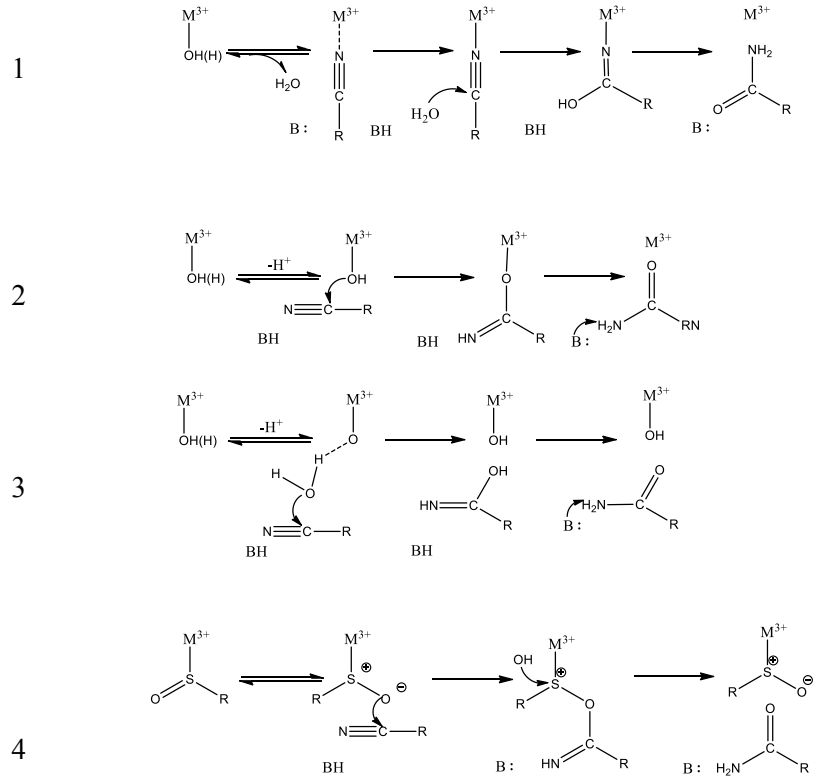

Figure 4. Proposed mechanisms. (1) Activated Substrate, (2) Directly Activated Nucleophile, (3) Indirectly Activated Nucleophile, (4) Activated Sulfenate.

Circumstantial evidence for direct nitrile binding to the axial position of the active site metal ion is gleaned from both model complexes and X-ray crystallography. First, synthetic inorganic biomimic complexes that serve as model for both the iron and cobalt active site readily bind nitriles.[27,28] Additionally, X-ray crystallography has shown that the sixth ligand in an Fe-type NHase from *Rhodococcus erythropolis* is NO when purified in the dark.[29] Upon exposure to light, the NO is exchanged for a water molecule from the solvent, indicating a labile, direct binding site to the metal ion.[30]

Crystallography has also revealed that upon addition of butyric acid, an NHase inhibitor, the carboxylate oxygen binds directly to the Co(III) active site in *Pt*NHase.[18] A blue shift of a UV-vis absorption corresponding to a $S^{2+} \rightarrow Fe^{3+}$ ligand to metal charge

transfer (LMCT) of an Fe-type NHase from *Pseudomonas chloraphis* B23 upon addition of proprionitrile is also indicative of direct substrate binding.[31]

The latter three mechanisms in Figure 4 are classified as outer sphere mechanisms in which the active site metal does not directly bind the nitrile substrate. The "directly activated nucleophile" mechanism suggests that a metal-bound hydroxide functions as the nucleophile.[32] In the third mechanism, the hydroxide ligand deprotonates a neighboring water molecule, which then functions as an "indirectly activated" nucleophile.[32] The last mechanism, "activated sulfenate", suggests that the sulfenate oxygen is the nucleophile.[33]

Activator Proteins

Transition metal centers in proteins typically aid in protein folding, stabilization, electron transport, or catalysis.[34] In NHase, it appears that the metal centers are necessary for catalysis and structural stabilization.[4] The trafficking and regulation of transition metal ions into metalloproteins is generally required for functionality, however, if metal movement is unregulated, it could be detrimental to cellular functions.[34] If metals are in excess, the cell will possibly die, or at least be seriously damaged. Too few metal ions will also result in loss of function. Cells use metallochaperones, storage proteins, and sequestration proteins to regulate the flow and concentration of metal ions to avoid any sort of disruption in cellular function.

NHase is unusual in that it can have either a low-spin Co(III) or Fe(III) ion in its active site. Iron (II) is the second most abundant metal in the cytoplasm (high μM), whereas cobalt (II) is extremely rare, being in the nM range.[35] Because the active sites are identical, one would expect that the more abundant metal would be routinely

assembled into the NHase active site with full activity. Instead, NHases are very specific for its respective metal ion.

Evidence of the specificity of NHase towards Co(III) or Fe(III) was observed in a series of metal substitution assays examining NHase activity.[36,18,37] Nojiri *et al*. successfully incorporated a cobalt ion into an Fe-type NHase from *Rhodococcus sp*. N-771 but reported only 5.9% of wild-type activity.[36] Miyanaga's group later attempted to insert iron into the Co-type NHase from *Pseudonocardia thermophila* (*Pt*NHase), but observed little cobalt incorporation, resulting in an apoenzyme.[18] Sari *et al.* substituted cobalt into an Fe-type *Comamonas testosteroni* (*Ct*NHase) using an *E. coli* GroESL chaperone system and obtained comparable activity to a wild type NHase; however, Holz's group later proved that *Ct*NHase does not need a chaperone protein to incorporate metal, bringing into question the significance of Sari's findings.[15, 37]

Combination of the findings from these studies have led to the hypothesis that the specificity of NHase for either Co^{3+} or Fe^{3+} is due to an accessory protein termed an "activator". Activator genes are present in almost all NHase gene clusters sequenced to date and have been shown to be required for full catalytic activity.[38] The activator gene is typically found downstream of the genes for α and β subunits, as shown in Figure 5. They are widely thought to function as metallochaperones. The activator protein in NHases may also be involved in cysteine oxidation of the active site, which is required for activity.[39]

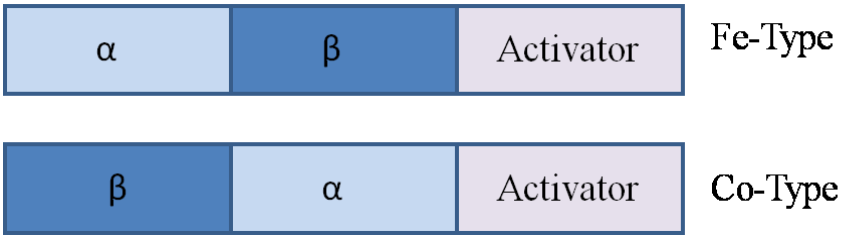

Figure 5. Arrangement of NHase genes with respect to metal type.

Iron-type Activators

Alignment of known Fe-type NHase activator protein sequences, shown in Table 1 reveals that they contain a highly conserved cysteine-rich motif.[38] This motif is a known metal binding site in other metallopchaperones, such as COX17 (copper) and Hyp proteins (nickel).[38,40] Interestingly the activator protein sequences for Fe-type and Co-type NHases are not homologous, which suggests the metallocenters are assembled by different mechanisms.[41] Co-type activators lack a cysteine rich binding site, are smaller, and have sequence homology with the Co-NHase β subunit.[42] Overall, very little is understood about the role of the Fe-type activator, whereas the role and mechanism of the Co-type activator is somewhat better understood.

Table 1. Conserved binding motif sequences of Fe-type activator homologues.[38]

Name	Species	Binding Motif
NHase Activator	*Rhodococcus sp*. N-771	68MTNGCICCTLR78
P44K protein	*Rhodococcus sp.* AJ270	68MTNGCICCTLR78
P47K	*Pseudomonas chloraphis* B23	68MSNGCICCTLR78
KB15K	*Rhodococcus equi* TG328-2	68MTNGCICCTLR78

The nitrile hydratase Fe-type activators share sequence homology with the G3E family of P-loop GTPases called COG0523.[41] The COG0523 family is a diverse set of

proteins that appear to be involved in metal transport in cells, which includes proteins critical to cobalamin synthesis and zinc transport. Figure 6 shows the most commonly conserved sequences in the COG0523 family of GTPases, which generally include a Walker A motif, a CxCC metal binding motif, a Walker B motif in which the there is a glutamate instead of aspartate, and a distal motif consisting of an NKxD sequence.[41] Less frequently, COG0523 proteins may also contain a histidine-rich region near the C-terminus of the protein.

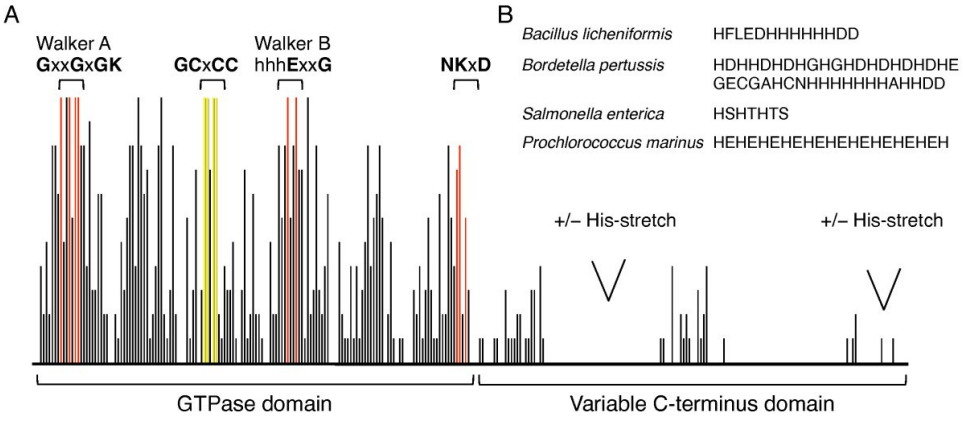

Figure 6. Conserved sequences in COG0523 family.[41]

GTPases bind and hydrolyze the γ-phosphate on GTP forming GDP (guanosine diphosphate) and inorganic phosphate.[43] GTPases are involved in signaling, protein biosynthesis, translocation, and regulation of cellular activities.[43] GTPases are typically structured with a central β-sheet surrounded by α-helices. An example of a P-loop GTPase is shown in Figure 7.[44]

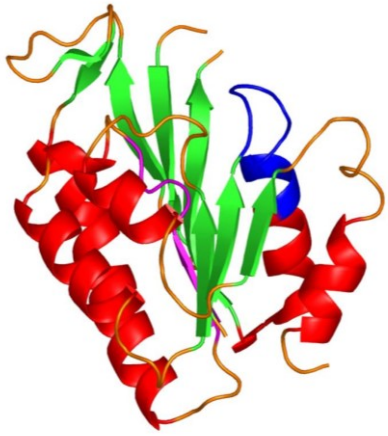

Figure 7. A P-loop GTPase with the Walker A and Walker B motifs in magenta and blue, respectively.[44]

Within the Fe-type activator and GTPase sequences is a Walker A motif, or P-loop, that is on a flexible loop between a β-strand and α-helix (Figure 7). The Walker A motif is responsible for binding and positioning the triphosphate group of GTP. Another feature of the COG0523 family of GTPases and the nitrile hydratase Fe-type activator sequence is a distal Walker B motif that is the site of magnesium binding, necessary for GTP hydrolysis.[43] The NHase activator from *Rhodococcus equi* TG328-2 (*Re*NHase TG328-2) contains a Walker A motif at the residues 13GFLGAGK21, a Walker B motif at 97LIIESSG104, and the previously described 72CICC75 sequence. As GTP hydrolysis is required in the assembly of several metalloproteins, including the nickel enzyme urease, it is likely to play a role in the incorporation of iron into Fe-type NHases.[45]

While no structural information is available for any Fe-type NHase activator, the structure of a related enzyme and a proposed GTPase in the COG0523 family, Yjia, was recently solved.[46] Because of the ability to obtain high quality diffraction data for Yjia

the metal binding and GTPase activity were investigated. These data suggest that GTPase activity is regulated by metal binding, some clue to the function of the COG0523 proteins.[46b] Given the sequence homology of Yjia with an Fe-type activator from *Rhodococcus equi* TG328-2, it can be hypothesized that the activator has a similar structure and function. Overall, the functions of COG0523 proteins are loosely related to metal transport, but the details of their function remain elusive.

Cobalt-type Activators

Currently, we can only postulate as to the true function and mechanism of the Fe-type NHase activators. Conversely, the Co-type NHase activators have been studied in more detail. A novel mechanism for cobalt uptake in *Rhodococcus rhodochrous* J1 was hypothesized to occur through "self-subunit swapping".[47] In this mechanism, a cobalt containing α-subunit is bound to two activator proteins. The cobalt containing α subunit then dissociates from the second activator protein and then binds to an apo α-subunit. Figure 8 is a graphical depiction of the mechanism.

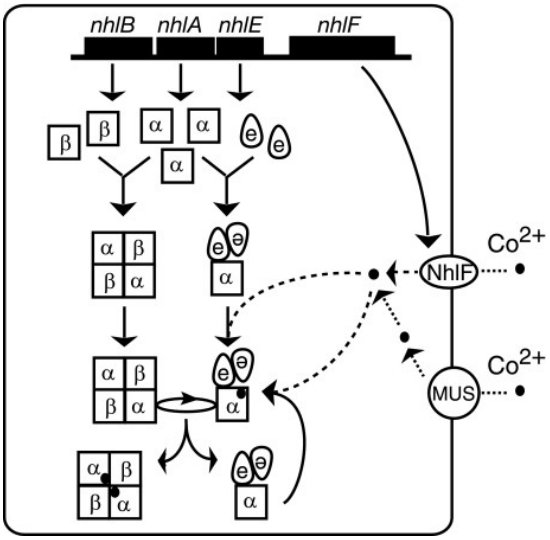

Figure 8. Self-subunit swapping mechanism in NHase. Activator is denoted as e.[10]

Evidence for the subunit swapping mechanism was most recently reported using dynamic light scattering (DLS) to detect the formation of large complexes.[42] Zhou's group also observed several intermediates using a combination of DLS and size exclusion chromatography, including a proposed αe_2 intermediate and an apoenzyme bound to the αe_2 intermediate. Based on these data, they concluded that all Co-type NHase activators are subunit swapping chaperones because of their high homology. The activator protein was also proposed to function as a metallochaperone as well as a subunit swapping chaperone by the failure of the apoenzyme to incorporate cobalt in the presence of the strong reducer dithiothreitol (DTT).[39] Moreover, post-translational modification of the cysteines was observed after insertion of the cobalt ion. These data were suggested to indicate that the activator has a redox role in the oxidation of the cysteines at the active site.[39]

Questions and Limitations of Nitrile Hydratase

Much is unknown about nitrile hydratases, in particular Fe-type enzymes, despite studies conducted by research groups in Japan, the United States, and France over the past 20 years. Even so, NHases have been widely utilized in industry.[18,8,9]

Understanding the catalytic mechanism of NHases is important for the future design of green catalysts. Once the method of substrate binding and selectivity is clear, better enzymes can be engineered to be more efficient, stable, and selective. Scientists would be able to create a tunable enzyme, which could be applied to other potential catalyst processes, advancing green industry.

For NHase to be active, it must have the metal ion in the active site. However the mode in which the metal ion is bound to the activator protein and escorted to the active

site is not known. The iron-type NHase activator has a cysteine-rich metal binding motif and a known GTP binding sequence that is found in other metal binding proteins in the poorly understood COG0523 family. If the function of the NHase activator is clarified, it can lead to better understanding of all COG0523 proteins with poorly defined functions.

In this thesis, I have worked to define the catalytic mechanism by trapping reaction intermediates and characterizing them kinetically and spectroscopically using an Fe-type NHase from *Rhodococcus equi*-TG328-2 (*Re*NHase-TG328-2). To understand the mechanism of metal insertion and GTPase function, examined the GTP and metal binding properties of the Fe-type activator from *Rhodococcus equi*-TG328-2 was examined. Therefore, the goals of my dissertation research are:

Aim 1: Identification and kinetic characterization of *Re*NHase-TG328-2 reaction intermediates.

Aim 2: EPR characterization of the *Re*NHase-TG328-2 active site in its resting state and with substrate bound.

Aim 3: Biophysical and kinetic analysis of the *Re*NHase-TG328-2 activator.

CHAPTER 2

IDENTIFICATION AND KINETIC CHARACTERIZATION OF RENHASE TG328-2 REACTION INTERMEDIATES

Summary

Stopped-flow kinetic data were obtained for the Fe-type nitrile hydratase from *Rhodococcus equi*-TG328-2 (*Re*NHase-TG328-2) using methacrylonitrile as the substrate. These data were globally fit providing a kinetic model that allows for the reversible binding of substrate, the presence of an intermediate, and the formation of product. Independent absorption spectra acquired between 0.005 and 0.5 s of the reaction reveal a significant increase in absorbance at 375, 460, and 550 nm along with the hypsochromic shift of an $Fe^{3+}\leftarrow S$ ligand-to-metal charge transfer (LMCT) band from 700 to 650 nm. The observed UV-Vis absorption bands for the Fe^{3+}-nitrile intermediate species are similar to low-spin Fe^{3+}-enzyme and model complexes bound by NO or N_3^-. These data provide spectroscopic evidence for the direct coordination of the nitrile substrate to the NHase active site low-spin Fe^{3+} center.

Introduction

Nitrile hydratases (NHases) catalyze the hydration of nitriles to their corresponding amides under ambient conditions and physiological pH (Figure 9).[19]. NHases have attracted substantial interest as biocatalysts in preparative organic chemistry and are already used in several industrial applications such as the large scale production of acrylamide and nicotinamide.[48,49]

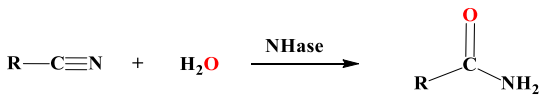

Figure 9. The hydration of a nitrile to its corresponding amide by nitrile hydratase.

For example, Mitsubishi Rayon Co. has developed a microbial process that produces ~95,000 tons of acrylamide annually using the NHase from *Rhodococcus rhodochrous* J1.[6] More than 3,500 tons of nicotinamide is produced per year *via* NHase, with yields of >99 % and without formation of troublesome byproducts such as acrylic acid.[50] NHases have also been employed as bioremediation agents to clean up nitrile-based pesticides, such as bromoxynil.[51] Because of their exquisite reaction specificity, the nitrile-hydrolyzing potential of NHase enzymes is becoming increasingly recognized as a truly new type of "Green" chemistry.

NHases contain either an Fe^{3+} ion ('Fe-type') or a Co^{3+} ion ('Co-type') in their active sites.[19] X-ray crystal structures of both Co- and Fe-NHase reveal that the M^{3+} ion is coordinated by three cysteines, two amide nitrogens, and a water molecule.[4] Two of the active site cysteine residues are post-translationally modified to cysteine-sulfinic acid ($–SO_2H$) and cysteine-sulfenic acid (–SOH) yielding an unusual metal coordination geometry, termed a "claw-setting". These Cys oxidation states are essential for NHase activity.[52]

The molecular characterization of both Fe-type and Co-type NHase enzymes has provided some insight into how molecular structure controls enzyme function. Based on these data, and several elegant studies on active site NHase model complexes, several possible reaction mechanisms have been proposed.[19] In each, imidate is produced as a

reaction intermediate, which then isomerizes to the corresponding amide. The most accepted catalytic mechanism for NHases involves the binding of the nitrogen of the nitrile substrate to the active site metal center; however, no direct evidence has been reported supporting such a mechanism.[19]

In an effort to identify the first example of a reaction intermediate for nitrile hydratases, stopped flow experiments were performed on an Applied Photophysics SX20 stopped flow instrument. *Re*NHase TG328-2 is an ideal system to use for stopped-flow experiments due to its high affinity towards methacrylonitrile (K_m = 0.19 mM) and its $t_{1/2}$ (10 msec) being well within the range of the stopped-flow instrument's capability. Additionally, the iron center allows for unique visible spectra with strong absorptions that are easily observed, unlike Co-type NHases. *Re*NHase can also be obtained in large quantities (~30 mg/L), necessary for the sample concentrations required of biophysical assays.

Herein we report the detection of an NHase reaction intermediate, using methacrylonitrile as the substrate that is observed using single-turnover stopped-flow UV-vis spectroscopy. These data provide the first direct spectroscopic evidence for nitrile binding to the Fe^{3+} active site in the nitrile hydratase from *Rhodococcus equi* TG328-2.

Results and Discussion

Pre-steady state stopped-flow experiments were initially run on *Re*NHase-TG328-2 at 5 ^{o}C using 25 mM methacrylonitrile at pH 7.0. An example progress curve is shown in Figure 10.

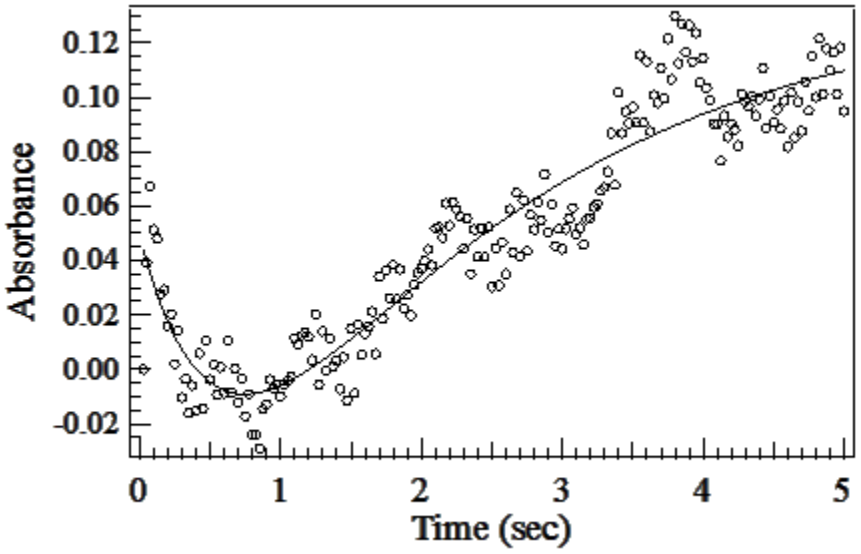

Figure 10. Stopped-flow data of *Re*NHase-TG328-2 assayed against MeACN.

A noticeable lag is present in the early portion of the reaction indicating at least two reaction steps. Independent absorption spectra were acquired at 242 nm over the time frame 0.005 to 10 s. These data were fit to a double exponential equation providing k_{obs1} and k_{obs2} for each phase of the reaction. k_{obs1} was designated the fast phase and k_{obs2} was designated as the slow phase. Based on these data, a minimal three-step kinetic model is proposed that allows for reversible substrate binding, the presence of an intermediate, and the formation of product, with product formation being the slow catalytic step (Figure 11).

$$E + S \underset{k_{-1}}{\overset{k_1}{\rightleftharpoons}} ES \underset{k_{-2}}{\overset{k_2}{\rightleftharpoons}} EI \xrightarrow{k_3} E + P$$

Figure 11. Proposed kinetic model for the hydration of methacrylonitrile by *Re*NHase TG328-2.

The concentration dependence of the reaction rate on methacrylonitrile was examined by plotting the fast and slow phases of the reaction against increasing substrate concentration (Figure 12). Microscopic rate constants for each step of the reaction were

extracted from the data plots through linear and non-linear regression analysis. The concentration dependence of the fast phase was fit to a linear equation where the slope is the second-order rate constant and the y-intercept is the sum of $k_{-1} + k_2 + k_{-2}$. This fit provided a k_1 value of 1.0 ± 0.1 $mM^{-1}s^{-1}$ and a $k_{-1} + k_2 + k_{-2}$ value of 12 ± 1 s^{-1}. The non-zero intercept and linear dependence implies that the binding step is reversible.

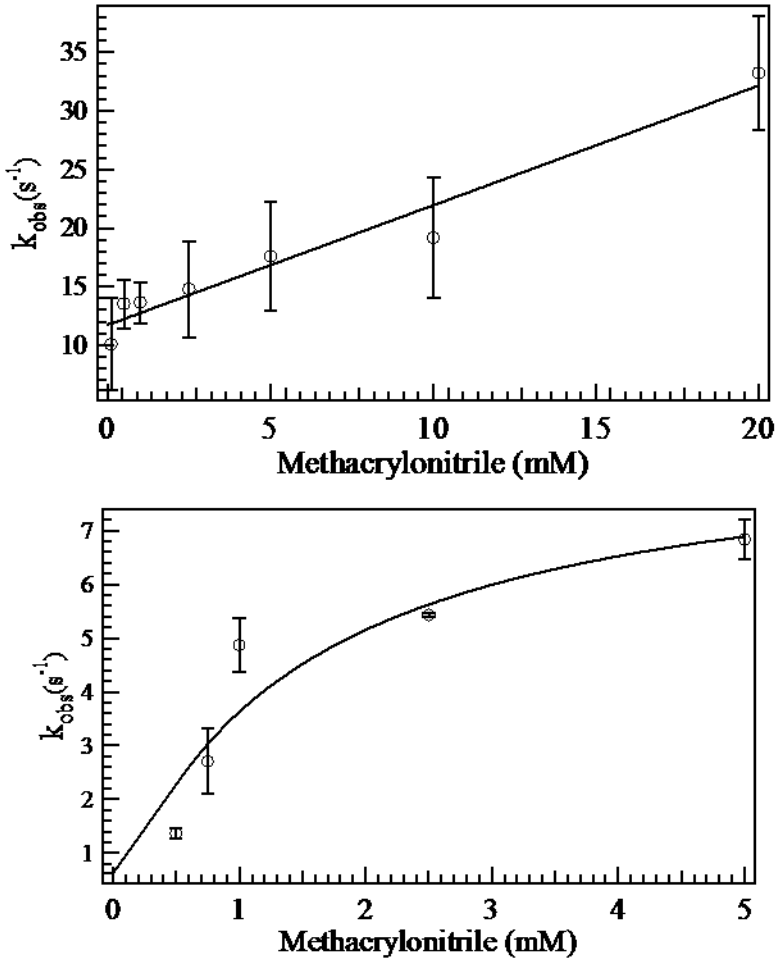

Figure 12. (A) Linear dependence of slow phase on substrate concentration. (B) Hyperbolic dependence of fast phase on substrate concentration.

The slow phase data were best fit to a hyperbolic curve, where k_{max} is the sum of $k_2 + k_{-2}$ and K_{d2} is the apparent dissociation constant of an intermediate form. k_{max} was

found to be 9 ± 2 s^{-1} and K_{d2} is 1.5 ± 0.8 mM. Subtracting k_{max} ($k_2 + k_{-2}$) from the intercept of the fast phase ($k_{-1} + k_2 + k_{-2}$) provides k_{-1}, which is 3 s^{-1}. The y-intercept of the slow phase provides k_{-2}, which is 1 s^{-1}. Therefore, k_2 is 8 s^{-1} and K_{d1}, which is k_{-1}/k_1, is 3 mM. The hyperbolic dependence of the slow phase indicates the presence of two reaction steps.

These data were compared to experimentally determined steady state kinetic data obtained at 5 ^oC for *Re*NHase-TG328-2 using 100 mM methacrylonitrile as the substrate at pH 7.0 and 242 nm. Under these conditions, the V_{max} value is 4.0 ± 0.2 s^{-1} and the K_m value is 6 ± 1 mM. Since k_2 is greater than k_{-1}, K_m is assumed to be greater than K_d, therefore, the steady state K_m value of 6 mM is in good agreement with the K_d value of 3 mM determined from stopped-flow data. These data indicate that a three step reaction mechanism is operative and provide microscopic rate constants.

The agreement of the theoretical constants calculated from the microscopic rates to steady state data also confirm that stopped flow experiments using UV detection were valid for the the NHase reaction. However, the high concentrations of substrate and subsequent product formation likely obscure potential transient intermediates. To overcome these limitations, single turnover stopped-flow experiments were performed, as only kinetically significant intermediates will be observed directly.

Single turnover stopped-flow experiments are typically not feasible due to the requirement that enzyme concentrations be similar to the K_m value of the substrate. For *Re*NHase-TG328-2, the K_m value for methacrylonitrile is 190 μM at 25 ^oC, which is low enough that the enzyme can be kept at a concentration that exceeds the substrate concentration. Additionally, the k_{cat} value determined at the K_m is 5 s^{-1}, placing the reaction well within the limits of the stopped-flow experiment. Therefore, independent

absorption spectra were acquired between 350 and 720 nm using 0.33 mM *Re*NHase-TG328-2 and 0.19 mM methacrylonitrile over 0.005 to 0.5 s of the reaction at 25 ºC (Figure 13).

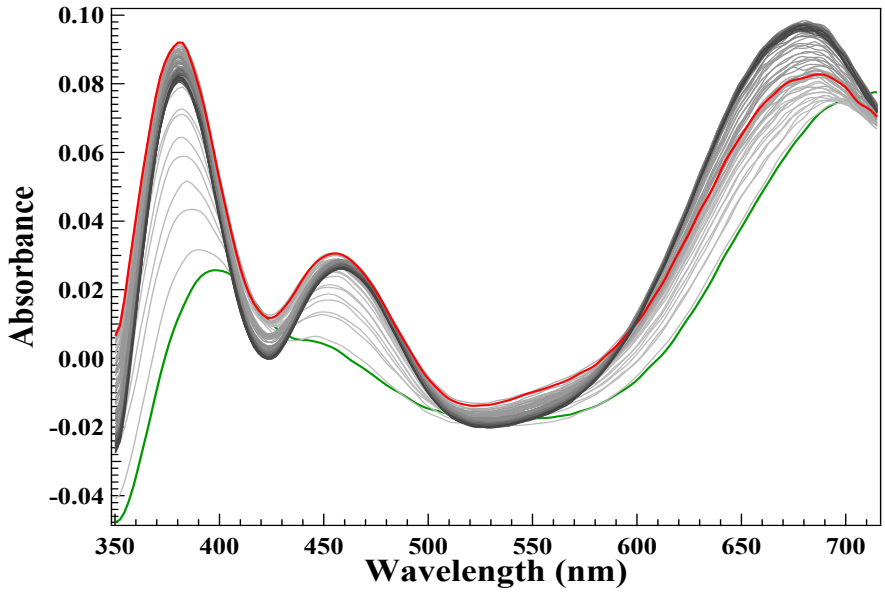

Figure 13. PDA raw absorption spectra of the single turnover reaction.

These transient spectra indicate the rapid formation of an Fe^{3+}-nitrile species that converts to the resting Fe^{3+} state and product. Independent spectra of potential enzyme intermediate complexes were extracted after singular value decomposition (SVD) was applied to the raw data in order to eliminate noise and to isolate species with significantly different absorption spectra. All spectra were then globally fit to several kinetic models using the Applied Photophysics ProK software, where the best fit corresponded to the kinetic model shown in Figure 11.

The best fit provided values for the forward rate constants k_1, k_2, and k_3 of 65 ± 10 mM^{-1} s^{-1}, 23 ± 3 s^{-1}, and 12 ± 4 s^{-1}, respectively. The reverse rate constants k_{-1} and k_{-2} were found to be 2.8 ± 0.1 s^{-1} and 1.1 ± 0.1 s^{-1}, respectively. All fitted data were verified

by residual analysis, observation of positive fitted spectra, and spectral simulation based on reactant concentrations. Theoretical k_{cat} and K_m values were calculated by inserting the microscopic rate constants obtained from single turnover into the following equations: $k_{cat} = k_2k_3/k_2+k_{-2}+k_3$ and $K_m = k_2k_3+k_{-1}k_{-2}+k_{-1}k_3/k_1(k_2+k_{-2}+k_3)$. The theoretical k_{cat} value of 8 s^{-1} and a K_m value of 128 μM are in good agreement with steady-state values of 5 s^{-1} and 190 μM, respectively.

These data indicate that the substrate-binding step is fast and reversible, while the product release step is rate-limiting. Product release was previously shown to be rate-limiting under steady-state conditions for both Fe- and Co-type NHase enzymes.[25] Concentration profiles for the progress of the reaction confirm a three-step reaction model (Figure 14) with the observed decrease in free enzyme concentration occurring concomitantly with the formation of an enzyme-substrate complex followed by an enzyme-intermediate complex and the consumption of substrate. The first transient species reaches its maximum concentration at ~0.03 s after which it begins to disappear and a second transient species peaks at ~0.1 seconds.

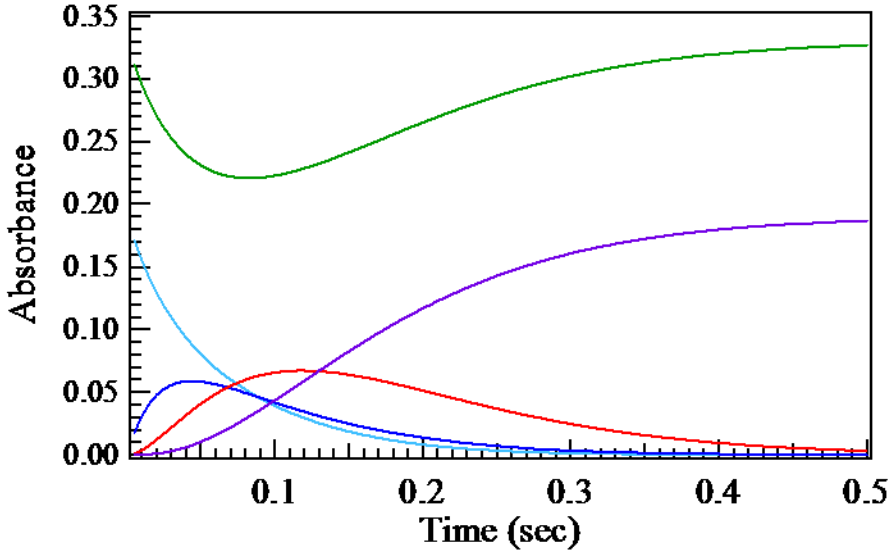

Figure 14. Concentration profile indicating the formation and decay of two intermediates (blue and red). Enzyme – green, product – purple, substrate – light blue.

Singular value decomposition identified four spectrally unique species, with one corresponding to native *Re*NHase-TG328-2 enzyme while the second is an Fe^{3+}-nitrile intermediate species (Figure 15). As the reaction proceeds, UV-vis absorption bands appear at 375, 450, 550, and 650 nm due to an Fe^{3+}-nitrile intermediate species. These absorption bands decrease in intensity as the reaction proceeds to product with the band at 550 nm disappearing completely.

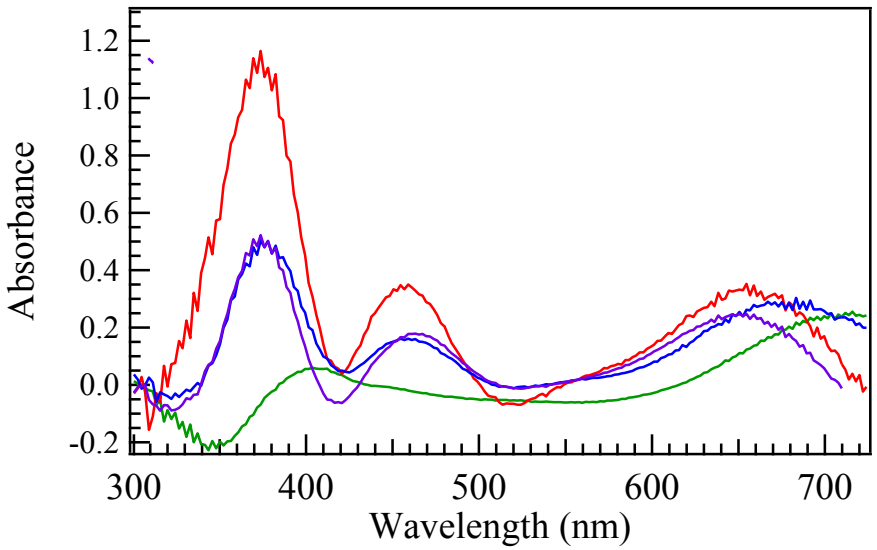

Figure 15. Extracted spectra of enzyme species. Green is resting, blue, red, and purple intermediates or product forms.

Extraction of the absorption data as a function of time at 375 nm and 550 nm provide curves that are identical to the first and second intermediates in the concentration profile. These data are consistent with the accumulation of an Fe^{3+}-nitrile intermediate species that degrades into the resting Fe^{3+} state and product. The origin of this absorption band is likely due to an Fe^{3+}←S ligand-to-metal charge transfer (LMCT) band resulting from the strong back-donation from the low-spin Fe^{3+} center to the nitrile N π* orbitals, similar to NHase-NO and Fe^{3+}-N_3 or –NO model complexes.[53]

Additional evidence for an Fe^{3+}-nitrile intermediate species comes from the observed absorption band at ~700 nm. In resting *Re*NHase-TG328-2, this band was assigned to an Fe^{3+}←S LMCT band. The observed hypsochromic shift from 700 to 650 nm upon the addition of substrate is indicative of a perturbation at the Fe^{3+} center due to nitrile binding.

Blue shifts of similar magnitude have been observed in NHase enzymes and model complexes upon the addition of NO or N_3^- and were attributed to an increase in π electron donation from the axial thiolate ligand to the Fe^{3+} ion to compensate for the π-accepting behavior of the bound ligand.[31] Similarly, the absorbance band observed at 450 nm, which has also been assigned as an Fe^{3+}←S LMCT band based on resonance Raman (RR) data and MCD model complex data, increases in intensity upon substrate binding.[53,29] Taken together, these data indicate that the observed enzyme-substrate complex is the result of the direct ligation of a nitrile to the active site low-spin Fe^{3+} center, which forms an Fe^{3+}-nitrile intermediate species.

Direct ligation of a nitrile to the low-spin Fe^{3+} center of *Re*NHase-TG328-2 is also consistent with the significant increase in absorption observed at 375 nm upon the addition of methacrylonitrile to resting *Re*NHase-TG328-2. In the presence of NO, Fe-type NHases show strong absorbance at 370 nm corresponding to an Fe^{3+}←S LMCT band that results from the direct coordination of the NO to the Fe^{3+} active site.[24, 54] Direct coordination of NO to the low-spin Fe^{3+} active site was confirmed by EPR and RR data, which suggested that NO displaces the axial water molecule forming an Fe^{3+}-NO complex that is inactive. The Fe^{3+}←S LMCT band observed at ~700 nm in resting Fe-type NHase is not observed in NO inhibited NHase enzymes but reappears upon light-induced activation.[29] However, in the enzyme-substrate intermediate complex the Fe^{3+}←S LMCT band at ~650 nm and a strong absorption at 375 nm are observed. This suggests that upon the addition of nitrile, the absorption band at 375 nm is due to an Fe^{3+}←S LMCT transition from nitrile coordination to the Fe^{3+} center in *Re*NHase TG328-2.

The single turnover data combined with previously reported kinetic data allow a catalytic mechanism to be proposed for Fe-type NHase enzymes that involves the direct ligation of the nitrile to the Fe^{3+} active site (Figure 16).[24,19] The rate constants provided herein suggest a fast second order step that involves binding of substrate to the enzyme followed by rearrangement and then product release, which is the rate-limiting step.

Displacement of the metal-bound water molecule by a nitrile and coordination to the low-spin Fe^{3+} center activates the CN bond towards nucleophilic attack by a sulfenic acid. Once nucleophilic attack occurs followed by proton transfer, the resulting imidate can tautomerize to form an amide with a subsequent proton transfer.[55] Finally, the amide product can be displaced by a water molecule and thus provide the regenerated catalyst.

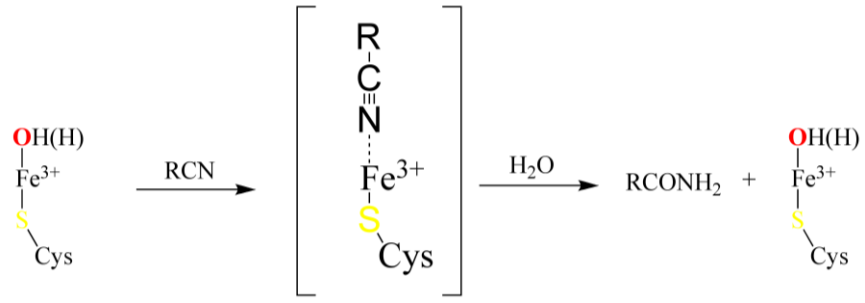

Figure 16. Proposed mechanism based on stopped flow data.

Materials and Methods

All reagents were purchased commercially and were the highest purity available.

Protein Expression

The *Re*NHase TG328-2 plasmid was kindly provided by Professor Uwe Bornscheuer. [56] The subunit and activator genes were sub-cloned into pET-21a(+) and pET-28a(+), respectively. *Re*NHase TG328-2 was transformed into NEB Turbo cells (New England Biolabs) for cloning and BL21(DE3) cells (Stratagene) for protein

expression. Cells were grown at 37°C in LB media supplemented with kanamycin (50 μg/mL) and ampicillin (100 μg/mL). The cultures were cooled for one hour upon reaching an optical density (OD) of 0.8. Cultures were induced with 0.1 mM Isopropyl-β-D-1-thiogalactopyranoside (IPTG) and 0.25 mM ferrous sulfate and shaken for 16 additional hours at 18°C. Cells were pelleted by centrifugation at 5000 rpm for 5 min.

Purification of ReNHase TG328-2

Cells containing *Re*NHase TG328-2 were resuspended in 50 mM sodium phosphate buffer at pH 7.5 containing 300 mM NaCl, 40 mM butyric acid, and 10 mM imidazole at a ratio of 3 mL/g of cells and lysed by ultrasonic probe (Misonix Sonicator 3000) in 30 s increments for 4 min. at 21W. The cell lysate was separated from cell debris by centrifugation for 40 min. at 12,500 rpm and purified using immobilized metal affinity chromatography (IMAC) on an AKTA FPLC Chromatographic System (GE) at 4°C. *Re*NHase TG328-2 was eluted with a linear gradient from 0-100% imidazole buffer (50 mM NaH_2PO_4 pH 7.5, 300 mM NaCl, 40 mM butyric acid, 500 mM imidazole) at 1 mL/min. followed by buffer exchange to remove butyric acid and imidazole using an Amicon centrifugal filter unit MWCO 30,000 (Millipore). Enzyme purity was assessed by sodium dodecyl sulfate-polyacrylamide gel electrophoresis (SDS-PAGE). A Bradford Assay was performed against bovine serum albumin (BSA) standards to determine protein concentration.

Steady State Kinetic Assay

*Re*NHase TG328-2 activity was examined using 100 mM methacrylonitrile as the substrate in 50 mM HEPES buffer, pH 7.0 and 25 °C at 242 nm (ε_{242} 3.2 $mM^{-1}cm^{-1}$) on a Shimadzu UV-2450 spectrometer. Initial reaction rates were monitored and fit to a

modified Hill equation y = V_{max}*(x/(k + x)) using Origin Pro. One unit of NHase activity was defined as the formation of 1 μmol of amide product formed per minute.

Stopped-Flow Experiments

*Re*NHase TG328-2 activity towards methacrylonitrile was examined in triplicate using a single mixing Applied Photophysics SX-20 stopped-flow UV-vis spectrophotometer. All data were fit using Pro-Data and Pro-K software by Applied Photophysics. *Re*NHase TG328-2 activity was monitored at 242 nm by acquiring stopped-flow data from 0.005 to 10 seconds at 5ºC using 10 μM enzyme and varying concentrations of methacrylonitrile (0.1 to 25 mM). These data were fit to the double exponential equation:

$$Y = A_1 e^{kobs1t} + A_2 e^{kobs2t} + C$$

Single turnover stopped-flow data were obtained using 0.33 mM *Re*NHase TG328-2 and 0.19 mM methacrylonitrile from 0.005 to 0.5 seconds. Data were reduced by Singular Value Decomposition (SVD) and globally fit to various mechanistic models.

CHAPTER 3

CHARACTERIZATION OF THE RESTING STATE OF NITRILE HYDRATASE FROM RHODOCOCCUS EQUI TG328-2 BY CW-EPR AND DFT

Summary

The nitrile hydratase from *Rhodococcus equi*-TG328-2 (*Re*NHase-TG328-2) contains a non-heme, low-spin Fe(III) ion in its active site, affording an S=1/2 ground state, which is ideal for electron paramagnetic resonance (EPR) spectroscopic analysis. As with most NHase enzymes, the resting state EPR spectrum of *Re*NHase-TG328-2 exhibits a rhombic EPR signal centered around $g = 2$, but contains several minor species with variable spin concentrations with batch-to-batch variability. As such, the use of EPR in mechanistic studies of NHase enzymes has been of limited utility. Reported herein, three species have been successfully assigned in the X-band EPR spectrum of *Re*NHase-TG328-2. The major component, N*a*, and the pH dependent interconversion of N*b* to N*c*, were attributed to the various protonation and oxidation states of the post-translationally modified cysteine ligands. Additionally, a simple method to standardize the resting enzyme was devised. Density Functional Theory (DFT) and the X-ray crystal structure of *Re*NHase-TG328-2 were used to support the EPR assignments of the major species.

Introduction

Nitrile hydratase (NHase) is an industrially and environmentally important metalloenzyme that hydrates nitriles to their commercially valuable amides.[19]

The reaction is outlined in Figure 17. The most current industrial method for the conversion of nitriles to amides requires harsh reaction conditions such as strongly acidic or basic conditions, high temperatures (200 – 400°C), and Raney copper catalysts.[5] These extreme conditions produce unwanted side reactions. NHases provide an attractive alternative as they can hydrate nitriles to amides in a regio-,enantio-, and chemo-selective fashion under mild reaction conditions (neutral pH, low temperature and pressure) that are also environmental compatible.

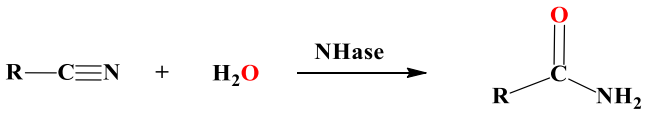

Figure 17. General reaction scheme for the conversion of nitrile to amide using nitrile hydratase.

NHases have been utilized in industrial bioprocesses as hydration catalysts most notably by the Mitsubishi Corporation, which produces up to 200,000 tons of acrylamide from acrylonitrile per year using whole cells that express NHases.[7] Amides, such as polyacrylamide and nicotinamide, are profitable precursors to rubbers, polymers (Nylon), paper fibers, animal feedstock, cosmetics, and textiles.[4] NHases have also proven to be useful in the bioremediation of chemical wastewater and runoff, specifically for the hydration of the pesticide bromoxynil.[10] The global demand for amide products emphasizes the importance of understanding the catalytic mechanism of NHase enzymes due to the large number of potential applications in chemical manufacturing and bioremediation.

NHases contain either a non-heme Fe(III) or non-corrin Co(III) ion in their active site.[32] NHases are $\alpha_2\beta_2$ heterotetramers, where the α and β subunits are approximately 28 kDa with some variation between bacterial sources.[4] The α subunit contains a

homologous cysteine rich amino acid sequence CXLCSCX (X = T,Y for Co type; S,T for Fe-type) that is the site of metal binding.[18] The metal ion is coordinated to six ligands and the geometry is conserved among all NHases.[19] Crystal structures for both Fe and Co-type NHase show that the metal ion is coordinated equatorially to two imido-nitrogen atoms from peptide backbone amides, two equatorial cysteine sulfurs, an axial cysteine sulfur, and either water for Co-type or NO for Fe-type NHase.[20] The equatorial cysteines are post-translationally modified to Cys-SOH (sulfenic acid) and Cys-SO_2H (sulfinic acid), which results in a unique metalloenzyme active site geometry called a "claw setting".[20] This configuration was confirmed by correlation Density Functional Theory (DFT) data, sulfur K-edge X-ray absorption spectroscopy (XAS) spectra, and vibrational and optical spectroscopy.[57, 58] The cysteines in the active site must be oxidized for the enzyme to be active.[21]

Given the unusual coordination geometry observed for NHases, the active site Fe(III) and Co(III) ions are low-spin, providing an S=1/2 center for the Fe(III) case, while Co(III) is S=0. The paramagnetic Fe(III) center is ideal for continuous wave - electron paramagnetic spectroscopy (CW-EPR or EPR) as EPR provides insight into the electronic properties, which are directly related to the structure and function of the active site. Previous EPR studies by Sugiura *et. al*[59,31] on two Fe-type NHases from *Rhodococcus* (formerly *Brevibacterium*) R312 (*Re*NHase-R312) and *Pseudomonas chloraphis* 23 (*Pc*NHase-23) provided rhombic EPR spectra typical of low-spin Fe(III) systems with g values at $g_1 = 2.28$, $g_2 = 2.15$, and $g_3 = 1.97$. Interestingly, the major g-values are similar between the two Fe-type NHases from different bacterial sources, however, there are significantly more minor species observed for *Pc*NHase-23. Electron

nuclear double resonance (ENDOR) spectroscopy identified the axial ligand as a water molecule at pH 7.5 and not a hydroxide.[60] Additionally, EPR was used to identify the enzyme resting state after photolysis of an Fe-type NHase, which releases NO.[61] Combination of these EPR data with DFT and X-ray crystallography has provided some insight into some the electronic properties that are common to all NHases.

However, a challenge to utilizing EPR methods to examine the electronic properties of Fe-type NHase enzymes is the observation of multiple minor species with *g*-values around 2.0. These minor species mask new catalytically relevant signals that result upon the addition of substrates or inhibitors as the resulting active site Fe(III) complex exhibits EPR resonances that lie within the range observed for the observed minor species. Therefore, characterization of the observed resting-state minor species is a necessary step in the utilization of EPR as a tool to examine changes in the electronic properties of the active site during catalytic turnover.

Results and Discussion

EPR Spectroscopy

EPR spectra were recorded on a Bruker EMXplus spectrometer at 10-30 K on 0.2-1 mM samples of *Re*NHase-TG328-2 in deuterated 50 mM HEPES buffer at pH 7.0. The resting state of *Re*NHase-TG328-2 shows at least three species, all of which are typical of low-spin (S=1/2) Fe(III) systems.[62,63] EPR spectra of the resting-state of two separate batches of *Re*NHase TG328-2 are shown in Figure 18.

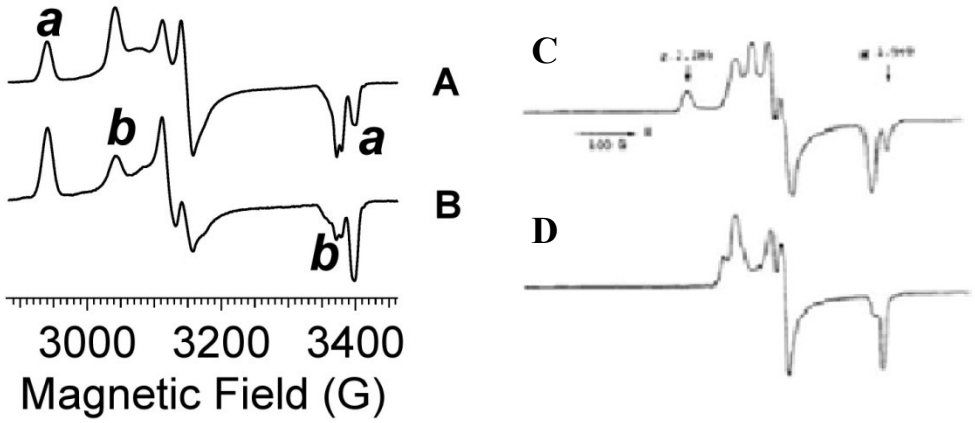

Figure 18. (A) and (B) Two purification batches of resting *Re*NHase-TG328-2. Resting spectrum of (C) *Rhodococcus* (formerly *Brevibacterium*[59]) R312 NHase and (D) *Pseudomonas chloraphis* 23.[31]

Interestingly, the resting-state EPR spectra observed for both batches of *Re*NHase-TG328-2, in general, resemble that reported for *Pc*NHase-23.[31] Similar to *Pc*NHase-23, the minor species appear in the same regions at different intensities. Clear turning points are exhibited in the spectrum of *Re*NHase-TG328-2 at 2941 G (peak), 3041 G (peak), 3077 G (small peak), 3120 G (crossover), 3149 G (crossover), 3376 G (split trough) and 3399 G (trough) (Figure 18). Small shoulders were also observed at about 3175 G and 3360 G.

These resonances correspond to *g*-values almost indistinguishable from those of *Pc*NHase-23 (after the resonant field values for *Re*NHase-TG328-2, *g*-values for the *Re*NHase-TG328-2 features are given in parentheses followed by the corresponding *Pc*NHase-23 values in brackets): 2941 G (2.281) [2.29]; 3041 G (2.206) [2.21]; 3077 G (2.180) [2.18]; 3120 G (2.150) [2.15]; 3149 G (2.131) [2.13]; 3376 G (1.987) [1.99]; and 3399 G (1.974) [1.97].

The relative intensities of these features differed in *Re*NHase-TG328-2 and *Pc*NHase-23 spectra and, indeed, in spectra from different batches of *Re*NHase-TG328-2 allowed unambiguous deconvolution of the spectrum into three species, termed here N*a*, N*b* and N*c* (to avoid confusion with NH_A, NH_C *etc.* employed elsewhere[61]). Resting-state EPR spectra of *Re*NHase-TG328-2 do not change in the presence of 10% glycerol or 10% methanol, typical buffer and assay components for Fe-type NHase enzymes. Therefore, the three species observed are not due to interactions of these buffer components with the low-spin Fe(III) center.

N*a* is the most anisotropic species and is characterized by $g_{(1,2,3)}$ = 2.281, 2.150, 1.974 (the outer resonances are labeled *a* on Trace A of Figure 18). In addition to its analog in *Pc*NHase-23, this species strongly resembles the as-prepared state of *Re*NHase-R312.[31, 61] Therefore, despite the inconsistency and complexity of *Re*NHase-TG328-2 EPR spectra, the primary EPR signal, N*a*, is identical in each enzyme.

One of the minor species, N*b*, has $g_{(1,2,3)}$-values of 2.206, 2.131 and 1.987. The g-tensor for N*b* is not only less anisotropic than that of N*a* ($g_1 - g_3$ = 0.219 *vs.* 0.307) but, perhaps more significantly, is markedly less rhombic; the rhombicities, R_B, for N*b* and N*a* are 0.69 and 0.85, respectively [here, "rhombicity", R_B, is defined as $R_B = 1 - [(|g_1 - 2g_2 + g_3|)/(g_1 - g_3)]$, where $R_B = 0$ for the axial cases of $g_1 = g_2$ and $g_2 = g_3$, and $R_B = 1$ for the most rhombic case of $[(g_1 - g_2) = (g_2 - g_3)]$. The closest analogies to N*b* in the literature, other than the corresponding species in *Pc*NHase-23, are the spectra obtained upon reaction of propionitrile with *Re*NHase-R312 ($g_{(1,2,3)}$ = 2.230, 2.163, 1.982; $g_1 - g_3$ = 0.248; R_B = 0.54) and, more so, the isobutyronitrile *Re*NHase-R312 complex ($g_{(1,2,3)}$ =

2.207, 2.124, 1.984; $g_1 - g_3 = 0.223$; $R_B = 0.74$).[31] An N*b* analog was not observed during illumination and annealing experiments on *Re*NHase-R312.[61]

The third minor species, N*c*, is less well characterized, as only the lowest field turning point is well-resolved, but tentative parameters are $g_{(1,2,3)} = 2.180, 2.114, 1.998$, $g_1 - g_3 = 0.182$, and $R_B = 0.73$. This appears to be the only example of a nitrile hydratase signal with $g_1 < 2.2$. While the orientation of the $g = 2.18$ feature in *Re*NHase-TG328-2 is not unambiguously clear, there seems little doubt that it is the lowest field resonance of a rhombic system in *Pc*NHase-23.

The presence of multiple species is a complicating factor in CW-EPR. Although there is some reassurance in the reproducibility of the nature of the three species between preparations of *Re*NHase-TG328-2 and between *Re*NHase-TG328-2 and *Pc*NHase-23, and the recapitulation of N*a* in the spectrum of *Re*NHase-R312, the irreproducibility of the proportions of N*a*, N*b* and N*c* in the spectra remains a concern. Even so, variability in resting-state CW-EPR spectra is a relatively common occurrence in metalloenzymes.[64,65,] For example, dimethyl sulfoxide reductase from *Rhodobacter sphaeroides* strain-16 exhibits several EPR species in the resting-state that were proposed to be due to a combination catalytically inactive enzyme species and a single catalytically relevant enzyme.[64-65,64] Therefore, it is likely that the same behavior is occurring in *Re*NHase-TG328-2, *Re*NHase-R312, and *Pc*NHase-23.

In order to find optimum conditions under which the catalytically relevant signal, N*a*, is maximized while minimizing the non-catalytically pertinent signals for resting *Re*NHase-TG328-2, the enzyme was turned over with acetonitrile (ACN) and methacrylonitrile (MeACN) (Figure 19). Upon the addition of ACN to *Re*NHase-TG328-

2 the N*a* signal was lost with ~60 % of the remaining EPR spins due to N*b* and the other ~40% due to a new signal (N*d*) with $g_{(1,2,3)}$-values 2.231, 2.148 and 1.986 (g_1 - g_3 = 0.245; R_B = 0.68).

The spectrum as a whole is very similar to that obtained by adding propionitrile to *Pc*NHase-23.[31] While it was not stated that the new signal obtained upon the addition of propionitrile was persistent in *Pc*NHase-23, unlike in *Re*NHase-R312 where the new EPR signal decayed to an N*a*-like resting state after exhaustion of the propionitrile substrate,[31] it appears that the only way that a single species (N*a*) could be elicited in *Pc*NHase-23 was to add mercury acetate.[31]

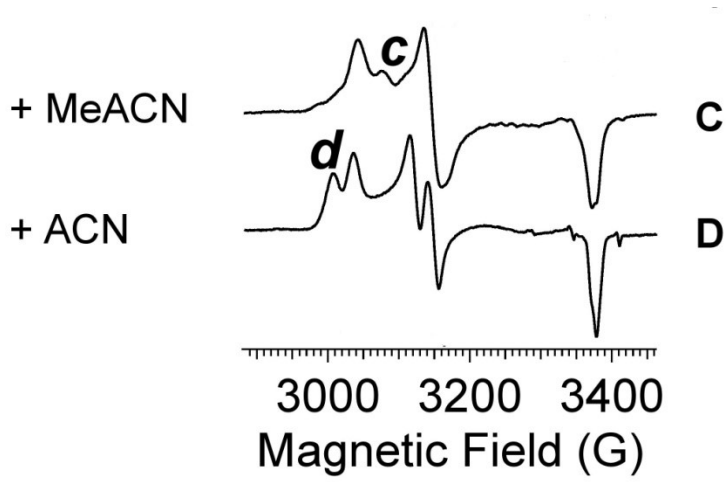

Figure 19. Spectra of *Re*NHase-TG328-2 samples frozen with ACN and turned over with methacrylonitrile.

Reaction of MeACN with *Re*NHase-TG328-2 provided an EPR spectrum consisting largely of N*b*, with small amounts of N*c* (Figure 19). Both species remain after exhaustive dialysis, however, the g_1 resonance shifted to higher field suggesting a mixture of substrate bound and unbound enzyme. These data are almost identical to *Pc*NHase-23 and *Re*NHase-R312 after reaction with proprionitrile,[31] in that the g_1 peak at

g = 2.28 corresponds to an unbound form of NHase and the peak at g = 2.24 corresponds to a substrate bound form of the enzyme.

The UV-vis and EPR spectra of resting *Re*NHase-TG328-2 were also recorded as a function of pH to determine if the observed minor species could be due to the protonation states of the active site sulfenic and sulfinic acid ligands and/or nearby amino acid residues. UV-vis spectra were recorded at pH values of 6.5, 7.0, 8.0, and 8.5 (Figure 20).

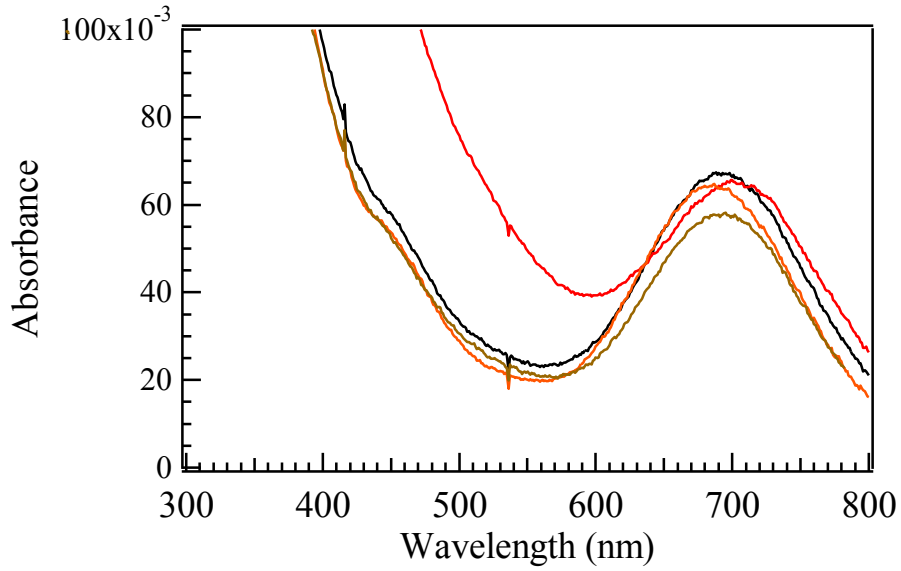

Figure 20. Visible spectra of 1 mM *Re*NHase-TG328-2 at pH 6-red, pH 7-black, pH 8-brown, pH 8.5-orange in 50 mM MES (pH 6.0) or 50 mM HEPES buffer.

Each spectrum is dominated by the Fe(III)←S ligand-metal charge-transfer (LMCT) band at ~700 nm due to π-back donation of electron density from the axial sulfur to the Fe(III) center.[53] At pH values of 7.0 and 8.0, the absorption maximum is 706 nm; however, decreasing the pH to 6.0 or increasing it to 8.5 results in a blueshift of this band to 690 and 683 nm, respectively. These data suggest an increase in π-back donation likely due to a decrease in the Fe-S bond length at low or high pH values.[66,31]

EPR spectra (Figure 21) of MeACN-turned over *Re*NHase-TG328-2, containing a mixture of N*b* and N*c*, were also recorded at pH values between 6.5 and 8.0. The proportion of N*c* decreased from ~35 % at pH 6.5 to <5% at pH 8.0, with a concomitant increase in N*b* providing an estimated pk_a value of 7.3. The loss of N*c* allowed N*b* and N*c* to be deconvoluted by subtracting the EPR spectrum obtained at pH 8.0 from the spectrum recorded at pH 6.5 providing a spectrum made up primarily of N*c*. (Figure 21)

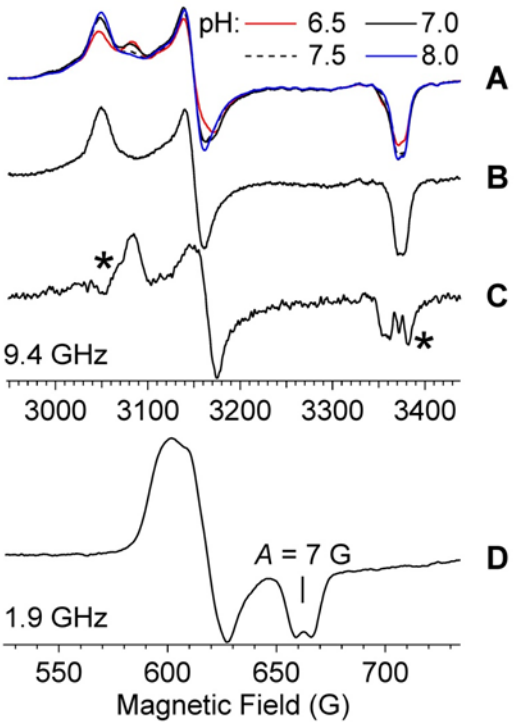

Figure 21. (A) Overlay of pH spectra of *Re*NHase-TG328-2. (B) and (C) Deconvoluted difference spectra. (D) 1.9 gHz spectra at pH 8.0.

Interestingly, the g_3 feature of the N*b* component exhibited a splitting, estimated at ~10 G that remained even in samples exchanged into >95% ^2H_2O. EPR spectra of *Pc*NHase-23 also suggested an unresolved broadening of g_3 whereas no such splitting was evident in spectra of *Re*NHase-R312.[31, 61] These data suggest that the splitting observed in the g_3 EPR signal is either due to a hyperfine interaction or two overlapping

signals with similar *g*-values. If the latter were the case, the splitting would be expected to collapse at low frequency due to the field dependence of the Zeeman interaction.[67]

In an effort to further examine the field dependence of the observed splitting in the g_3 resonance, EPR spectra of MeACN-turned over *Re*NHase-TG328-2 at pH 8.0 were recorded at 1.9 GHz (Figure 21D). The splitting observed on the high-field signal (g_3) became well-resolved as a result of line narrowing due to a decrease in *g*-strain.[67] These data clearly show that the observed splitting is field-independent and therefore, must be due to either a hyperfine interaction with a non-exchangeable $I = {}^1/_2$ nucleus such as a proton coordinated to a carbon or oxygen atom or a dipolar interaction with a nearby $S = {}^1/_2$ spin system. In the absence of a candidate for the latter, which would itself exhibit an EPR signal, the former is proposed.

The most likely candidate is a strongly coupled proton of a coordinated water/hydroxyl; however, this feature was insensitive to pH changes between 6.5 and 8.0, in contrast to the shift in the g_1 resonant field and therefore could be due to a protonated sulfenic acid ligand. Combination of the UV-vis and EPR data obtained at various pH values suggest that two ionizable groups interact with the low-spin Fe(III) ion, one of which appears to be due to a metal ligand and one that is likely not a ligand but still influences electronic structure.

The UV-vis and EPR data obtained for *Re*NHase-TG328-2 at various pH values correlate with kinetic data obtained on the Fe-type NHase from *Comamonas testosteroni* Nil (*Ct*NHase) as well as a Co-type NHase from *Pseudonocardia thermophila* JCM-3095 (*Pt*NHase).[55, 68,69] Kinetic data obtained over the pH range 3.2 to 11.0 for both *Ct*NHase and *Pt*NHase indicate that two protons are transferred in the rate-limiting step with pK_a

values of 5.8 and 9.1 and a normal isotope effect. As expected, these pK_a's clearly do not correspond to the pK_a value determined from EPR data of 7.3 for the pH dependent interchange of the two species N*b* and N*c*.

As the recent kinetic and X-ray crystallographic data on *Pt*NHase bound by boronic acid inhibitors suggests that one proton is transferred from the αCys113−OH ligand, which functions as a nucleophile in the catalytic reaction, to the nitrile N-atom while a second proton transfer occurs between a water molecule that reforms αCys113−OH (protonated sulfenic acid) and the newly forming imidate N-atom, the pK_a obtained from EPR data is possibly due to an active site residue that is not a ligand to the metal center but can affect the electronic properties of the Fe(III) ion.[68]

Previous studies on Fe-type NHases prepared in the dark (termed "NH_{dark}") indicate that they are inactive and EPR-silent.[61,29] Illumination of NH_{dark} at 2 - 4 K yields "NH_C", which exhibits EPR signals that are less anisotropic (g_1 - g_3 = 0.2) than those exhibited by Fe-type NHase enzymes activated upon exposure to ambient light at room temperatures ("NH_{light}"; g_1 - g_3 = 0.3).[61] Upon illumination of NH_{dark} at 20 K followed by annealing at 77 K, the NH_C EPR signal is lost; however, illumination of NH_{dark} at 2 - 4 K followed by controlled annealing at 20 - 77 K produced a procession of EPR signals with increasing anisotropies, from 0.2 (*c.f.* NH_C) to 0.3 (*c.f.* NH_{light}), with at least three additional intermediate species.

The involvement of nitric oxide (NO) was inferred by X-ray crystallographic data and the differential electronic effects observed for inhibitors that act on NH_{light} and NH_C or NH_{dark}.[21] Therefore, another possibility for the origin of the minor species observed in resting-state EPR spectra of *Re*NHase-TG328-2, is the presence of photolyzable NO. A

liquid sample of resting state *Re*NHase-TG328-2 irradiated at ~0°C with a projector lamp for 5 min prior to freezing in liquid N_2 (Figure 22) were identical those obtained without irradiation (Figure 18A & 18B).

Therefore, NO is not involved in the formation of the observed minor signals. An unusually broad radical signal, however, was observed upon illumination. It is well documented that HEPES can generate HOOH when illuminated by visible light.[70,71] Therefore, it is likely that this radical signal is due to a HEPES-generated peroxide that has undergone Fenton chemistry at the iron site to generate free radicals that subsequently react with protein residues.

Interestingly, a free radical signal associated with an Fe-type NHase was previously reported an suggested to be due to an essential pyrroloquinoline quinone (PQQ) cofactor.[72] A PQQ cofactor has never been observed for any NHase so it is highly unlikely that PQQ is required for catalytic activity, though the clear EPR finding that a free radical can be elicited in NHase samples under certain conditions is intriguing.

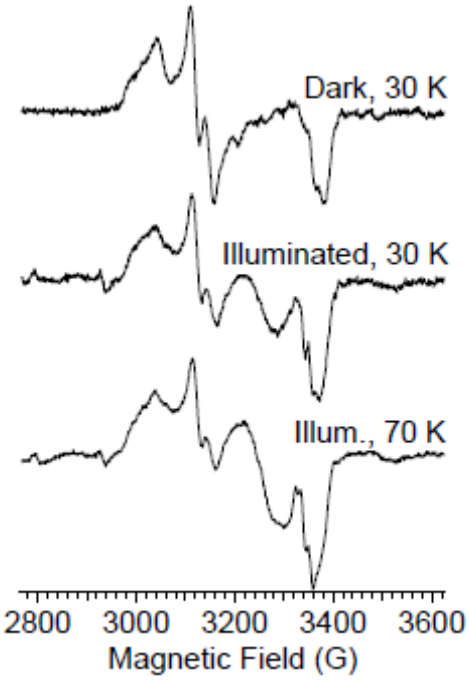

Figure 22. EPR spectra of illuminated and dark *Re*NHase samples.

Density Functional Theory

EPR data collected for the resting-state of *Re*NHase-TG328-2 was further examined using the ORCA computational package, developed by Dr. Frank Neese, which has proven enormously successful in treating transition-metal species.[53] DFT studies of NHase spin-Hamiltonian parameters require initial "calibration" through examination of suitable model complexes with well-defined structures and EPR spectra. In collaboration with Professor Adam Fielder at Marquette University, a coupled-perturbed self-consistent field (CP-SCF) equations for spin-orbit coupling (as implemented in ORCA) and a combined DFT/ligand-field approach that uses excited-state energies from time-dependent DFT calculations (TD-DFT) as inputs into the equations developed by Taylor for low-spin Fe(III) systems , were employed.[53,73]

EPR parameters for an Fe-type NHase model complex ($[Fe^{3+}(ADIT)_2]^+$) reported by Kovacs *et. al*[57] (Figure 23) were examined as the oxidation and protonation states of one of the thiolates was systematically altered and provided different EPR spectra.

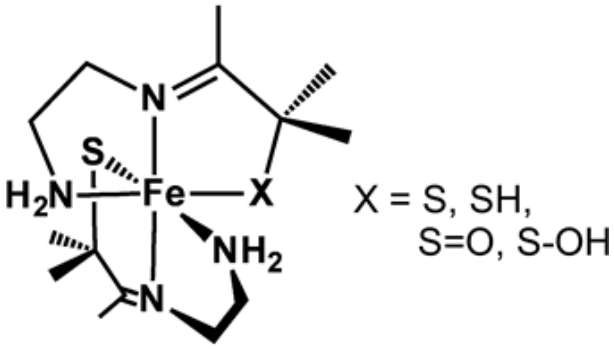

Figure 23. Fe-type NHase model complex used for DFT studies.

Both CP-SCF and the combined TD-DFT/LF approaches reproduce key elements of the experimental EPR data reported for the $[Fe^{3+}(ADIT)_2]^+$ complexes (Table 2). The TD-DFT/LF results, in particular, are very encouraging, given the excellent agreement between the calculated g-values and the experimental data (rms deviations of ~0.02). Importantly, the calculations replicate changes in the g-tensor that occurs upon the mechanistically significant protonation and/or oxidation of the thiolate ligand to an –S=O donor.

On the other hand, CP-SCF consistently predicts a g_3-value much greater than 2.0, whereas the experimental g_3 is always less than 2.0, and has *g*-value rms deviations ~4 time higher than TD-DFT/LF. In addition, CP-SCF underestimates the g_1-value. These data, in combination with the observed *g*-values for the minor species N*b* and N*c* observed for *Re*NHase-TG328-2, suggest that N*b* is due to a deprotonated form of the enzyme and N*c* is due to a protonated form.

Table 2. Experimental and computed *g*-values for $[Fe^{3+}(ADIT)_2]^+$ and its derivatives.

X		g_1	g_2	g_3	g_{ave}	g-aniso[a]	g-rhomb[b]	rms dev[c]
S	exper	2.17	2.11	1.99	2.090	0.180	0.333	
	DFT/LF	**2.160**	**2.129**	**1.990**	**2.093**	**0.170**	**0.182**	**0.021**
S–H	exper	2.22	2.15	1.97	2.113	0.250	0.280	
	DFT/LF	**2.201**	**2.163**	**1.980**	**2.115**	**0.221**	**0.172**	**0.025**
S=O	exper	2.20	2.16	1.98	2.113	0.220	0.182	
	DFT/LF	**2.175**	**2.162**	**1.980**	**2.106**	**0.195**	**0.067**	**0.025**
S–OH	exper	2.24	2.15	1.97	2.120	0.270	0.333	
	DFT/LF	**2.202**	**2.160**	**1.970**	**2.111**	**0.232**	**0.181**	**0.010**

[a] g-aniso = $g_1 - g_3$; [b] g-rhomb = $(g_1 - g_2)/(g_1 - g_3)$; [c] rms dev = root-mean-square deviation between computed and experimental g-values.

X-Ray Crystallography

In an effort to clearly define the structure of *Re*NHase-TG328-2 along with the catalytically relevant residues that constitute the active site, we have solved the X-ray crystal structure to 2.3Å resolution (Figure 24). The structure was solved by molecular replacement using the NHase from *Rhodococcus erythropolis* AJ270 (*Re*NHase-AJ270; PDB ID: 2QDY) as a template.[16] The parameters are summarized in Table 2. The template was selected due to its sequence homology to ReNHase-TG328-2 (82% identity for the α-subunit and 70% identity for the β-subunit).

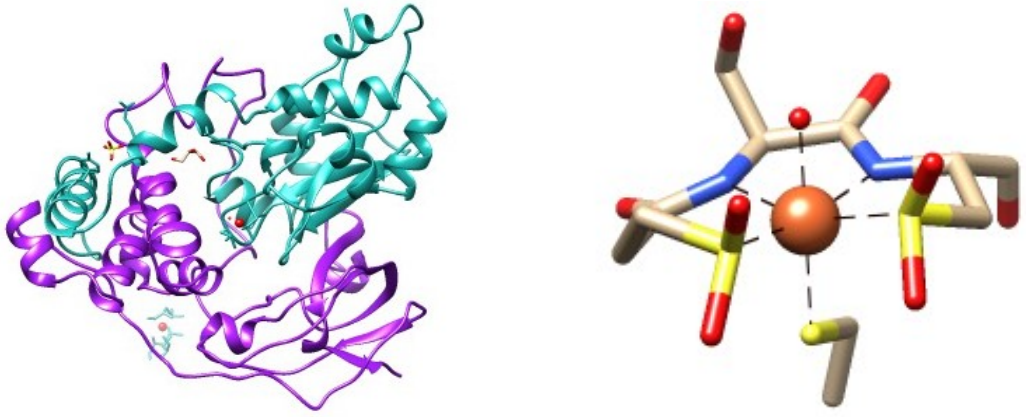

Figure 24. (Left) Crystal structure of the heterodimer of *Re*NHase-TG328-2. (Right) Active site of *Re*NHase-TG328-2 displaying the "claw" geometry.

Similar to other Fe-type NHases, the active site is buried at the interface of the α and β subunits. The Fe(III) ion in ReNHase TG328-2 is six-coordinate and bound by αC109, αC112, and αC114 as well as two backbone amide nitrogens from αSer113 and αC114, where αC112 and αC114 are both oxidized to cysteine sulfinic acids (Figure 24). The complete oxidation of αC112 and αC114 is due to the fact that ReNHase-TG328-2 was crystallized under anaerobic conditions and the first crystal appeared after a three month time period. As expected, the sixth ligand is a water molecule.

Table 3. Data collection and refinement statistics of *Re*NHase TG328-2.

Data Processing	
Space group	I23
Cell dimension	
α, β, γ (°)	90.0; 90.0; 90.0
a, b, c (Å)	184.9; 184.9; 184.9
Resolution (Å)	41.4 - 2.57
[a]R_{merge} (%)	0.149 (0.485)[b]
I/σ (I)	6.9
Completeness (%)	99.8
Multiplicity	6.2 (4.4)
No. Reflections	210086
No. Unique Reflections	33630
Refinement	
Average B factor (Å^2)	40.72
[c]R_{work}/[d]R_{free} (%)	18.04/22.47
No. of Atoms	
Protein	6503
Water	174
[e]RMSD	
Bond length (Å)	0.012
Bond angle (°)	1.221
Ramachandran plot	
Most Favored (%)	94.71
Allowed (%)	3.81
Outliers (%)	1.48

[a] $R_{merge} = \Sigma|I_{obs}-I_{avg}|/ \Sigma I_{avg}$

[b] The values for the highest resolution bind are in parentheses.
[c] $R_{work} = \Sigma|F_{obs}-F_{calc}|/ \Sigma F_{obs}$.
[d] Five percent of the reflection data were selected at random as a test set and only these data were used to calculate R_{free}.
[e] RMSD, root mean square deviation

Bond distances were calculated for ligands bound to the Fe(III) center and summarized in Table 3. Given that the crystal of *Re*NHase-TG328-2 was prepared from a sample not treated with any nitrile substrate, it is likely that an EPR spectrum of the sample prior to crystallization, which would contain sulfenic and sulfinic acid ligands would be dominated by N*a*, the catalytically relevant species.

Table 4. Bond distances at the active site of *Re*NHase-TG328-2.

Bonded Atoms	**Bond Distance (Å)**
Fe-αCys112	2.10
Fe-O (H_2O or OH^-)	1.90
Fe-α(S)Cys109	2.19
Fe-α(N)Ser113	2.16
Fe-α(S)Cys114	2.07
Fe-α(N)Cys114	2.25

Conclusion

We have identified and characterized three signals that are observed in different proportions in resting *Re*NHase-TG328-2 using EPR spectroscopy. Based on EPR analysis including the pH dependence of the Na and Nb, along with DFT and X-ray crystallography, N*a* is assigned as a catalytically relevant species since it is almost completely extinguished (5% remaining) by MeACN. The two minor species, N*b* and N*c*, are related signals that interconvert depending on pH. The protonation states of the active site cysteine and cysteine sulfenic and sulfinic acid ligands were suggested to be Cys-S^-, CysSOH and a $CysSO_2^-$ based on sulfur K-edge EXAFS and geometry-optimized DFT calculations at pH 7.0.[57] Therefore, N*c* is likely due to the catalytically active

protonated cysteine sulfenic acid (CysSOH) form of *Re*NHase-TG328-2 while N*b* is due to the catalytically inactive deprotinated cysteine sulfenic acid ($CysSO^-$) form with a pK_a value for process of ~7.3. TD-DFT/LF DFT analysis is also consistent with these assignments. Understanding the resting-state EPR spectrum of *Re*NHase-TG328-2 enhance our understanding of the electronic structure of the active site and provides the foundation to utilize pulsed EPR methods to characterizing NHase reaction intermediates.

Materials and Methods

All reagents were purchased commercially and were the highest purity available.

Protein Expression

The *Re*NHase-TG328-2 plasmid was provided by Professor Uwe Bornscheuer [74]. The subunit and activator genes were sub-cloned into pET-21a(+) and pET-28a(+), respectively. *Re*NHase-TG328-2 was transformed into NEB Turbo cells (New England Biolabs) for subcloning and BL21(DE3) cells (Stratagene) for protein expression. Cells were grown at 37°C in LB media supplemented with kanamycin (50 μg/mL) and ampicillin (100 μg/mL). Upon reaching an optical density (OD) of 0.8, the cultures were cooled to the induction temperature of 18°C. Cultures were induced with 0.1 mM isopropyl-β-D-1-thiogalactopyranoside (IPTG) and 0.25 mM ferrous sulfate and shaken for 16 additional hours at 18°C.

Purification of ReNHase -TG328-2

Cells were pelleted by centrifugation at 5000 rpm for 5 min. Cells containing *Re*NHase-TG328-2 were resuspended in 50 mM sodium phosphate buffer at pH 7.5 containing 300 mM NaCl, 40 mM butyric acid, and 10 mM imidazole at a ratio of 3 mL/g of cells and lysed by ultrasonic probe (Misonix Sonicator 3000) in 30 s increments for 4

min. at 21W. The cell lysate was separated from cell debris by centrifugation for 40 min. at 12,500 rpm and purified using immobilized metal affinity chromatography (IMAC) on an AKTA FPLC Chromatographic System (GE) at 4°C. *Re*NHase-TG328-2 was eluted with a linear gradient from 0-100% imidazole buffer (50 mM NaH_2PO_4 pH 7.5, 300 mM NaCl, 40 mM butyric acid, 500 mM imidazole) at 1 mL/min. followed by buffer exchange to remove butyric acid and imidazole using an Amicon centrifugal filter unit MWCO 30,000 (Millipore). Enzyme purity was assessed by sodium dodecyl sulfate-polyacrylamide gel electrophoresis (SDS-PAGE). A Bradford Assay was performed against bovine serum albumin (BSA) standards to determine protein concentration.

Steady State Kinetic Assay

*Re*NHase-TG328-2 activity was examined using 100 mM methacrylonitrile as the substrate in 50 mM HEPES buffer, pH 7.0 and 25 ^{o}C at 242 nm (ε_{242} 3.2 $mM^{-1}cm^{-1}$) on a Shimadzu UV-2450 spectrometer. Initial reaction rates were monitored and fit to a modified Hill equation $y = V_{max}*(x/(k + x))$ using Origin Pro. One unit of NHase activity was defined as the formation of 1 μmol of amide product formed per minute. No attempt was made to limit exposure to light throughout purification and sample preparation, and neither extended (> 4 h) exposure to ambient light nor storage at 4 °C in the dark were observed to elicit any changes in the activities or EPR signals of samples.

Electron Paramagnetic Resonance

All *Re*NHase-TG328-2 samples were prepared in deuterated buffers at 0.2 mM - 1 mM, with 10% glycerol added for cryogenic storage. Resting *Re*NHase-TG328-2 was prepared in deuterated HEPES pH 7.0 at 0.2 mM. Where other buffer conditions (*e.g.* MES pH 6.0; glycerol; $^{2}H_2O$ substitution) are indicated, buffer exchange was effected

using Amicon centrifugal concentrators. Substrate was either added directly and rapidly mixed manually,[64] or else was added using a rapid-freeze-quench apparatus described elsewhere.[75] Samples were generally examined immediately and then stored in the dark at 77 K prior to any subsequent re-examination. No storage-dependent changes in signals were observed. Continuous-wave (CW) X-band EPR was recorded on either a Bruker EMXplus spectrometer (ER4116DM resonator, Oxford ESR900 helium flow cryostat & ITC503 temperature controller) or an EleXsys E600 spectrometer (ER4116DM & Super-Hi-Q resonators, Oxford ESR900 helium flow cryostat & ITC503 temperature controller). L-band EPR was recorded on a home-built spectrometer equipped with a loop-gap resonator that accommodated the 4 mm O.D. tubes,[76] and with non-adiabatic rapid scanning (NARS) capability.[77] A turnover sample was prepared by adding 0.2 mM MeACN to 0.2 mM of *Re*NHase-TG328-2. The sample was incubated at 25˚C for 5 minutes. Methylacrylamide product and residual MeACN was removed from the enzyme using an Amicon centrifugal concentrator.

Crystal Structure

*Re*NHase-TG328-2 was concentrated to 20 mg/mL and exchanged into 50 mM HEPES pH 7.0 using an Amicon Ultrafiltration device, MWCO 50,000. Sitting drop vapor diffusion crystal screens were set up using an Art Robbins Crystal Gryphon robot at 10 mg/ mL and 20 mg/mL. Screens employed were Wizard 1 and 2 from Emerald Biosystems and Index Screen 1 and 2, PEG/Ion 1 and 2, and Crystal Screen 1 and 2 from Hampton Research. Screens were stored at 20˚C. A single cubic shaped crystal was obtained in 0.1 bis-tris pH 5.5 and 2.0 M ammonium sulfate. The crystal was flash frozen with liquid nitrogen in a cryoprotectant solution containing the crystallization

condition and 40% glycerol. Crystallographic data sets were collected at the SBC beamline 19-ID at the Advanced Photon Source at Argonne National Laboratory. Data sets were processed using the HKL2000. The structure was determined by molecular replacement of the template structure from *Rhodococcus erythropolis* NHase AJ270 using PHASER. NHase AJ270. Model building and refinement were performed with Coot. The structure was refined using a combination of CCP4 and Phenix.

CHAPTER 4

IDENTIFICATION OF NITRILE HYDRATASE INTERMEDIATES USING RFQ-EPR

Summary

Efforts to structurally characterize an actual nitrile intermediate of nitrile hydratase have been unsuccessful. While inhibitor complexes have yielded some information regarding the catalytic mechanism of nitrile hydratases, they cannot completely define the mechanism like a true, nitrile-enzyme intermediate complex. Prior spectrokinetic, crystallographic, and Density Functional Theory (DFT) data provided the foundation for rapid-freeze-quench (RFQ) electron paramagnetic resonance (EPR) studies on the Fe-type nitrile hydratase from *Rhodococcus equi*-TG328-2 (*Re*NHase-TG328-2). RFQ-EPR data using methylacrylonitrile (MeACN) as the substrate provide evidence for a short-lived intermediate that is strongly indicative of a nitrile-bound complex. These data provide new insight into the catalytic mechanism of NHase enzymes.

Introduction

Nitrile hydratases (NHases) catalyze the stereo and regio-specific hydration of nitriles to their corresponding higher value amides under ambient conditions and physiological pH.[19] NHases have attracted substantial interest as biocatalysts in preparative organic chemistry and are already used in several industrial applications such as the large scale production of acrylamide [48] and nicotinamide.[49] For example, Mitsubishi Rayon Co. has developed a microbial process that produces ~200,000 tons

of acrylamide annually using the NHase from *Rhodococcus rhodochrous* J1.[7] More than 3,500 tons of nicotinamide are produced per year *via* NHase hydration, with yields of >99 % and without the formation of troublesome byproducts such as acrylic acid.[50] NHases have also been employed as bioremediation agents to clean up nitrile-based pesticides, such as bromoxynil.[51] Because of their exquisite reaction specificity, the nitrile-hydrolyzing potential of NHase enzymes is becoming increasingly recognized as a truly new type of "Green" chemistry.

NHases contain either a low-spin Fe(III) ion ('Fe-type') or a Co(III) ion ('Co-type') in their active sites.[19] X-ray crystal structures of both Co- and Fe-type NHases reveal that the active site metal ion is coordinated by three cysteines, two amide nitrogens, and a water molecule.[4] Two of the active site cysteine residues are post-translationally modified to cysteine-sulfinic acid ($-SO_2H$) and cysteine-sulfenic acid (–SOH) yielding an unusual metal coordination geometry, termed a "claw-setting". These Cys oxidation states are essential for NHase activity.[38, 57] The protonation states were suggested to be Cys-S^-, CysSOH and a $CysSO_2^-$ based on sulfur K-edge EXAFS and geometry-optimized Density Functional Theory (DFT) calculations.[57] Although the structures of Fe- and Co-type NHases are very similar, Fe-type NHases only bind Fe(III) and Co-type NHases only bind Co(III). Despite the industrial and bioremediation importance of NHase enzymes and the wealth of structural information vailable, details of their reaction mechanism remain poorly understood.

Based on several elegant studies on NHase enzymes and biomimetic model complexes, several possible reaction mechanisms have been proposed.[19, 78] In each, imidate is produced as a reaction intermediate, which then isomerizes to the

corresponding amide.

The most accepted catalytic mechanism for NHases involves the binding of the nitrogen atom of the nitrile substrate to the active site metal center.[19, 79] A nitrile-bound intermediate and an additional intermediate of unknown structure was recently detected using single-turnover stopped-flow spectroscopy (Chapter 2), providing the first spectroscopic evidence for nitrile binding to the low-spin Fe(III) active site in the nitrile hydratase from *Rhodococcus equi*-TG328-2 (*Re*NHase-TG328-2).[80] More recently, X-ray crystal structures of a Co-type NHase from *Pseudonocardia thermophila* JCM-3095 (*Pt*NHase) with boronic acid inhibitors bound to the active site Co(III) ion, provided further support for direct substrate binding to the active metal center.[68] Additionally, the structure of butane boronic acid (BuBA) bound to *Pt*NHase reveals a covalent bond between the oxygen atom of the sulfenic acid ligand and the boron atom of the boronic acid. These data provide the first experimental evidence that the sulfenic acid can function as a nucleophile, which was supported by DFT calculations.[68] Taken together, these data indicate the direct coordination of the nitrile substrate to the active site metal ion followed by nucleophilic attack by the sulfenic acid ligand oxygen atom.

Even though the boronic acid structures provide evidence that the αCys-OH ligand can function as a nucleophile, a previously unknown role for this ligand, it remains unclear if a similar covalently bound intermediate-state exists for an actual nitrile substrate and if this structure represents the transition-state of the NHase catalytic reaction. Herein, we provide evidence for two nitrile bound transient intermediate species and a product complex for *Re*NHase-TG328-2 obtained using rapid-freeze quench (RFQ) techniques coupled with electron paramagnetic resonance (EPR).

Multiple EPR techniques were used to characterize *Re*NHase-TG328-2 samples generated by RFQ including CW-EPR, ENDOR, and ESEEM. The generation of catalytic intermediates by rapid reaction with substrate and characterization with advanced EPR techniques verifies the direct coordination of the nitrile nitrogen atom to the active site metal ion and is consistent with the sulfenic acid functioning as the nucleophile.

Results and Discussion

Single turnover stopped-flow experiments carried out on *Re*NHase-TG328-2 using methacrylonitrile (MeACN) as the substrate revealed the formation of a reaction intermediate within 10 msec of the reaction timeframe.[80] Therefore, a detailed RFQ-EPR study of the reaction of MeACN with *Re*NHase-TG328-2 at high substrate concentration (5 mM) was undertaken (Figure 25). EPR spectra of a 1 mM sample of *Re*NHase-TG328-2 in 50 mM HEPES buffer, pH 7.0 reacted at 2˚C and quenched by freezing after 10 ms, 26 ms, 75 ms, and 1 minute were recorded at 30K. The as-prepared sample of *Re*NHase TG328-2 contained a mixture of species defined as N*a*, N*b* and N*c* in roughly equimolar proportions.

After reaction of *Re*NHase-TG328-2 with 5 mM MeACN for 10 ms, well within the expected turnover time of 5 s^{-1}, N*c* was undetectable and the spin density of both N*a* and N*b* decreased by >40 % and continued to decrease with an approximate apparent time constants $\tau_{app.} \approx 5.5$ ms. Although disappearance of N*a* and N*b* are not fast and residual N*a* and N*b* persisted long beyond the exhaustion of substrate, they both disappear in a catalytically competent manner. Since pH studies discussed in the previous chapter indicate that N*c* is converted to N*b* as the pH is increased from 6.5 to

8.0, the loss of N*c* upon reaction of MeACN is consistent with it being catalytically competent.

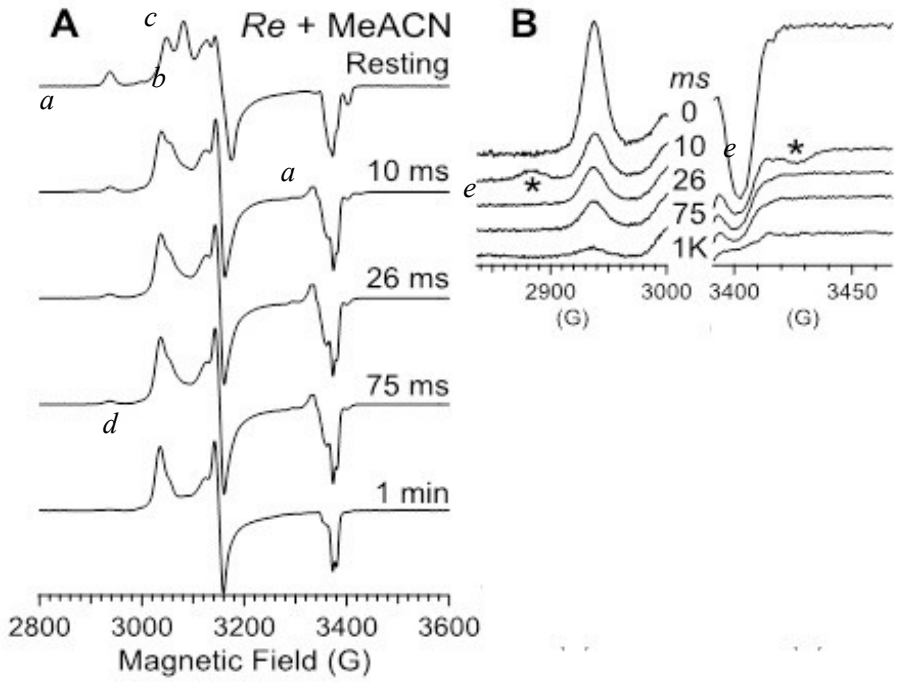

Figure 25. **(**A) RFQ-EPR time course of *Re*NHase-TG328-2 with 5 mM MeACN at 2 °C. (B) Identification of a highly anisotropic transient intermediate (*) in the reaction.

Careful examination of the EPR spectra in Figure 25A reveal a completely new species (N*e*) that appears within 10 ms and is extinguished by 26 ms (Figure 25B). The g_2 feature of this signal could not be deconvoluted, but the outer resonances were well separated from the other spectral features, with $g_1 = 2.366$ (at 2884 G) and $g_3 = 1.958$ (at 3427 G). This species, with $g_1 - g_3 = 0.408$, is > 30 % more anisotropic than any of the other reported signals from any Fe-type NHase and indicates a distortion in the electronic structure of the active site Fe(III) ion. The species at g_3 also reduces in magnitude over the time course, with the doublet collapsing into a single peak. Because the new species appears and disappears faster than enzyme turnover it is clearly part of the catalytic

process and is likely due to an ES-like complex. However, this intermediate is observed with only very low intensity, which severely complicates its study.

Stopped-flow kinetic data obtained for *Re*NHase-TG328-2 suggested a minimal three-step kinetic model that allows for the reversible binding of substrate, the presence of an intermediate, and the formation of product.[80] Moreover, the product-release step was shown to be the rate-limiting step and is on the order of 12 s^{-1}, at 25 ^{o}C. Based on these microscopic rate constants, a build-up of ES is predicted at low [S] whereas an accumulation of EP is expected at high [S].

Reaction of *Re*NHase-TG328-2 with high MeACN concentrations (5 mM) for 10 ms at 2 ^{o}C also revealed another new signal (N*d*) with a g_1 resonant field intermediate between N*a* and N*b* [$g_{(1,2,3)}$-values 2.231, 2.148 and 1.986 (g_1 - g_3 = 0.245; R_B = 0.68)]. This signal develops with catalytic competence (Figure 25A) and is clearly the major species at 26 ms. N*d* continued to increase in intensity over the course of the reaction timeframe with the concomitant loss of N*a* and N*b*. These data suggest that N*d* is due to the formation of an EP bound form.

In order to further examine the origins of the observed EP complex EPR signal, the competitive inhibitors butane boronic acid (BuBA) and phenyl boronic acid (PBA) were examined.[68] Boronic acids act as transition-state analogs, as boron contains an empty p-orbital making it is a good Lewis acid and susceptible to nucleophilic attack. X-ray crystal structures of the *Pt*NHase-BuBA complex formed by either co-crystallization or soaking, have been reported at 1.5 and 1.6 Å resolution, respectively. The *Pt*NHase-PBA structure was also reported at1.3 Å resolution where the complex was obtained *via* co-crystallization.

For the BuBA complex, electron density corresponding to the boronic acid inhibitor was present at the active site replacing the axial water molecule (Figure 26). Interestingly, the oxygen atom of the sulfenic acid ligand (αCys^{113}-OH) is covalently bound to the boron atom of BuBA with a bond distance of 1.6 Å. This covalent bond, which has not been observed previously, is the result of nucleophilic attack of the sulfenic acid oxygen atom on the empty p_z orbital of the boron atom and the subsequent loss of a boronic acid oxygen atom.

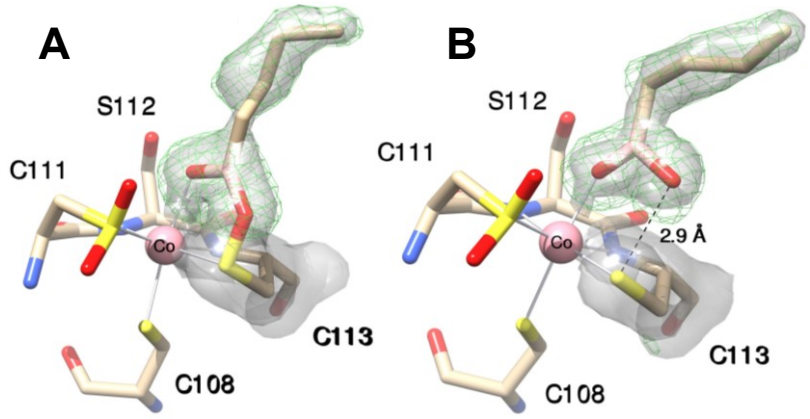

Figure 26. X-ray crystal structure of *Pt*NHase-3095 bound by BuBA after (A) soaking a crystal of WT *Pt*NHase-3095 in cryo-protectant containing 10 mM BuBA for 20 s followed by flash freezing in liquid nitrogen and (B) co-crystallization of WT *Pt*NHase-3095 and 10 mM BuBA.

On the other hand, the *Pt*NHase-BuBA structure obtained *via* co-crystallization of WT *Pt*NHase and 10 mM BuBA, reveals that the S-O boronic acid oxygen interaction (2.9 Å) is significantly diminished (Figure 26B). While this distance is still within the van der Waals radii of sulfur and oxygen, which is ~3.3 Å, it is clear that the αCys^{113}-OH interaction is considerably weakened compared to that observed in the *Pt*NHase-BuBA structure obtained *via* soaking. This weak S-O interaction is likely due to the initial dissociation of boronic acid from the active site and not the initial binding step, which

would require that the αCys^{113} residue is in its fully reduced form. Since αCys^{113} is clearly oxidized to its sulfenic acid form in the WT *Pt*NHase structure, the observed S-O elongation is assigned to boronic acid dissociation.

Since these two structures represent a "snapshot" of two potential intermediate- or product-bound states in nitrile hydration by depicting nucleophilic attack by the sulfenic acid ligand and the initial stage of the product-release step, UV-vis and EPR spectra were recorded for *Re*NHase-TG328-2 after the addition of three equivalents of BuBA and PBA. The addition of BuBA or PBA to *Re*NHase-TG328-2 resulted in an immediate change in color from the characteristic green to blue. UV-vis spectra indicate a blue shift in the characteristic Fe(III)←S ligand-to-metal charge transfer (LMCT) band from 700 to 650 nm (Figure 27).

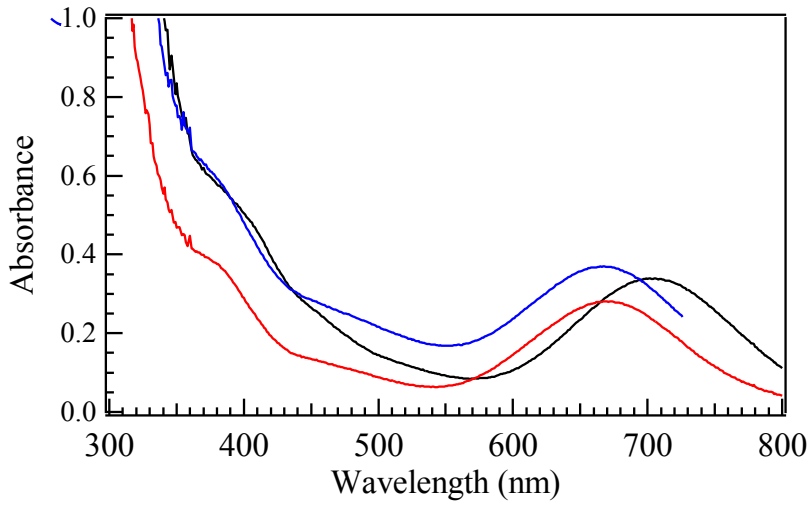

Figure 27. UV-visible spectra of free *Re*NHase-TG328 (Black), BuBA-bound (Red), and PBA-bound (Blue).

The observed UV-Vis absorption bands for the Fe(III)-boronic acid complexes are similar to Fe(III)-nitrile intermediate species observed in stopped-flow studies with MeACN as well as those obtained for NO or N_3^- binding.[29, 53, 80-81] These data provide

spectroscopic evidence for the direct coordination of boronic acids to the NHase active site low-spin Fe(III) center consistent with the X-ray crystal structures of the Co-type *Pt*NHase bound by BuBA and PBA.

Interestingly, EPR spectra obtained on the *Re*NHase-TG328-2 BuBA and PBA complexes are dominated by signals identical to the new EPR signal, N*d*, a species suggested to be a substrate or product-inhibited complex (Figure 28, Table 5). Both EPR spectra contained significant amounts of N*b* (15 - 30 %), and the BuBA complex also contained about 20 % of an N*c*-like component.

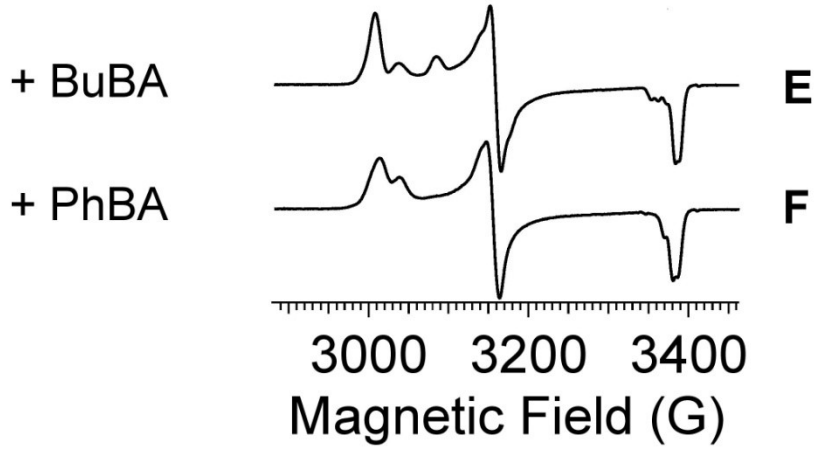

Figure 28. EPR spectra of *Re*NHase-TG328 complexed with boronic acid inhibitors.

Combination of these data with the X-ray structures of the *Pt*NHase-BuBA and PBA complexes, indicate that N*d*, which is observed when *Re*NHase-TG328-2 is reacted with MeACN, is likely the EP complex of the hydration reaction. The 1:2:1 triplet observed for the g_3 feature in the MeACN product complex spectrum suggests two equivalent protons, consistent with a nitrogen-coordinated amide that was not replicated in the boronic acid complexes.

Table 5. *g*-values for *Re*NHase-TG328-2.

Sample	g_1	g_2	g_3
Resting *Re*NHase	2.28	2.15	1.97
pH 6.0	2.28	2.15	1.97
pH 7.0	2.28	2.15	1.97
RFQ with MeACN	2.20	2.14	1.98
BuBA	2.17	2.13	1.98
PBA	2.21	2.13	1.98
Native R312[31]	2.28	2.14	1.97
R312 with proprionitrile[31]	2.23	2.16	1.98
B23 with proprionitrile[31]	2.22	2.16	1.98

Further confirmation of the electronic and structural aspects of the N*e* species, was gleaned from Electron Spin Echo Envelope Modulation (ESEEM) experiments. ESEEM was used to investigate the interactions between the Fe(III) unpaired electron and nuclei from groups ligated to the low-spin Fe(III) ion. The RFQ-EPR sample of WT *Re*NHase-TG328-2 and *Re*NHase-TG328-2 reacted with 5 mM MeACN that was frozen at 10 ms was analyzed using ESEEM obtained for g_2 and g_3 orientations (Figure 29).

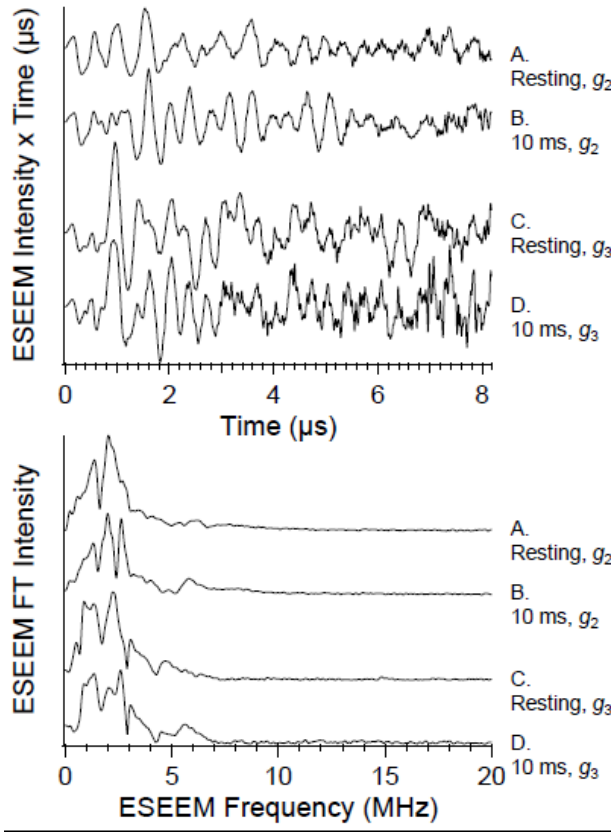

Figure 29. ESEEM data with a weakly coupled nitrogen at around 5.5 MHz.

Fourier transform of the raw data obtained for both WT *Re*NHase-TG328-2 and *Re*NHase-TG328-2 reacted with MeACN reveal new double quantum peaks at around 3 MHz, which are likely due to additional protons in the N*d* species that couple to the Fe(III) center, and another at 5.5 MHz. It has been observed that equatorial heme nitrogens and axial imidazole nitrogens have almost isotropic couplings of about 5 MHz when bound to low spin Fe(III) centers.[82] Therefore, the peak observed at 5.5 MHz is likely due to a higher population of weakly coupled nitrogen's in the RFQ sample than in the resting sample suggesting a new nitrogen signal due to a metal-bound nitrogen. Quantitation of the observed ESEEM signals at 5.5 MHz is difficult due to multiple overlapping EPR-active species; nevertheless, the simplest explanation for the clear

increase in the resonance at 5.5 MHz in the RFQ sample is the addition of a substrate derived nitrile nitrogen that binds directly to the low-spin Fe(III) active site. These data are consistent with single-turnover stopped-flow, kinetics, X-ray, and EPR data obtained for boronic acid inhibitors, which take together establishes that the nitrile nitrogen displaces the axial water ligand and binds directly to the active site metal ion.

Conclusion

The RFQ-EPR and ESEEM data presented herein revealed two new species, N*d* and N*e*, where N*d* is very likely an EP complex while N*e*, which is a transient species is likely the Michaelis complex. Combination of these data along with the UV-vis and EPR data for boronic acid binding to *Re*NHase-TG328-2 along with kinetic stopped-flow, X-ray crystallographic, and biomimetic model complex data,[21, 24-25, 80] allow a novel catalytic mechanism to be proposed for NHase enzymes. All of the current spectroscopic and crystallographic data clearly indicate the direct ligation of the nitrile substrate nitrogen atom to the active site low-spin Fe(III) ion as the first step in the catalytic mechanism of NHase enzymes (Figure 30). Displacement of the metal-bound water molecule by the nitrile substrate activates the CN bond towards nucleophilic attack by the αCys-OH sulfenic acid ligand.[69] Once nucleophilic attack of the nitrile carbon occurs, two protons are transferred in the rate-limiting step.[25, 55] One proton transfer is proposed to occur between the αCys-OH ligand and the nitrile N-atom, while the second transfer occurs between a water molecule that reforms the αCys-OH and the N-atom of the newly forming imidate, consistent with the observed normal isotope effect.[25, 55]

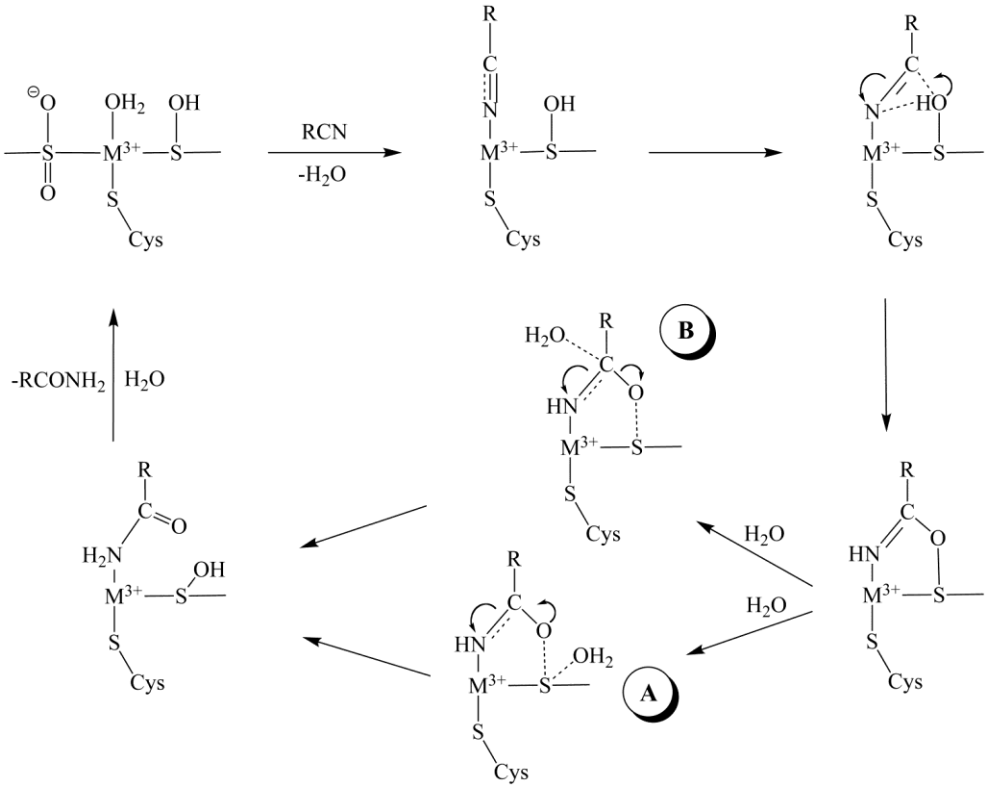

Figure 30. Proposed catalytic mechanism of nitrile hydratase.

That the αCys-OH ligand is protonated, was suggested by sulfur K-edge XAS and DFT data.[57] Once proton transfer occurs, the resulting covalently bound imidate can tautomerize to form an amide upon nucleophilic attack by a water molecule on αCys (pathway **A**). Alternatively, nucleophilic attack by water molecule at the C-atom of the imidate intermediate could occur (pathway **B**), such that the oxygen atom of the amide product would be derived from H_2O, not the sulfenic group. In this alternative, the active site metal ion and the sulfenic acid group work together to form and stabilize the imidate intermediate, which can then be hydrated with sulfenic acid functioning as the leaving group. Finally, the amide product complex, which was verified by ESEEM data, can be displaced by a water molecule and thus provide the regenerated catalyst.

Materials and Methods

All reagents were purchased commercially and were the highest purity available.

Protein Expression

The *Re*NHase-TG328-2 plasmid was provided by Professor Uwe Bornscheuer [74]. The subunit and activator genes were sub-cloned into pET-21a(+) and pET-28a(+), respectively. *Re*NHase-TG328-2 was transformed into NEB Turbo cells (New England Biolabs) for subcloning and BL21(DE3) cells (Stratagene) for protein expression. Cells were grown at 37°C in LB media supplemented with kanamycin (50 μg/mL) and ampicillin (100 μg/mL). Upon reaching an optical density (OD) of 0.8, the cultures were cooled to the induction temperature of 18°C. Cultures were induced with 0.1 mM isopropyl-β-D-1-thiogalactopyranoside (IPTG) and 0.25 mM ferrous sulfate and shaken for 16 additional hours at 18°C.

Purification of ReNHase TG328-2

Cells were pelleted by centrifugation at 5000 rpm for 5 min. Cells containing *Re*NHase-TG328-2 were resuspended in 50 mM sodium phosphate buffer at pH 7.5 containing 300 mM NaCl, 40 mM butyric acid, and 10 mM imidazole at a ratio of 3 mL/g of cells and lysed by ultrasonic probe (Misonix Sonicator 3000) in 30 s increments for 4 min. at 21W. The cell lysate was separated from cell debris by centrifugation for 40 min. at 12,500 rpm and purified using immobilized metal affinity chromatography (IMAC) on an AKTA FPLC Chromatographic System (GE) at 4°C. *Re*NHase-TG328-2 was eluted with a linear gradient (0-100% imidazole buffer; 50 mM NaH_2PO_4 pH 7.5, 300 mM NaCl, 40 mM butyric acid, 500 mM imidazole) at 1 mL/min. followed by buffer exchange to remove butyric acid and imidazole using an Amicon centrifugal filter unit

MWCO 30,000 (Millipore). Enzyme purity was assessed by sodium dodecyl sulfate-polyacrylamide gel electrophoresis (SDS-PAGE). A Bradford Assay was performed against bovine serum albumin (BSA) standards to determine protein concentration.

Steady State Kinetic Assay.

*Re*NHase-TG328-2 activity was examined using 100 mM methacrylonitrile as the substrate in 50 mM HEPES buffer, pH 7.0 and 25 ^{o}C at 242 nm (ε_{242} 3.2 $mM^{-1}cm^{-1}$) on a Shimadzu UV-2450 spectrometer. Initial reaction rates were monitored and fit to a modified Hill equation $y = V_{max}*(x/(k + x))$ using Origin Pro. One unit of NHase activity was defined as the formation of 1 μmol of amide product formed per minute. No attempt was made to limit exposure to light throughout purification and sample preparation, and neither extended (> 4 h) exposure to ambient light nor storage at 4 °C in the dark elicited any changes in the activities or observed EPR signals.

EPR spectroscopy

Samples for EPR spectroscopy were concentrated in 50 mM HEPES buffer to1 mM by ultracentrifugation. Where other buffer conditions (*e.g.* MES pH 6.0; glycerol; $^{2}H_2O$ substitution) are indicated, buffer exchange was affected by ultracentrifugation. Substrate was either added directly and rapidly mixed manually,[64] or else was added using a rapid-freeze-quench apparatus described elsewhere.[75] Samples were examined immediately and then stored in the dark at 77 K prior to any subsequent re-examination. No storage-dependent changes in signals were observed.

Continuous-wave (CW) X-band EPR spectra were recorded on either a Bruker EMXplus spectrometer (ER4116DM resonator, Oxford ESR900 helium flow cryostat & ITC503 temperature controller) or an EleXsys E600 spectrometer (ER4116DM & Super-

Hi-Q resonators, Oxford ESR900 helium flow cryostat & ITC503 temperature controller). Pulsed X-band EPR was recorded on a Bruker E580 spectrometer (EN4118X-MD-4W resonator, ER4118CF helium flow cryostat, Oxford ITC503 temperature controller, ASE 2 kW TWT microwave amplifier, DICE ENDOR unit, ENI A300 & 3100L RF amplifiers). For pulsed EPR, the same samples used for CW-EPR in 4 mm O.D. EPR tubes (Wilmad 706-SQ-250M) were loaded into the bottom of the pre-cooled resonator.

CHAPTER 5

THE IRON-TYPE NITRILE HYDRATASE ACTIVATOR IS A GTPASE

Summary

The iron-type nitrile hydratase activator from *Rhodococcus equi* TG328-2 (*Re*NHase-TG328-2) was successfully expressed and purified in a soluble form, allowing for in-depth biophysical characterization. Divalent metal ions were titrated into the activator to gain insight into the structural and electronic properties of a putative metal-activator complex and K_d values for Co(II) (26 ± 6 μM) and Ni(II) (75 ± 25 μM) were determined. Sequence analysis of the protein revealed that it shares sequence homology with the G3E family of P-loop GTPases called COG0523, suggesting it may exhibit GTPase activity. Kinetic analysis of the *Re*NHase-TG328-2 activator protein revealed that it is capable of hydrolyzing GTP to GDP with a k_{cat} value of 1.2 x 10^{-3} s^{-1} and a K_m value of 40 μM in the presence of 5 mM $MgCl_2$ at pH 8.0. The *Re*NHase-TG328-2 activator protein is also capable of hydrolyzing both ATP and UTP but at slower rates. Circular dichroism spectra indicate that GTP binding to the *Re*NHase-TG328-2 activator protein significantly impacts the secondary structure, suggesting that the GTP and GDP bound forms of the activator protein exist in two different conformations. Finally, a three-dimensional homology structure of the *Re*NHase-TG328-2 activator protein was generated using the X-ray crystal structure of the proposed GTPase, Yjia (PDB : 1NIJ) as the template. This homology structure provides insight into to the divalent metal and GTP binding sites.

Introduction

Nitrile hydratases (NHase) are metalloenzymes that contain either a low-spin Fe(III) (Fe-type) or Co(III) (Co-type) ion in their active site.[19] Though the active site ligands are practically identical for both Fe- and Co-type NHases, they are very specific for their respective metal ion. It is hypothesized that the specificity of NHase for either Co(III) or Fe(III) is due to an accessory protein termed an "activator", which is present in almost all NHase gene clusters sequenced to date.[38] The activator gene is typically found downstream from the α- and β- subunit genes (Figure 31) and is required for full catalytic activity.

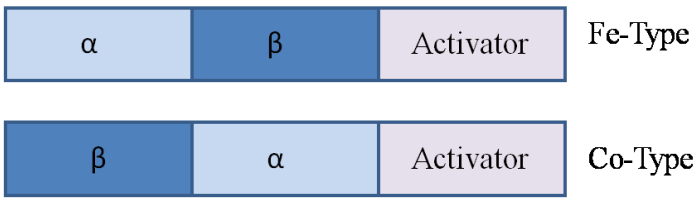

Figure 31. Arrangement of NHase genes with respect to metal type.

The activator protein has also been suggested to function as a metallochaperone and also play a role in cysteine ligand oxidation to a sulfinic (Cys-SO_2H) and sulfenic (Cys-SOH) acids, which are required for catalytic activity; however, no definitive evidence has been reported to verify this hypothesis.[39] To date, no X-ray crystal structure data for any NHase activator protein has been reported.

Interestingly the activator protein sequences for Fe-type and Co-type NHases are not homologous, which suggests the metallocenters are assembled by different mechanisms.[41] Co-type activators are smaller and have sequence homology with the Co-NHase β subunit.[42] On the other hand, alignment of Fe-type NHase activator protein sequences reveals that they contain a highly conserved cysteine-rich motif (Table 6).[38]

This motif is a known metal binding site in other metallochaperones, such as the COX17 (copper) and Hyp proteins (nickel).[38,40]

Table 6. Conserved binding motif sequences of Fe-type activator homologues.[38]

Database Name	**Species**	**Binding Motif**
NHase Activator	*Rhodococcus sp*. N-771	66VEMTNGCICCTLR-DLLSEISALAR90
P44K protein	*Rhodococcus sp.* AJ270	65LVEMTNGCICCTLR-DLLSEISALAR89
P47K	*Pseudomonas chloraphis* B23	69LIEMSNGCICCTLRADLLEQISDLAR94
KB15K	*Rhodococcus equi* TG328-2	65LVEMTNGCICCTLREDLLAEIGRLA89

Fe-type activators also share sequence homology with the G3E family of P-loop GTPases called COG0523.[41] GTPases bind and hydrolyze the γ-phosphate of guanosine triphosphate (GTP) to form guanosine diphosphate (GDP) and inorganic phosphate. They are involved in signaling, protein biosynthesis, translocation, and regulation of cellular activities.[43] GTP hydrolysis is also required in the assembly of some metalloproteins, including the nickel enzyme urease.[45] Recently, the X-ray crystal structures of proposed GTPases in the COG0523 family, Yjia and YeiR, were solved.[46b,46a,83] These data suggested that GTPase activity is regulated by divalent metal ion binding, providing insight into the function of the COG0523 proteins.

In an effort to clearly define the biochemical properties of the Fe-type nitrile hydratase activator protein from *Rhodococcus equi* TG328-2 (*Re*NHase-TG328-2), which

is required for expression of the fully metallated and active form of *Re*NHase-TG328-2,[15] the gene encoding for this protein was expressed in *E. coli* with an N-terminal TEV-MBP-His_6 tag. The functional expression of the *Re*NHase-TG328-2 activator protein has, for the first time, allowed the metal and GTP binding properties to be investigated *via* kinetic, electronic absorption, and circular dichroism (CD) spectroscopy. These data verify that the Fe-type activator protein from *Re*NHase-TG328-2 binds divalent metal ions utilizing at least one cysteine residue and can function as a GTPase, a previously unknown role for Fe-type NHase activator proteins.

Results and Discussion

Cloning and Purification of Activator Protein

A major limitation in examining the proposed metallochaperone properties of an Fe-type NHase activator protein is the lack of an expression system that provides ample amounts of a soluble form of the protein. We have overcome these issues by sub-cloning the *Re*NHase-TG328-2 activator gene into the pMCSG9 plasmid, which contains an N-terminal tobacco etch virus (TEV) protease cleavage site followed by maltose-binding protein (MBP) and a His_6 tag. The MBP was incorporated to aid protein folding and solubility during expression while the His_6 tag allows rapid purification *via* immobilized metal ion affinity chromatography (IMAC). This plasmid was then transformed into BL21(DE3) (Stratagene) cells for protein expression.

The activator protein was initially expressed then purified *via* IMAC in standard buffer conditions of 50 mm sodium phosphate buffer pH 7.5 containing 300 mM NaCl, and 10 mM imidazole using a 10-100 mM imidazole linear gradient (Figure 32). The

MBP-His_6 tag was cleaved from the activator using TEV protease, which resulted in the precipitation of the *Re*NHase TG328-2 activator protein.

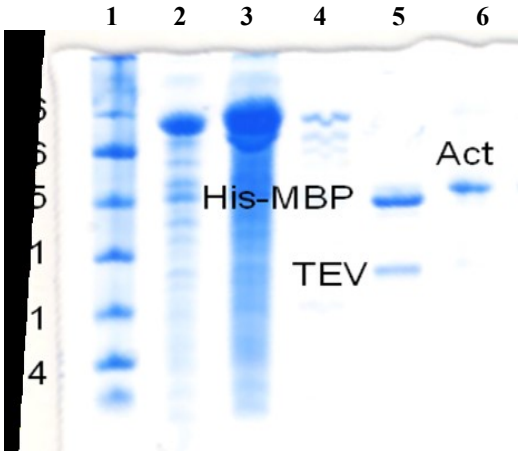

Figure 32. SDS-PAGE of the Fe-type *Re*NHase-TG328-2 activator protein. Lane 1. Protein Marker; Lane 2. Crude; Lane 5. Cleaved Tag; Lane 6. Cleaved activator.

Optimal conditions for solubilizing the activator protein were found by employing a solubility screen, which provided the following conditions: 50 mM HEPES, pH 8.0, 300 mM NaCl, and 10% glycerol to maintain solubility of the *Re*NHase TG328-2 activator protein upon TEV cleavage. Under these conditions, ~5 mg of *Re*NHase TG328-2 activator protein/L cell culture was obtained after purification and the protein remained soluble at 4˚C for >3 days.

Divalent Metal Binding to the ReNHase-TG328-2 Activator Protein

Interestingly, the as purified activator did not contain any bound metal ions even though it contains a cysteine-rich motif, which was proposed to be the metal binding site (Table 1). The lack of a bound metal ion in the as-purified *Re*NHase-TG328-2 activator protein was hypothesized to be the result of IMAC purification given the >50 mM imidazole was used in the purification process or disulfide formation. In order to examine the metal binding properties of the *Re*NHase-TG328-2 activator protein, a free

thiol assay was performed to identify any potential disulfide bonds in the protein that would prevent metal binding and perhaps, provide evidence for which cysteine residues are capable of functioning as metal ligands. A total of 5.5 ± 0.5 free thiols were identified, which is consistent with five cysteines being present in the protein sequence. The free thiol assay indicated that no disulfide bonds are present in the apo-activator protein and that all of the cysteines present could potentially bind divalent metal ions.

UV-vis spectroscopy was utilized with Co(II) as the spectroscopic probe as the position and molar absorptivities of Co(II) d-d bands reflect the coordination number and geometry of the metal ion.[84,85] Optical absorption spectra were recorded at 25 ^{o}C on a 100 μM sample of the *Re*NHase-TG328-2 activator protein in a buffered solution prepared with metal-free water (50 mM HEPES, 300 mM NaCl, and 10% glycerol) at pH 8.0 (Figure 33).

The addition of one equivalent of Co(II) to the *Re*NHase-TG328-2 activator protein resulted in absorption bands at 312 nm (ε_{312} =3,188 $M^{-1}cm^{-1}$) and 530 nm (ε_{530} = 396 $M^{-1}cm^{-1}$). The absorption band at 312 nm is very characteristic of a S → Co(II) ligand-to-metal charge-transfer (LMCT) band and the molar absorptivity is consistent with two Co(II)-S-thiolate interactions.[84,85] These data suggest that two cysteine thiols are bound to a single Co(II) ion.

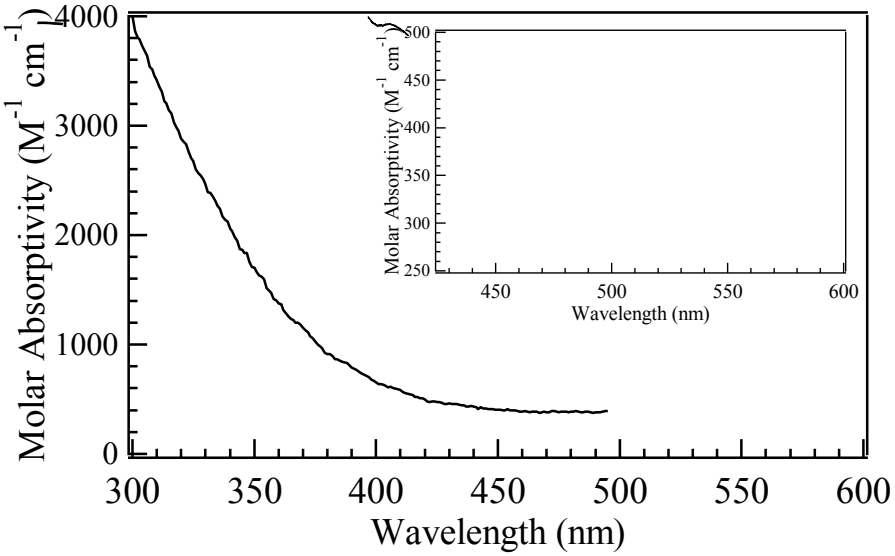

Figure 33. UV-vis spectrum of one molar equivalent of Co(II) bound to the *Re*NHase-TG328-2 activator protein.

Ligand-field theory predicts that optical transitions of four-coordinate Co(II) complexes give rise to intense absorptions ($\varepsilon > 300\ M^{-1}cm^{-1}$) in the 625 ± 50 nm region due to a comparatively small ligand-field stabilization energy, while five-coordinate Co(II) shows features with moderate absorption intensities ($50 < \varepsilon < 250\ M^{-1}cm^{-1}$) with several maxima between 525 and 625 nm.[86] Based on the molar absorptivities and *d-d* absorption maxima of the Co(II)-form of the *Re*NHase-TG328-2 activator protein, the Co(II) ion likely binds in a distorted four coordinate geometry.

The Co(II)- and Ni(II)-binding properties of the *Re*NHase-TG328-2 activator protein were further investigated using electronic absorption spectroscopy by titrating both Co(II) and Ni(II) into apo-*Re*NHase-TG328-2 activator protein (1 mM) and monitoring the absorption at 312 nm for Co(II) and 310 nm for Ni(II) **(**Figure 34**).** The dissociation constant (K_d) for Co(II) and Ni(II) binding was obtained by fitting these titration data to equation 1:[87]

$$r = pC_S/(K_d + C_S) \quad (1)$$

where p is the number of sites for which interaction with Co(II) or Ni(II) is governed by the intrinsic dissociation constant, K_d and r is the binding function calculated by conversion of the fractional saturation (f_a) using equation 2.

$$r = f_a p \quad (2)$$

C_s, the free metal concentration, was calculated using equation 3

$$C_S = C_{TS} - rC_A \quad (3)$$

where C_{TS} and C_A are the total molar concentrations of metal and enzyme, respectively. Values for K_d were obtained by fitting these data *via* an iterative process that allowed both K_d and p to vary (Figure 5). The best fits obtained provided a p value of 1.2 ± 0.1and a K_d value of 26 ± 5 μM for Co(II)-binding and a p value of 1.3 ± 0.3 with a K_d value of 75 $\pm$ 25 μM for Ni(II)-binding.

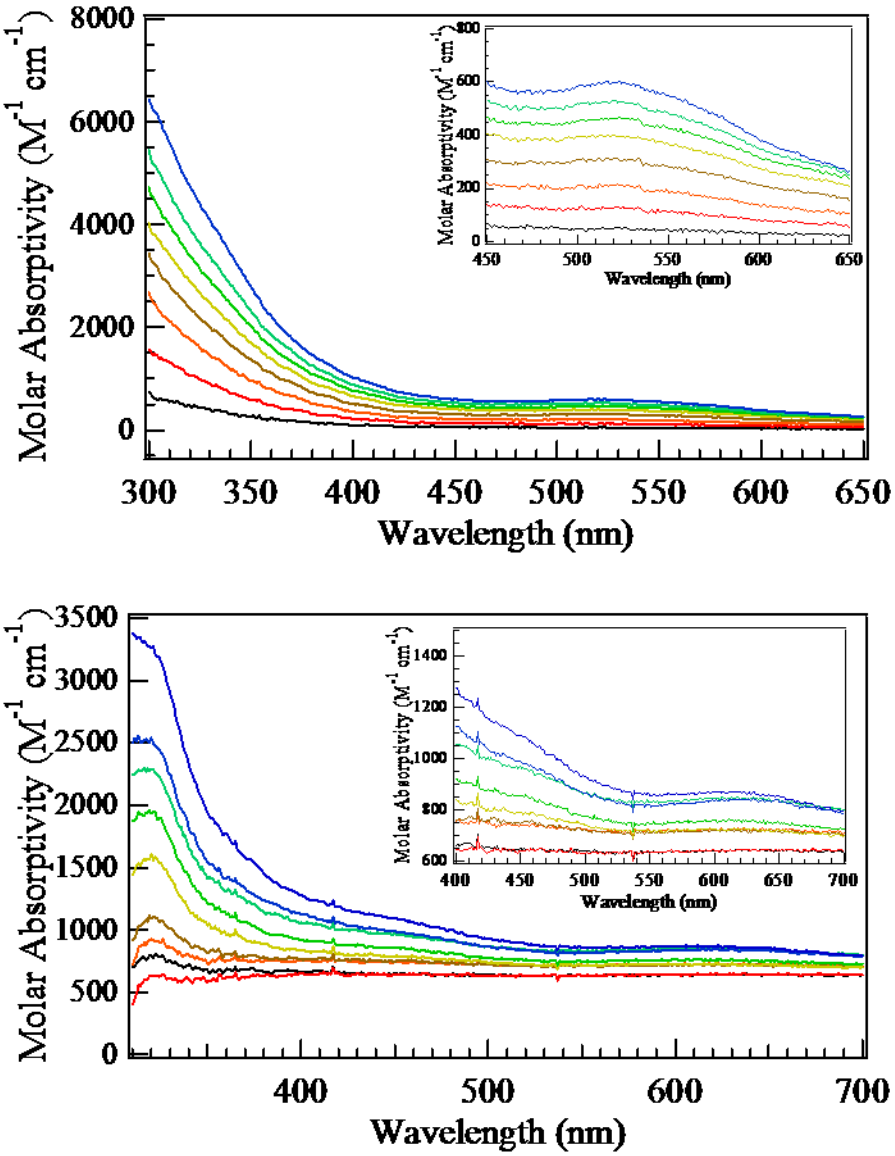

Figure 34. Top. Co(II) binding spectra with inset for enlarged view of broad peak at 525 nm. Bottom. Nickel binding spectra with inset for enlarged view for shoulder at 440 nm and peak at 640 nm.

These K_d values are comparable to K_d values obtained for other metallochaperones and are also similar to the related protein Yjia, which exhibits K_d values of 20 ± 10 μM and 3.7 ± 0.3 μM for Co(II) and Ni(II), respectively.[88,46b]

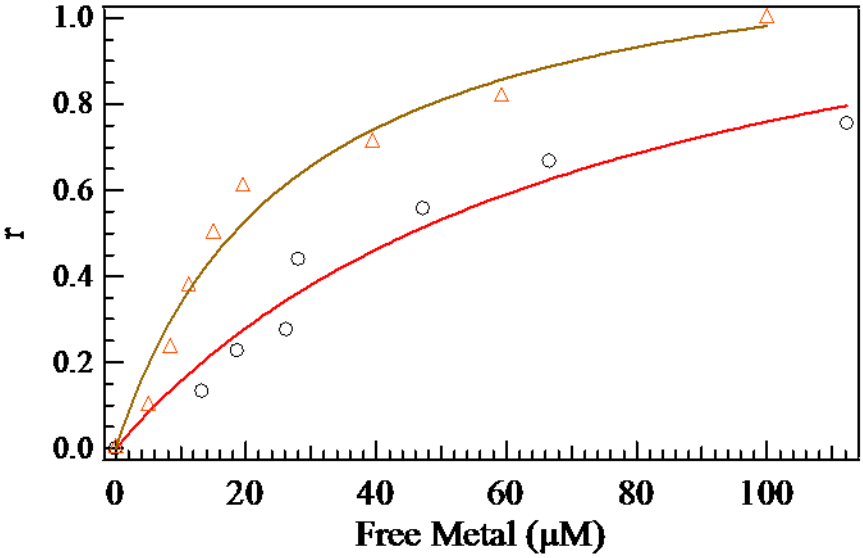

Figure 35. Plot of Binding function-r, *vs*. the Free Metal concentration in solution for Co(II) (triangles) and Ni(II) (circles) titration into the *Re*NHase-TG328-2 activator protein.

GTPase Activity

The COG0523 family of GTPases is a diverse set of proteins that appear to be involved in cellular metal transport processes.[43,41] GTPases are typically structured with a central β-sheet surrounded by α-helices. Within the protein sequence is a Walker A motif (or P-loop) that resides on a flexible loop between a β-strand and α-helix. The Walker A motif is responsible for binding and positioning the triphosphate group of GTP. Another prominent feature of GTPase sequences is a distal Walker B motif that is the site of magnesium binding, necessary for GTP hydrolysis.[43] In the COG0523 family of GTPases, the Walker motifs flank a CXCC metal binding motif. Additionally, the Walker B motif contains a glutamate instead of an aspartate and a distal motif consisting of an NKxD sequence.[41] GTPase functionality has not been proposed for Fe-type NHase activator proteins, but the presence of Walker A and B motifs in the *Re*NHase-TG328-2 activator protein suggests GTPase activity.

Therefore, the *Re*NHase-TG328-2 activator protein was examined for GTPase activity in 50 mM HEPES buffer at pH 8.0 in the presence of 1 mM GTP and 5 mM $MgCl_2$. Reaction times up to 4 hours were examined by quantifying the formation of free phosphate by complexation with malachite green-molybdate, which provides a strong absorption at 630 nm. Remarkably, the *Re*NHase-TG328-2 activator protein is capable of hydrolyzing GTP with a k_{cat} value of $(1.2 \pm 0.5) \times 10^{-3}$ s^{-1} and a K_m value of 40 ± 20 μM (Table 7).

Table 7. Kinetic data for the *Re*NHase-TG328-2 activator protein towards nucleotide triphosphates.

NTP	k_{cat} (s^{-1})	K_m (μM)	k_{cat}/K_m (s^{-1} M^{-1})
GTP	$(1.2 \pm 0.5) \times 10^{-3}$	40 ± 20	30 ± 20
GTP + Cobalt	$(3.1 \pm 1.3) \times 10^{-3}$	170 ± 80	20 ± 10
ATP	$(1.0 \pm 0.2) \times 10^{-3}$	70 ± 30	13 ± 9
UTP	$(3.2 \pm 0.5) \times 10^{-4}$	90 ± 20	4 ± 1

The *Re*NHase-TG328-2 activator protein was also capable of hydrolyzing adenosine triphosphate (ATP) and uridine triphosphate (UTP) with similar rates to GTP, but with weaker affinity resulting in poorer catalytic efficiencies. This promiscuity could be due to the guanine binding sequence of the activator having a serine instead of a glutamate in the sequence SKxD, reducing selectivity for GTP.

Comparison of the *Re*NHase-TG328-2 activator proteins ability to hydrolize GTP to other GTPases within the COG0523 family suggests that the *Re*NHase-TG328-2 activator protein exhibits comparable GTPase activity. For example, the sequence-related protein Yjia exhibits a k_{cat} value of 6×10^{-3} s^{-1}, while YeiR hydrolyzes GTP with a k_{cat} of 3×10^{-3} s^{-1}.[46b,83] Similarly, the small, monomeric Ras GTPase exhibits a k_{cat} value

of 3.4 x 10^{-4} s^{-1}.[89] Interestingly, the addition of a divalent metal ion to the reaction mixture of Yjia did not alter the observed k_{cat} value for GTP hydrolysis while both k_{cat} and K_m were enhanced with the addition of metal to YeiR.[83] Interestingly, the affinity of GTP for GTPases outside of the COG0523 family is typically in the picomolar to nanomolar range.[89] The *Re*NHase-TG328-2 activator protein's affinity towards GTP was found to be in the micromolar range similar to Yjia, suggesting that the observed GTPase activity for the *Re*NHase-TG328-2 activator protein is regulated differently than GTPases outside of the COG0523 family. These data also suggest that unlike typical GTPases, the *Re*NHase-TG328-2 activator protein does not require accessory proteins to release GTP.

The addition of Co(II) to the reaction mixture resulted in a k_{cat} value of (3.1 ± 1.3) x 10^{-3} s^{-1} and a K_m value of 170 ± 30 μM for GTP. The nearly three-fold increase in k_{cat} suggests that the GTPase activity exhibited by the *Re*NHase-TG328-2 activator protein is potentially related to the metal homeostasis process.[90] However, the four-fold decrease in the K_m value for GTP in the presence of Co(II) suggests that Co(II) may compete with Mg(II) for GTP binding. An alternative explanation might be that Co(II) binding induces a conformational change as observed for other GTPases.[91]

For Yjia, YeiR, and UreG, metal binding induced oligomerization but it was unclear if oligomerization is necessary for GTPase functionality.[46b,83,92] No metal induced oligomerization was not observed for the *Re*NHase-TG328-2 activator protein upon Co(II) or Ni(II) binding. However, Zn(II) binding induced dimerization for UreG but Ni(II) did not, suggesting metal ion specific oligomerization.[92] Clearly, metal binding affects GTPase activity for the *Re*NHase-TG328-2 activator protein and the observed GTPase activity may have a regulatory function in metal-protein interactions.

Circular Dichroism

In order to determine if Co(II) or GTP binding to the *Re*NHase-TG328-2 activator protein induces a conformational change, as observed for other GTPases, circular dichroism (CD) spectra were recorded at 25 ºC in 50 mM HEPES buffer at pH 8.0 (Figure 36). All CD data were quantified using the CDSSTR algorithm providing approximate percentages for the secondary structure (Table 8). For the as-purified *Re*NHase-TG328-2 activator protein, the most prominent feature occurs at 222 nm indicative of α-helical character (Figure 36A). However, this feature is shallower relative to the peak at 208 nm, indicating the presence of random coil and/or β-sheet structure. The addition of 1 mM GTP or GDP significantly altered the secondary structure, with a marked decrease in ordered α-helical character and an increase in protein disorder (Table 8). The CD spectra of the *Re*NHase-TG328-2 activator protein bound by GTP or GDP are similar but not identical, indicating structural differences exist between the GTP and GDP-bound forms.

The binding of ATP and UTP to *Re*NHase-TG328-2 activator protein was also investigated (Figure 36C). Interestingly, both ATP and UTP significantly affect the secondary structure of the activator protein and nearly double the amount of ordered α-helices (Table 8). The CD spectra of the ATP and UTP *Re*NHase-TG328-2 activator protein complexes do not resemble the GTP or GDP activator complex. The preference of GTP over ATP or UTP for the activator *Re*NHase-TG328-2 activator protein is perhaps explained by secondary structural changes exhibited.

CD spectra were also recorded for the *Re*NHase-TG328-2 activator protein in the presence of Mg(II) and GTP + Mg(II) (Figure 36B). Aside from a decrease in absorption

intensity, the addition of 5 mM Mg(II) to the activator is nearly identical to the as-purified activator.

Upon the addition of 1 mM GTP, the CD spectrum of the GTP + Mg(II) *Re*NHase-TG328-2 activator protein complex is nearly identical to the activator in the presence of only GTP. CD spectra were also recorded for the *Re*NHase-TG328-2 activator protein in the presence of 1 eq. of Co(II) (Figure 36B). Similar to Mg(II), the presence of Co(II) does not affect the secondary structure of the protein. Taken together, these data suggest that a conformational change occurs upon GTP binding, which is common for small GTPases,[43] but that Co(II) or Mg(II) binding does not affect the secondary structure of the activator protein.

Table 8. Calculated percentages of secondary structure derived from CD.

Sample	**Helix 1**	**Helix 2**	**Strand 1**	**Strand 2**	**Turns**	**Unordered**
Activator	23%	11%	19%	11%	17%	19%
GTP	6%	14%	16%	11%	27%	26%
GDP	4%	13%	18%	12%	26%	27%
Mg(II)	21%	10%	18%	11%	19%	20%
Mg(II) + GTP	6%	14%	20%	12%	25%	24%
Co(II)	21%	10%	19%	11%	17%	21%
ATP	37%	8%	15%	11%	10%	20%
UTP	40%	10%	19%	11%	17%	21%

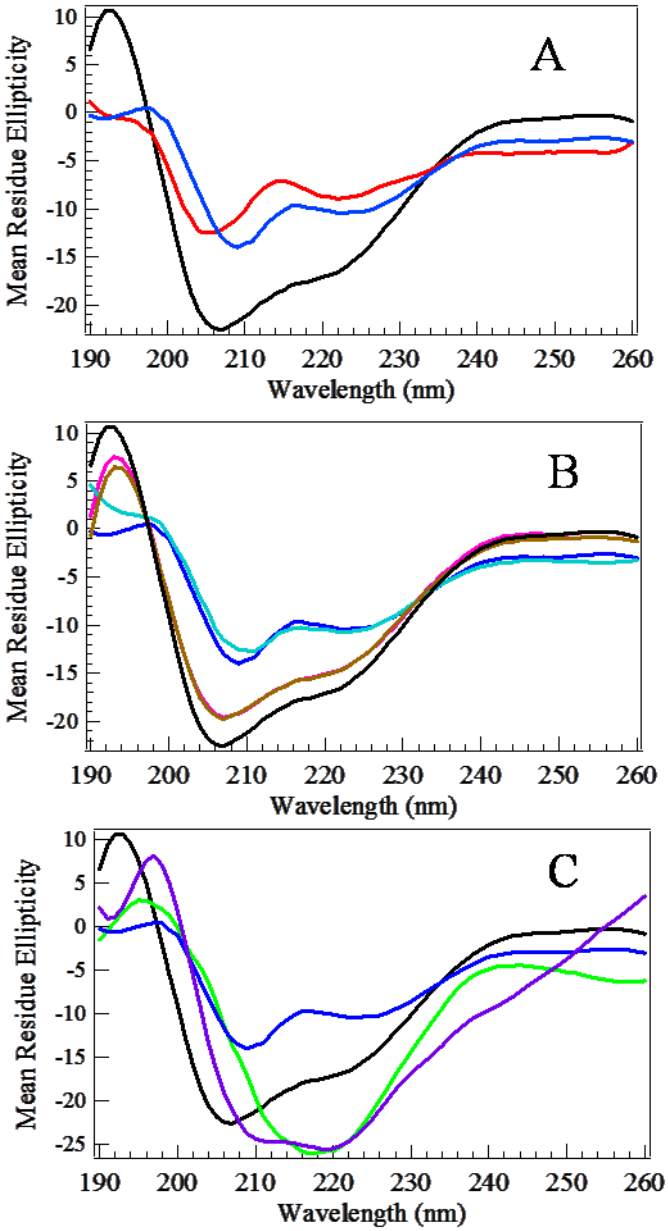

Figure 36. CD data of *Re*NHase TG328-2 activator protein (Black) bound to: (A) GTP (blue) and GDP (red), (B) Cobalt (pink), Mg^{2+} (brown), GTP and Mg^{2+} (light blue), (C) ATP (green), UTP (purple).

Homology Model

Currently, no structural data exists for any Fe-type NHase activator. While the current lack of structural data preclude definitive assignment of the active site residues involved in divalent metal or GTP binding, a three-dimensional homological structure of

the *Re*NHase-TG328-2 activator protein was generated using the X-ray crystal structure of the Yjia (PDB : 1NIJ) protein as a template. Sequence analysis of the target and template show that these two proteins share broad sequence similarity (31% sequence identity and 49 % similarity). The activator was also aligned with YeiR, however, only an identity of 16% and similarity of 27% exist and with the only similarities occurring in the GTPase motifs and the metal-binding region. The initial alignment of the *Re*NHase-TG328-2 activator protein and Yjia was performed in DeepView and refined manually (Figure 37).

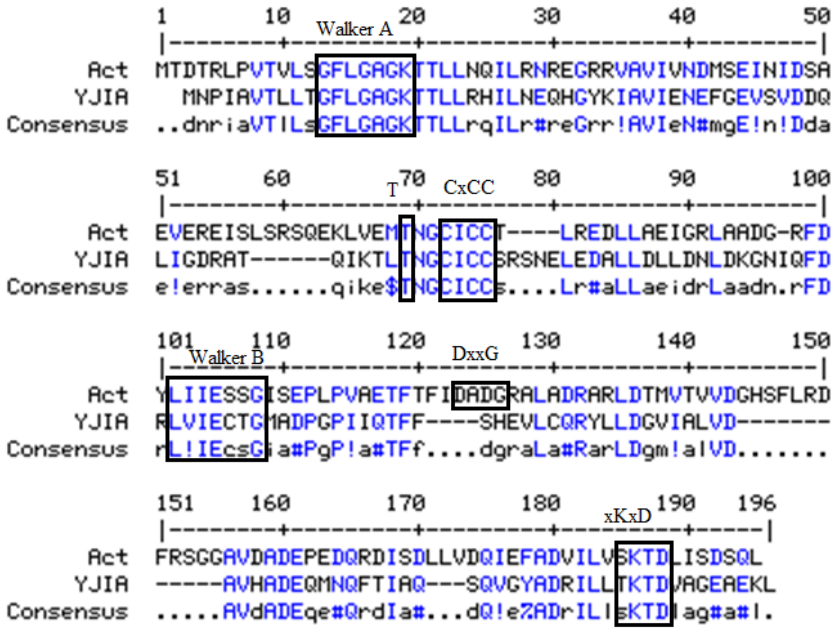

Figure 37. Sequence alignment of the ReNHase-TG328-2 activator protein with Yjia. Consensus GTPase sequences are annotated and boxed.

The SwissModel-based homology building server was used to construct a structural homology model of the *Re*NHase-TG328-2 activator protein. The model was validated by ProCheck and Verify 3D software, highlighting regions of model certainty. The regions of the homology model with the highest degree of sequence similarity and

least amount of modeling error are highlighted in blue in Figure 38, coinciding with the GTPase and metal binding motifs. Verify 3D was also run on the template Yjia structure to assess the quality of the template, showing that certain sequence regions in the structure were of low quality. Because of this, the quality of the homology model of the activator protein was impacted in those same regions.

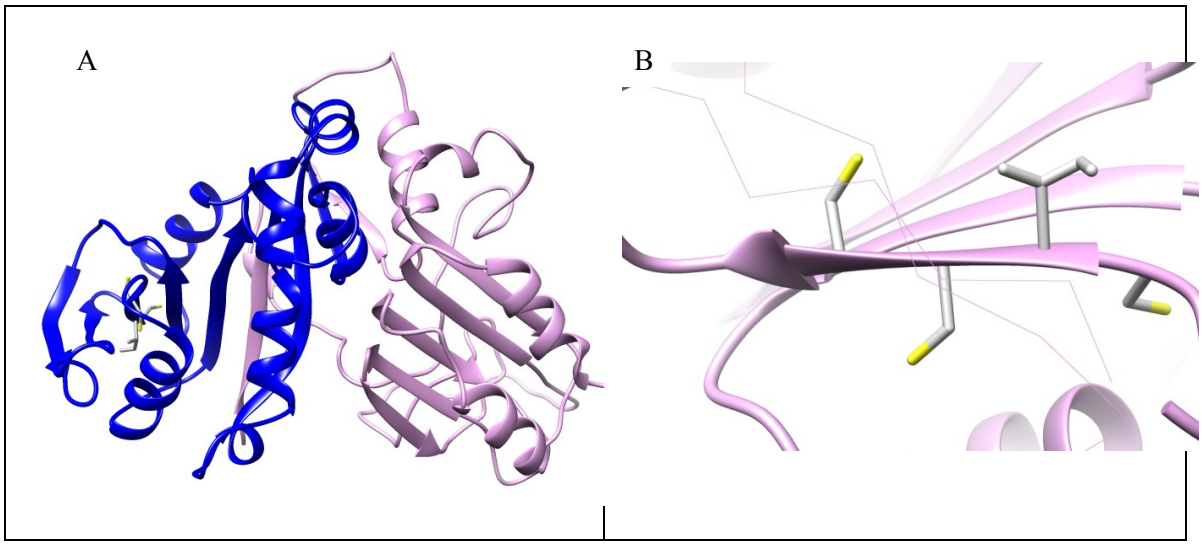

Figure 38. (A) Homology model of the *Re*NHase-TG328-2 activator protein, with blue highlighting the regions of high homology. (B) The metal binding motif showing the orientation of cysteine ligands.

Additionally, the N-terminus of the activator had no template to be modeled on, due to the Yjia protein being roughly 100 residues shorter than the activator. Despite that, the overall QMEAN score was 0.51 and the Verify 3D assessment showed that a majority of the protein was in the positive region, validating the model.[93,94]

The *Re*NHase-TG328-2 activator protein contains a Walker A motif between residues ^{13}GFLGAGK^{21}, a Walker B motif between ^{97}LIIESSG^{104}, and the previously described ^{72}CICC^{75} sequence, which was suggested to be the divalent metal binding site.[38] Interestingly, three of the four cysteine residues of the proposed metal binding loop (Figure 38B) are located on a β-sheet, with the fourth cysteine residue on a loop.

The orientation of these residues suggests that only one or possibly two can function as ligands for divalent metal binding, consistent with the UV-Vis data.

The homology modal indicates that the Walker A, or P-loop, and the Walker B motif are located on an α-helix, similar to other GTPase enzymes.[91] A conserved threonine at position 69 has been shown to be necessary for catalysis by coordinating to the phosphate of GTP.[43] A sequence corresponding to ^{115}DxxG^{118} is present and may function as the Mg(II) binding site along with the γ-phosphate of GTP. The sequence NKxD typically found in P-loop GTPases that is responsible for the specificity of guanine over other bases is also present. In the *Re*NHase-TG328-2 activator protein, this sequence is ^{177}SKxD^{180}, which may affect the GTP selectivity. The presence of these motifs is consistent with the observed GTPase activity for the *Re*NHase-TG328-2 activator protein.

Conclusion

The Fe-type *Re*NHase-TG328-2 activator protein has been expressed and purified in a soluble form for the first time. UV-Vis spectra of the Co(II)-bound form of the activator, indicates that Co(II) binds to two cysteine thiolates and resides in a distorted four-coordinate geometry. Titration of Co(II) and Ni(II) into the *Re*NHase-TG328-2 activator protein indicates the presence of only one divalent metal binding site, consistent with binding to the ^{72}CICC^{75} sequence. Surprisingly, the *Re*NHase-TG328-2 activator protein can catalyze the hydrolysis of GTP at a rate similar to other GTPases. The addition of Co(II) accelerated the hydrolysis of GTP by the activator protein, suggesting that GTP hydrolysis and the proposed metal chaperone function of the *Re*NHase-TG328-2 activator protein are interdependent. While Co(II) binding does not significantly alter

the secondary structure of the activator protein, GTP and GDP binding markedly increased the percentage of disordered helices. Therefore, the *Re*NHase-TG328-2 activator protein is a member of the COG0523 sub-family of G3E P-loop GTPases, which are known to play a role in metal homeostasis. Based on previous studies on the Yjia and YeiR proteins, it is clear that the iron-type activator is involved in NHase active site assembly and that this function is likely regulated by GTP hydrolysis.

Materials and Methods

All reagents were purchased commercially and of the highest purity required. Primers were synthesized by Integrated DNA Technologies Inc. (IDT). Genes were verified by sequencing performed at the University of Chicago, Cancer Research Center for DNA Sequencing Facility. The *Re*NHase-TG328-2 plasmid was obtained from Dr. Uwe Bornscheuer of the Department of Biotechnology & Enzyme Catalysis at Greifswald University.[56]

*Expression and Purification of the Re*NHase-*TG328-2 activator protein*

NHase is more active when the genes for the α- and β-subunits and the activator are co-expressed in different plasmids.[95] Since the *Re*NHase-TG328-2 plasmid had all three genes in tandem, the subunit and activator genes were isolated and then sub-cloned into pET-21a (+) and pET-28a (+), respectively. The activator was digested out of pET-28a (+) then ligated into pMCSG9. The plasmid containing activator was then transformed into BL21(DE3) (Stratagene) cells for protein expression. Cells were grown at 37°C in LB media supplemented with the kanamycin (50 μg/mL) and ampicillin (100 μg/mL). The cultures were cooled for one hour upon reaching 0.8 optical-density (OD). Cultures were induced with 0.1 mM Isopropyl-β-D-1- and thiogalactopyranoside (IPTG)

then shaken for 16 additional hours at 18°C for protein expression. Cells were pelleted by centrifugation at 5000 rpm for 5 minutes. Cells were resuspended in 50 mm sodium phosphate buffer pH 8.0 containing 300 mM NaCl, 10% glycerol, and 10 mM imidazole at a ratio of 3 mL/g of cells. Cells were lysed by ultrasonic probe (Misonix Sonicator 3000) in 30 second increments for 4 minutes at 21W. Cell lysate was separated from cell debris by centrifugation for 40 minutes total at 12,500 rpm. Cell lysate was purified using immobilized metal affinity chromatography (IMAC) on an AKTA FPLC Chromatographic System (GE) at 4°C.

The protein was eluted from a nickel nitrilotriacetic acid (Ni-NTA) column (100 mg protein/5mL column) with a linear gradient from 0-100% of a high imidazole content buffer (50 mM NaH_2PO_4 pH 8.0, 300 mM NaCl, 10% glycerol, 500 mM imidazole) at 1 mL/min. Fractions containing activator were treated with TEV protease (5% w/w) and 2mM dithiothreitol (DTT) and stirred gently overnight at 4°C. Cleaved protein was purified with IMAC by eluting unbound protein with 100% 10 mM imidazole buffer. The protein was then concentrated to 2 mL and loaded onto a 25 mL DEAE-Sepharose (diaminoethyl) column equilibrated with anion exchange buffer A (10 mM Tris, pH 8.0, 10 mM NaCl). The protein was eluted in a stepwise gradient at 50% of buffer B (10 mM Tris, pH 8.0, 500 mM NaCl). The purified protein was then buffer exchanged using an Amicon centrifugal concentrator (Millipore) into 50 mM HEPES pH 8.0, 300 mM NaCl). Purification of the activator was confirmed by sodium dodecyl sulfate-polyacrylamide gel electrophoresis (SDS-PAGE). A Bradford Assay was performed at 595 nm against bovine serum albumin (BSA) standards to determine protein concentration.

Solubility Screen

Solubility screening of activator was performed according to Jancarik's procedure.[96] 100 mM buffers prepared were sodium acetate pH 4.5, sodium citrate pH 5.5, MES pH 6.5, HEPES pH 7, HEPES pH 7.5, HEPES or Tris pH 8.0, and CHES pH 9.5. Briefly, buffer solutions were prepared at a range of pH's (4.5-9.5), salt concentrations (0-1.0 M), and glycerol concentrations (0-20%). 200 µL of each solution was transferred into a 48-well crystallization plate. The protein was mixed in a 1:1 ratio with the buffer solution on a glass slide and left at ambient temperature. Conditions were eliminated upon formation of protein precipitate. The condition with the no precipitation after 3 days at room temperature and minimal additives was selected as the optimal buffer solution for solubility.

Homology Modeling

The sequence of the *Re*NHase TG328-2 activator was aligned and fit against the template protein Yjia (PDB: 1NIJ) using DeepView Swiss PDB Viewer. The model was submitted the SwissModel server for modeling and model quality assessment. The structure was exported to Deepview Swiss PDB Viewer for further refinement and model validation. ProCheck and Verify 3D was run on the homology model to validate the model.

Free Thiol Assay

Stock solutions of A) 2 mM 5,5′-dithio-bis-(2-nitrobenzoic acid) (DTNB) in 50 mM sodium acetate and B) 1M Tris pH 8.0 were prepared. For exposed thiols, sample solutions consisting of 50 µL of A, 100 µL of B, 10 µL of sample, and 840 µL of water were prepared, mixed, and incubated at room temperature for 5 minutes. Samples were

also prepared with the addition of 8M urea to quantify the amount of buried thiols. Absorbance was measured at 412 nm. The concentration of 2-nitro-5-thiobenzoate (TNB) formed in the reaction was determined using the molar absorption coefficients $\varepsilon_{low\ salt}$ = 14,150 M^{-1} cm^{-1} and ε_{urea} = 14290 M^{-1} cm^{-1}. One mole of TNB formed was equivalent to one mole of free thiol in solution.

Circular Dichroism

A 3μM sample of purified activator was prepared in 10 mM sodium phosphate pH 7.5. Sample was analyzed in a 2000 μL cylindrical quartz cell with a 0.1 cm pathlength on an Olis DSM CD. Sample was scanned from 260 to 190 nm and spectra collected using Olis software. CD raw data was submitted to Birkbeck College University of Londen's online server DICHROWEB. The program CDSSTR (reference set 4) was used to analyze the secondary structure of the activator. Additional samples incubated with GTP, ATP, G1P, Mg^{2+}, and Co^{2+} were prepared at 0.1 mM, 0.5 mM, and 1.0 mM.

Metals Analysis

Purified activator protein was digested in a 5% nitric acid (HNO_3) solution for 15 minutes at 70°C. The digested protein was filtered through a 0.2 μm Supor membrane (Whatman). All glassware was washed with 1M HNO_3 prior to use. Filtered sample was then sent for inductively coupled plasma-atomic emission spectroscopy (ICP-AES) analysis at the Integrated Molecular Structure Education and Research Center (IMSERC) at Northwestern University. Metal ions detected were assayed against a standard consisting of iron (238.204 and 259.940 nm), nickel (230.299, 231.604 nm), and zinc (202.548, 213.857 nm)

Free Phosphate Determination

NTPase activity was assayed using a malachite green assay developed by Fusare et al.[97] The reaction consisted of 50 mM HEPES (pH 8.0), 1-3 μM activator, 5mM $MgCl_2$, and 0.05 to 1 mM GTP, ATP, G6P, and 1 mM Co(II) in a total volume of 50 μl. The mixture was incubated at 37˚C for 5 to 240 minutes, with aliquots taken at individual timepoints. The reaction was stopped with the addition of 375 μL of malachite green color reagent (2.6 mM Malachite Green, 1.5% ammonium molybdate, and 0.2% Tween 20). The solution was incubated at room temperature for 1 minute. Sodium citrate was added to the reaction medium to a final concentration of 3.5 mM. The absorbance was measured at 630 nm on a BioTek Synergy 2 Multi-mode microplate reader. One unit of enzymatic activity is defined as the amount of enzyme catalyzing the formation of 1 μmol PP_i/min under the above-specified conditions. A standard curve was constructed and linearity calculated to be in the range of 1 μM to 25 μM phosphate.

Spectrophotometric Determination of Metal Binding Constants

The activator protein was incubated with 10 mM EDTA and 20 mM TCEP at 4ºC under anaerobic conditions for 24 hours. The EDTA and TCEP was removed by dialysis into metal-free 50 mM HEPES pH 8.0. 50 μM of activator protein was titrated with $CoCl_2$ and $NiCl_2$ in from 10 μM to 150 μM, with initial increments of 10 μM with an increase to 25 μM then finally, 50 μM. UV-vis spectra were collected from 200 nm to 800 nm on a Shimadzu 2450 UV-vis spectrophotometer. An apo-activator spectrum was collected, then subtracted from titrations to obtain a difference spectrum.

CHAPTER 6

CONCLUSION

The application of nitrile hydratases as an industrial enzyme, has made great progress since its discovery in the late 1970s.[6] The full potential use of NHase, however, has been limited because of the absence of knowledge about fundamental aspects of the enzyme; that is its catalytic mechanism and active site biosynthesis. The research conducted and detailed within this dissertation has provided vital and novel information about both of these facets of NHase. First, *Re*NHase reaction intermediates were kinetically and spectroscopically characterized, giving key structural evidence of the orientation and mode of binding of nitrile substrates. Secondly, soluble expression and purification of the activator protein allowed for the first biophysical characterization of an Fe-type activator, which resulted in finding a previously unknown function that hints at a much more complex metallocenter assembly process than initially assumed.

At the start of the project, the most supported catalytic mechanism involved direct binding of the nitrile substrate to the metal center of the enzyme, however, no direct evidence existed.[19] We aimed to confirm this mechanism using a combination of pre-steady state kinetics and EPR spectroscopy. Unlike previous methods used to determine the catalytic mechanism, an Fe-type NHase enzyme and its preferred nitrile substrate were reacted and directly analyzed. This approach eliminated some inherent uncertainty due to biomimetic inorganic model complexes that do not hydrate nitriles under

physiological conditions, computational error, or inhibitors and substrate analogs not binding in identical ways.

Data from multiple turnover pre-steady state kinetics defined the minimal reaction model as a 3-step mechanism, the rate-limiting step as product release, and that substrate binding is reversible. Single turnover stopped-flow kinetics provided significant spectroscopic evidence for the direct coordination of the nitrile of methacrylonitrile to the Fe(III) center of *Re*NHase-TG328-2, due to shift in the signature LMCT band for $Fe^{3+} \leftarrow S^{2+}$ from 700 nm to 650 nm. It also provided a time scale (10 ms) in which reaction intermediates formed in high concentrations, which was useful for RFQ-EPR experiments.

The recent proposal by the Holz group that the active site Cys-sulfenic acid functions as the nucleophile during catalysis provides an interesting direction for future stopped-flow work. Mutation of the Cys-sulfenic acid to an alanine will certainly affect intermediate complex formation during catalysis. Single turnover stopped-flow can be used to examine this and add further insight into the role of the sulfenic acid and the individual catalytic steps that are affected by removing the proposed nucleophile. Additionally, questions still remain regarding the role of the axial thiolate ligand. It has been proposed that the axial thiolate ligand acts as a π donor to the Fe^{3+} ion to compensate for the π-accepting behavior of the bound nitrile. Mutation of the conserved axial thiolate to a weaker π donor like serine or to alanine should help to estimate the degree to which electron donation is necessary for active site binding. It is expected that a serine mutant will exhibit a slower catalytic rate. Again, applying the stopped-flow method will provide further insight to the axial thiolate ligand's role during catalysis.

CW-EPR studies on *Re*NHase-TG328-2 resulted in the characterization of minor species in the EPR spectra. The first of the minor species is a catalytically relevant component, while the latter two minor species are pH dependent interconversions. These minor species were initially of concern because they interfere with spectra from advanced EPR techniques. Therefore, a method to eliminate most of the minor species and obtain a standardized resting state by first turning the enzyme over with methacrylonitrile was developed. DFT calculations were performed using X-ray crystallographic and EPR data for NHase enzymes and model complexes. The success of the preliminary experiments shows that DFT will be an alternative technique to characterize other unidentified minor species in the NHase resting EPR spectrum, in which the crystal structure of *Re*NHase-TG328-2 will become indispensible.

With the timescale and concentrations of reactants for maximum intermediate formation derived from single turnover experiments and a standardized resting *Re*NHase-TG328-2 EPR spectrum, RFQ-EPR experiments were optimized and performed. These experiments revealed the presence of two new species, the first being a substrate or product bound inhibited form of the enzyme and the second, a transient Michaelis complex that was only present in the 10 ms RFQ sample. The identity of the transient intermediate was probed further by collecting ESEEM data, where the frequency of a peak of interest is very likely an increased population of nitrogen interacting with the low spin Fe(III) center. Though the signal is complicated by overlapping spectra, it provides the first structural evidence of the nitrogen of an actual nitrile substrate binding directly to the active site metal. CW-EPR spectra were also collected on enzyme samples bound to boronic acid (BA) inhibitors. These spectra were dominated by a species thought to

correspond to a substrate or product bound inhibited enzyme. These data and the observed hypsochromic shift in the visible spectrum upon BA binding are further evidence of direct binding to the active site. The stopped-flow and EPR data acquired, coupled with X-ray crystal structures of BA-*Pt*NHase allow for a new and more complete proposed catalytic mechanism, as discussed in detail in Chapter 5.

To confirm if the intermediate formed during RFQ experiments is a Michaelis complex, it will be necessary to either increase the concentration of the intermediate, which is difficult to control, or to use isotopically labeled substrates. Upon acquisition of N^{15}-MeACN and N^{14}-MeACN, pulsed EPR experiments (ESEEM for N^{14} and ENDOR for N^{15}) can be performed to closely and selectively study nitrogen coupling. Once these samples are prepared, the electronic spin and molecular vibrations of the active site will be further studied *via* magnetic circular dichroism (MCD) and resonance Raman spectroscopy. Mossbauer spectroscopy may also be used for further characterization of the electronic structure at the NHase active site.

Lastly, much progress was made in the characterization of the iron-type activator protein from *Re*NHase TG328-2. Soluble expression and purification in itself was a big step forward, as it was the key reason why the activator had not been studied earlier. The protein binds one molar equivalent of Co(II) or Ni (II) ions with micromolar affinity. The UV-Vis spectra suggest that two thiolate ligands are bound to the Co(II) ion. Sequence analysis of the protein placed it in the COG0523 subfamily of G3E P-loop GTPases. Therefore, GTP binding and hydrolysis was investigated with the now purified activator protein. Binding of NTPs greatly affected the secondary structure of the activator, with GTP CD spectra differing greatly from those of ATP and UTP. Also

interesting is that the activator has GTPase activity, with rates comparable to typical GTPases. This activity was increased with the addition of Co(II) which is the first time an iron-type activator has shown GTPase activity, expanding the possible role of the activator protein.

Of the many diverse proteins in the COG0523 family, only two others have been investigated. The main conclusions that can be drawn from Yjia, YeiR, and now, *Re*NHase-TG328-2 activator is that GTPase activity plays a role in metal homeostasis in the cell. Currently, it is unclear if metal transfer to the active site will occur if GTPase activity is disabled, which is well worth investigating through mutations of key GTPase motifs. It would be valuable as well to identify potential effector proteins that enhance GTPase activity, as is the case for most GTPases.[91,43] Metal binding studies will also be important on the activator containing mutations at the cysteine-rich metal binding motif, so as to isolate the cysteine residue responsible for binding. Kinetic assays, CD, and stopped-flow kinetics should be performed anaerobically, so that Fe(II) may be investigated. Of course, an existing goal for the project that has not come to fruition would be to obtain a crystal structure of the activator, which will answer many questions involving binding sites. If successful, molecular dynamics simulations may be performed to attempt to model the conformational changes that occur during GTP hydrolysis. Overall, the exciting discovery of GTPase activity and subsequent divalent metal binding data opens up a new direction of research that will lead to a better understanding of the formation of the NHase active site.

REFERENCES

1. Legras, J. L.; Chuzel, G.; Arnaud, A.; Galzy, P., Natural nitriles and their metabolism. *World J Microbiol Biotechnol* **1990,** *6* (2), 83-108.

2. Houtz, R. C., "Orlon" Acrylic Fiber: Chemistry and Properties. *Textile Research Journal* **1950,** *20* (11), 786-801.

3. Fleming, F. F.; Yao, L.; Ravikumar, P. C.; Funk, L.; Shook, B. C., Nitrile-Containing Pharmaceuticals: Efficacious Roles of the Nitrile Pharmacophore. *Journal of Medicinal Chemistry* **2010,** *53* (22), 7902-7917.

4. Banerjee; Sharma, The nitrile-degrading enzymes: current status and future prospects. *Appl. Microbiol. Biotechnol.* **2002,** *60* (1), 33-44.

5. Nagasawa, T.; Yamada, H., Microbial production of commodity chemicals. *Pure Appl. Chem* **1995,** *67*, 1241-1256.

6. Prasad, S.; Bhalla, T. C., Nitrile hydratases (NHases): At the interface of academia and industry. *Biotechnology Advances* **2010,** *28* (6), 725-741.

7. Sakashita, T.; Hashimoto, Y.; Oinuma, K.-I.; Kobayashi, M., Transcriptional Regulation of the Nitrile Hydratase Gene Cluster in Pseudomonas chlororaphis B23. *Journal of Bacteriology* **2008,** *190* (12), 4210-4217.

8. Chuck, R., Technology development in nicotinate production. *Applied Catalysis A: General* **2005,** *280* (1), 75-82.

9. van Pelt, S.; Quignard, S.; Kubac, D.; Sorokin, D. Y.; van Rantwijk, F.; Sheldon, R. A., Nitrile hydratase CLEAs: The immobilization and stabilization of an industrially important enzyme. *Green Chemistry* **2008,** *10* (4), 395-400.

10. Müller, D.; Gabriel, J., Bacterial degradation of the herbicide bromoxynil byAgrobacterium radiobacter in biofilm. *Folia Microbiol* **1999,** *44* (4), 377-379.

11. Cupples, A. M.; Sanford, R. A.; Sims, G. K., Dehalogenation of the Herbicides Bromoxynil (3,5-Dibromo-4-Hydroxybenzonitrile) and Ioxynil (3,5-Diiodino-4-Hydroxybenzonitrile) by Desulfitobacterium chlororespirans. *Applied and Environmental Microbiology* **2005,** *71* (7), 3741-3746.

12. Kohyama, E.; Yoshimura, A.; Aoshima, D.; Yoshida, T.; Kawamoto, H.; Nagasawa, T., Convenient treatment of acetonitrile-containing wastes using the tandem combination of nitrile hydratase and amidase-producing microorganisms. *Appl. Microbiol. Biotechnol.* **2006,** *72* (3), 600-606.

13. Guebitz, G. M.; Cavaco-Paulo, A., Enzymes go big: surface hydrolysis and functionalisation of synthetic polymers. *Trends in Biotechnology* **2008,** *26* (1), 32-38.

14. Tauber, M. M.; Cavaco-Paulo, A.; Robra, K.-H.; Gübitz, G. M., Nitrile Hydratase and Amidase fromRhodococcus rhodochrous Hydrolyze Acrylic Fibers and Granular Polyacrylonitriles. *Applied and Environmental Microbiology* **2000,** *66* (4), 1634-1638.

15. Kuhn, M. L.; Martinez, S.; Gumataotao, N.; Bornscheuer, U.; Liu, D.; Holz, R. C., The Fe-type nitrile hydratase from Comamonas testosteroni Ni1 does not require an activator accessory protein for expression in Escherichia coli. *Biochem Biophys Res Commun* **2012,** *424* (3), 365-370.

16. Song, L.; Wang, M.; Shi, J.; Xue, Z.; Wang, M.-X.; Qian, S., High resolution X-ray molecular structure of the nitrile hydratase from Rhodococcus erythropolis AJ270 reveals posttranslational oxidation of two cysteines into sulfinic acids and a novel biocatalytic nitrile hydration mechanism. *Biochemical and Biophysical Research Communications* **2007,** *362* (2), 319-324.

17. Miyanaga, A.; Fushinobu, S.; Ito, K.; Wakagi, T., Crystal Structure of Cobalt-Containing Nitrile Hydratase. *Biochemical and Biophysical Research Communications* **2001,** *288* (5), 1169-1174.

18. Miyanaga, A.; Fushinobu, S.; Ito, K.; Shoun, H.; Wakagi, T., Mutational and structural analysis of cobalt-containing nitrile hydratase on substrate and metal binding. *European Journal of Biochemistry* **2004,** *271* (2), 429-438.

19. Kovacs, J. A., Synthetic Analogues of Cysteinate-Ligated Non-Heme Iron and Non-Corrinoid Cobalt Enzymes. *Chemical Reviews* **2004,** *104* (2), 825-848.

20. Yano, T.; Ozawa, T.; Masuda, H., Structural and Functional Model Systems for Analysis of the Active Center of Nitrile Hydratase. *Chemistry Letters* **2008,** *37* (7), 672-677.

21. Hashimoto, K.; Suzuki, H.; Taniguchi, K.; Noguchi, T.; Yohda, M.; Odaka, M., Catalytic Mechanism of Nitrile Hydratase Proposed by Time-resolved X-ray Crystallography Using a Novel Substrate, tert-Butylisonitrile. *Journal of Biological Chemistry* **2008,** *283* (52), 36617-36623.

22. Shearer, J.; Jackson, H. L.; Schweitzer, D.; Rittenberg, D. K.; Leavy, T. M.; Kaminsky, W.; Scarrow, R. C.; Kovacs, J. A., The First Example of a Nitrile Hydratase Model Complex that Reversibly Binds Nitriles. *Journal of the American Chemical Society* **2002,** *124* (38), 11417-11428.

23. Hopmann, K. H.; Guo, J.-D.; Himo, F., Theoretical Investigation of the First-Shell Mechanism of Nitrile Hydratase. *Inorganic Chemistry* **2007,** *46* (12), 4850-4856.

24. Yamanaka, Y.; Hashimoto, K.; Ohtaki, A.; Noguchi, K.; Yohda, M.; Odaka, M., Kinetic and structural studies on roles of the serine ligand and a strictly conserved tyrosine residue in nitrile hydratase. *J Biol Inorg Chem* **2010,** *15* (5), 655-665.

25. Mitra, S.; Holz, R. C., Unraveling the catalytic mechanism of nitrile hydratases. *Journal of Biological Chemistry* **2007,** *282* (10), 7397-7404.

26. Hopmann, K. H.; Himo, F., On the Role of Tyrosine as Catalytic Base in Nitrile Hydratase. *European Journal of Inorganic Chemistry* **2008,** *2008* (22), 3452-3459.

27. Shearer, J.; Kung, I. Y.; Lovell, S.; Kaminsky, W.; Kovacs, J. A., Why Is There an "Inert" Metal Center in the Active Site of Nitrile Hydratase? Reactivity and Ligand Dissociation from a Five-Coordinate Co(III) Nitrile Hydratase Model. *Journal of the American Chemical Society* **2000,** *123* (3), 463-468.

28. Shearer, J.; Scarrow, R. C.; Kovacs, J. A., Synthetic Models for the Cysteinate-Ligated Non-Heme Iron Enzyme Superoxide Reductase: Observation and Structural Characterization by XAS of an FeIII−OOH Intermediate. *Journal of the American Chemical Society* **2002,** *124* (39), 11709-11717.

29. Noguchi, T.; Hoshino, M.; Tsujimura, M.; Odaka, M.; Inoue, Y.; Endo, I., Resonance Raman Evidence that Photodissociation of Nitric Oxide from the Non-Heme Iron Center Activates Nitrile Hydratase from Rhodococcus sp. N-771†. *Biochemistry* **1996,** *35* (51), 16777-16781.

30. Shigehiro, S.; Nakasako, M.; Dohmae, N.; Tsujimura, M.; Tokoi, K.; Odaka, M.; Yohda, M.; Kamiya, N.; Endo, I., Novel non-heme iron center of nitrile hydratase with a claw setting of oxygen atoms. *Nature Structural Biology* **1998,** *5* (5), 347-351.

31. Sugiura, Y.; Kuwahara, J.; Nagasawa, T.; Yamada, H., Nitrile hydratase. The first non-heme iron enzyme with a typical low-spin iron (III)-active center. *Journal of the American Chemical Society* **1987,** *109* (19), 5848-5850.

32. Huang, W.; Jia, J.; Cummings, J.; Nelson, M.; Schneider, G.; Lindqvist, Y., Crystal structure of nitrile hydratase reveals a novel iron centre in a novel fold. *Structure* **1997,** *5* (5), 691-699.

33. Heinrich, L.; Mary-Verla, A.; Li, Y.; Vaissermann, J.; Chottard, J.-C., Cobalt(III) Complexes with Carboxamido-N and Sulfenato-S or Sulfinato-S Ligands Suggest that a

Coordinated Sulfenate-S is Essential for the Catalytic Activity of Nitrile Hydratases. *European Journal of Inorganic Chemistry* **2001,** *2001* (9), 2203-2206.

34. Holm, R. H.; Kennepohl, P.; Solomon, E. I., Structural and Functional Aspects of Metal Sites in Biology. *Chemical Reviews* **1996,** *96* (7), 2239-2314.

35. Giedroc, D. P.; Arunkumar, A. I., Metal sensor proteins: nature's metalloregulated allosteric switches. *Dalton Transactions* **2007,** (29), 3107-3120.

36. Nojiri, M.; Nakayama, H.; Odaka, M.; Yohda, M.; Takio, K.; Endo, I., Cobalt-substituted Fe-type nitrile hydratase of Rhodococcus sp. N-771. *FEBS Letters* **2000,** *465* (2), 173-177.

37. Sari, M.-A.; Jaouen, M.; Saroja, N. R.; Artaud, I., Influence of cobalt substitution on the activity of iron-type nitrile hydratase: Are cobalt type nitrile hydratases regulated by carbon monoxide? *Journal of Inorganic Biochemistry* **2007,** *101* (4), 614-622.

38. Lu, J.; Zheng, Y.; Yamagishi, H.; Odaka, M.; Tsujimura, M.; Maeda, M.; Endo, I., Motif CXCC in nitrile hydratase activator is critical for NHase biogenesis in vivo. *FEBS Letters* **2003,** *553* (3), 391-396.

39. Zhou, Z.; Hashimoto, Y.; Kobayashi, M., Self-subunit Swapping Chaperone Needed for the Maturation of Multimeric Metalloenzyme Nitrile Hydratase by a Subunit Exchange Mechanism Also Carries Out the Oxidation of the Metal Ligand Cysteine Residues and Insertion of Cobalt. *Journal of Biological Chemistry* **2009,** *284* (22), 14930-14938.

40. Cheng, T.; Li, H.; Yang, X.; Xia, W.; Sun, H., Interaction of SlyD with HypB of Helicobacter pylori facilitates nickel trafficking. *Metallomics* **2013,** *5* (7), 804-807.

41. Haas, C.; Rodionov, D.; Kropat, J.; Malasarn, D.; Merchant, S.; de Crecy-Lagard, V., A subset of the diverse COG0523 family of putative metal chaperones is linked to zinc homeostasis in all kingdoms of life. *BMC Genomics* **2009,** *10* (1), 470.

42. Zhou, Z.; Hashimoto, Y.; Cui, T.; Washizawa, Y.; Mino, H.; Kobayashi, M., Unique Biogenesis of High-Molecular Mass Multimeric Metalloenzyme Nitrile Hydratase: Intermediates and a Proposed Mechanism for Self-Subunit Swapping Maturation. *Biochemistry* **2010,** *49* (44), 9638-9648.

43. Leipe, D. D.; Wolf, Y. I.; Koonin, E. V.; Aravind, L., Classification and evolution of P-loop GTPases and related ATPases. *Journal of Molecular Biology* **2002,** *317* (1), 41-72.

44. RoSZbach, M.; Daumke, O.; Klinger, C.; Wittinghofer, A.; Kaufmann, M., Crystal structure of THEP1 from the hyperthermophile Aquifex aeolicus: a variation of the RecA fold. *BMC Structural Biology* **2005,** *5* (1), 7.

45. Farrugia, M. A.; Macomber, L.; Hausinger, R. P., Biosynthesis of the Urease Metallocenter. *Journal of Biological Chemistry* **2013,** *288* (19), 13178-13185.

46. (a) Khil, P. P.; Obmolova, G.; Teplyakov, A.; Howard, A. J.; Gilliland, G. L.; Camerini-Otero, R. D., Crystal structure of the Escherichia coli YjiA protein suggests a GTP-dependent regulatory function. *Proteins: Structure, Function, and Bioinformatics* **2004,** *54* (2), 371-374; (b) Sydor, A. M.; Jost, M.; Ryan, K. S.; Turo, K. E.; Douglas, C. D.; Drennan, C. L.; Zamble, D. B., Metal Binding Properties of Escherichia coli YjiA, a Member of the Metal Homeostasis-Associated COG0523 Family of GTPases. *Biochemistry* **2013,** *52* (10), 1788-1801.

47. Zhou, Z.; Hashimoto, Y.; Shiraki, K.; Kobayashi, M., Discovery of posttranslational maturation by self-subunit swapping. *Proceedings of the National Academy of Sciences* **2008,** *105* (39), 14849-14854.

48. Petrillo, K. L.; Wu, S.; Hann, E. C.; Cooling, F. B.; Ben-Bassat, A.; Gavagan, J. E.; Dicosimo, R.; Payne, M. S., Over-expression in Escherichia coli of a thermally stable and regio-selective nitrile hydratase from Comamonas testosteroni 5-MGAM-4D. *Appl Microbiol Biotechnol.* **2005**, in press.

49. Padmakumar, R.; Oriel, P., Bioconversion of acrylonitrile to acrylamide using a thermostable nitrile hydratase. *Appl Biochem Biotechnol.* **1999,** *77-79*, 671-679.

50. Mylerova, V.; Martinkova, L., Synthetic applications of nitrile-converting enzymes. *Cur. Org. Chem.* **2003,** *7*, 1-17.

51. Baxter, J.; Cummings, S. P., The current and future applications of microorganism in the bioremediation of cyanide contamination. *Antonie van Leeuwenhoek* **2006,** *90* (1), 1-17.

52. Tsujimura, M.; Odaka, M.; Nakayama, H.; Dohmae, N.; Koshino, H.; Asami, T.; Hoshino, M.; Takio, K.; Yoshida, S.; Maeda, M.; Endo, I., A novel inhibitor for Fe-type nitrile hydratase: 2-cyano-2-propyl hydroperoxide. *J Am Chem Soc.* **2003,** *125*, 11532-11538.

53. Kennepohl, P.; Neese, F.; Schweitzer, D.; Jackson, H. L.; Kovacs, J. A.; Solomon, E. I., Spectroscopy of Non-Heme Iron Thiolate Complexes: Insight into the Electronic Structure of the Low-Spin Active Site of Nitrile Hydratase. *Inorganic Chemistry* **2005,** *44* (6), 1826-1836.

54. Noguchi, T.; Hoshino, M.; Tsujimura, M.; Odaka, M.; Inoue, Y.; Endo, I., Resonance Raman evidence that photodissociation of nitric oxide from the non-heme iron center activates nitrile hydratase from Rhodococcus sp. N-771. *Biochemistry* **1996,** *35*, 16777-16781.

55. Rao, S.; Holz, R. C., Analyzing the Catalytic Mechanism of the Fe-Type Nitrile Hydratase from Comamonas testosteroni Ni1†. *Biochemistry* **2008,** *47* (46), 12057-12064.

56. Rzeznicka, K.; Schatzle, S.; Bottcher, D.; Klein, J.; Bornscheuer, U. T., Cloning and functional expression of a nitrile hydratase (NHase) from Rhodococcus equi TG328-2 in Escherichia coli, its purification and biochemical characterisation. *Appl. Microbiol. Biotechnol.* **2010,** *85* (5), 1417-1425.

57. Dey, A.; Chow, M.; Taniguchi, K.; Lugo-Mas, P.; Davin, S.; Maeda, M.; Kovacs, J. A.; Odaka, M.; Hodgson, K. O.; Hedman, B.; Solomon, E. I., Sulfur K-Edge XAS and DFT Calculations on Nitrile Hydratase: Geometric and Electronic Structure of the Non-heme Iron Active Site. *Journal of the American Chemical Society* **2005,** *128* (2), 533-541.

58. Shearer, J.; Callan, P. E.; Amie, J., Use of Metallopeptide Based Mimics Demonstrates That the Metalloprotein Nitrile Hydratase Requires Two Oxidized Cysteinates for Catalytic Activity. *Inorganic Chemistry* **2010,** *49* (19), 9064-9077.

59. Duran, R., New shuttle vectors for Rhodococcus sp. R312 (formerly Brevibacterium sp. R312), a nitrile hydratase producing strain. *Journal of Basic Microbiology* **1998,** *38* (2), 101-106.

60. Doan, P. E.; Nelson, M. J.; Jin, H.; Hoffman, B. M., An Implicit TRIPLE Effect in Mims Pulsed ENDOR: A Sensitive New Technique for Determining Signs of Hyperfine Couplings. *Journal of the American Chemical Society* **1996,** *118* (29), 7014-7015.

61. Popescu, V.-C.; Münck, E.; Fox, B. G.; Sanakis, Y.; Cummings, J. G.; Turner, I. M.; Nelson, M. J., Mössbauer and EPR Studies of the Photoactivation of Nitrile Hydratase†. *Biochemistry* **2001,** *40* (27), 7984-7991.

62. Nishida, Y.; Oshio, S.; Kida, S., ESR spectra of low-spin iron(III) complexes with several quadridentate schiff bases. *Inorganica Chimica Acta* **1977,** *23* (0), 59-61.

63. Gaffney, B. J., EPR of mononuclear non-heme iron proteins. In *High Resolution EPR*, Springer: 2009; pp 233-268.

64. Bennett, B.; Benson, N.; McEwan, A. G.; Bray, R. C., Multiple states of the molybdenum centre of dimethylsulphoxide reductase from *Rhodobacter capsulatus* revealed by EPR spectroscopy. *Eur. J. Biochem.* **1994,** *225*, 321-331.

65. Fourmond, V.; Burlat, B. n. d.; Dementin, S. b.; Arnoux, P.; Sabaty, M.; Boiry, S. v.; Guigliarelli, B.; Bertrand, P.; Pignol, D.; Léger, C., Major Mo(V) EPR Signature of Rhodobacter sphaeroides Periplasmic Nitrate Reductase Arising from a Dead-End Species That Activates upon Reduction. Relation to Other Molybdoenzymes from the DMSO Reductase Family. *The Journal of Physical Chemistry B* **2008,** *112* (48), 15478-15486.

66. Scarrow, R. C.; Brennan, B. A.; Cummings, J. G.; Jin, H.; Duong, D. J.; Kindt, J. T.; Nelson, M. J., X-ray Spectroscopy of Nitrile Hydratase at pH 7 and 9†. *Biochemistry* **1996,** *35* (31), 10078-10088.

67. Hagen, W. R., *Biomolecular EPR spectroscopy*. CRC press: 2008.

68. Martinez, S.; Wu, R.; Sanishvili, R.; Liu, D.; Holz, R., The Active Site Sulfenic Acid Ligand in Nitrile Hydratases Can Function as a Nucleophile. *Journal of the American Chemical Society* **2014,** *136* (4), 1186-1189.

69. Banci, L.; Bertini, I.; Luchinat, C.; Donaire, A.; Martinez, M.-J.; Moratal Mascarell, J. M., *Comments Inorg. Chem.* **1990,** *9*, 245.

70. Kirsch, M.; Lomonosova, E. E.; Korth, H.-G.; Sustmann, R.; de Groot, H., Hydrogen Peroxide Formation by Reaction of Peroxynitrite with HEPES and Related Tertiary Amines IMPLICATIONS FOR A GENERAL MECHANISM. *Journal of Biological Chemistry* **1998,** *273* (21), 12716-12724.

71. Zigler Jr, J.; Lepe-Zuniga, J.; Vistica, B.; Gery, I., Analysis of the cytotoxic effects of light-exposed HEPES-containing culture medium. *In Vitro Cellular & Developmental Biology* **1985,** *21* (5), 282-287.

72. Sugiura, Y.; Kuwahara, J.; Nagasawa, T.; Yamada, H., Singificant interaction between low-spin iron(III) site and pyrroloquinoline quinone in active center of nitrile hydratase. *Biochemical and Biophysical Research Communications* **1988,** *154* (2), 522-528.

73. Taylor, C., The EPR of low spin heme complexes Relation of the τ< sub> 2g</sub> hole model to the directional properties of the< i> g</i> tensor, and a new method for calculating the ligand field parameters. *Biochimica et Biophysica Acta (BBA)-Protein Structure* **1977,** *491* (1), 137-148.

74. Rzeznicka, K.; Schätzle, S.; Böttcher, D.; Klein, J.; Bornscheuer, U., Cloning and functional expression of a nitrile hydratase (NHase) from Rhodococcus equi TG328-2 in Escherichia coli, its purification and biochemical characterisation. *Appl. Microbiol. Biotechnol.* **2010,** *85* (5), 1417-1425.

75. Garrity, J. D.; Bennett, B.; Crowder, M. W., Direct Evidence That the Reaction Intermediate of Metallo-β-lactamase L1 Is Metal Bound†. *Biochemistry* **2004,** *44* (3), 1078-1087.

76. (a) Hyde, J. S.; Bennett, B.; Walter, E. D.; Millhauser, G. L.; Sidabras, J. W.; Antholine, William E., EPR of Cu2+ Prion Protein Constructs at 2 GHz Using the g¥ Region to Characterize Nitrogen Ligation. *Biophysical journal* **2009,** *96* (8), 3354-3362; (b) Kowalski, J. M.; Bennett, B., Spin Hamiltonian Parameters for Cu(II)−Prion Peptide Complexes from L-Band Electron Paramagnetic Resonance Spectroscopy. *Journal of the American Chemical Society* **2011,** *133* (6), 1814-1823.

77. Hyde, J. S.; Bennett, B.; Kittell, A. W.; Kowalski, J. M.; Sidabras, J. W., Moving difference (MDIFF) non-adiabatic rapid sweep (NARS) EPR of copper(II). *Journal of Magnetic Resonance* **2013,** *236* (0), 15-25.

78. Desai, L. V.; Zimmer, M., Substrate selectivity and conformational space available to bromoxynil and acrylonitrile in iron nitrile hydratase. *Dalton Trans.* **2004,** *6*, 872-877.

79. Wegman, M. A.; van Langen, L. M.; van Rantwijk, F.; Sheldon, R. A., A two-step, one-pot enzymatic synthesis of cephalexin from D-phenylglycine nitrile. *Biotechnol Bioeng.* **2002,** *79*, 356-361.

80. Gumataotao, N.; Kuhn, M. L.; Hajnas, N.; Holz, R. C., Identification of an Active Site-bound Nitrile Hydratase Intermediate through Single Turnover Stopped-flow Spectroscopy. *Journal of Biological Chemistry* **2013,** *288* (22), 15532-15536.

81. Rose, M. J.; Betterley, N. M.; Oliver, A. G.; Mascharak, P. K., Binding of Nitric Oxide to a Synthetic Model of Iron-Containing Nitrile Hydratase (Fe-NHase) and Its Photorelease: Relevance to Photoregulation of Fe-NHase by NO. *Inorganic Chemistry* **2010,** *49* (4), 1854-1864.

82. García-Rubio, I.; Mitrikas, G., Structure and spin density of ferric low-spin heme complexes determined with high-resolution ESEEM experiments at 35 GHz. *J Biol Inorg Chem* **2010,** *15* (6), 929-941.

83. Blaby-Haas, C. E.; Flood, J. A.; Crecy-Lagard, V. d.; Zamble, D. B., YeiR: a metal-binding GTPase from Escherichia coli involved in metal homeostasis. *Metallomics* **2012,** *4* (5), 488-497.

84. May, S. W.; Kuo, J.-Y., Preparation and properties of cobalt(II) rubredoxin. *Biochemistry* **1978,** *17* (16), 3333-3338.

85. Vasák, M.; Kägi, J. H., Metal thiolate clusters in cobalt(II)-metallothionein. *Proceedings of the National Academy of Sciences* **1981,** *78* (11), 6709-6713.

86. MacColl, R.; Eisele, L. E.; Stack, R. F.; Hauer, C.; Vakharia, D. D.; Benno, A.; Kelly, W. C.; Mizejewski, G. J., Interrelationships among biological activity, disulfide bonds, secondary structure, and metal ion binding for a chemically synthesized 34-amino-acid peptide derived from α-fetoprotein. *Biochimica et Biophysica Acta (BBA) - General Subjects* **2001,** *1528* (2–3), 127-134.

87. Winzor, D. J.; Sawyer, W. H., *Quantitative Characterization of Ligand Binding*. Wiley-Liss: New York, 1995.

88. Xiao, Z.; Wedd, A. G., The challenges of determining metal-protein affinities. *Natural Product Reports* **2010,** *27* (5), 768-789.

89. Song, B. D.; Schmid, S. L., A Molecular Motor or a Regulator? Dynamin's in a Class of Its Own†. *Biochemistry* **2003,** *42* (6), 1369-1376.

90. Siderovski, D. P.; Willard, F. S., The GAPs, GEFs, and GDIs of heterotrimeric G-protein alpha subunits. *International journal of biological sciences* **2005,** *1* (2), 51.

91. Bourne, H. R.; Sanders, D. A.; McCormick, F., The GTPase superfamily: conserved structure and molecular mechanism. *Nature* **1991,** *349* (6305), 117-127.

92. Cai, F.; Ngu, T.; Kaluarachchi, H.; Zamble, D., Relationship between the GTPase, metal-binding, and dimerization activities of E. coli HypB. *J Biol Inorg Chem* **2011,** *16* (6), 857-868.

93. Liithy, R.; Bowie, J. U.; Eisenberg, D., Assessment of protein models with three-dimensional profiles. *Nature* **1992,** *356* (6364), 83-85.

94. Bowie, J.; Luthy, R.; Eisenberg, D., A method to identify protein sequences that fold into a known three-dimensional structure. *Science* **1991,** *253* (5016), 164-170.

95. Verseck, S. H., DE), Osswald, Steffen (Rodenbach, DE), Phong, Wai-yee (Singapore, SG), Liebeton, Klaus (Zwingenberg, DE), Eck, Jurgen (Bensheim, DE) Expression of Nitrile Hydratases in a Two-Vector Expression System. 2008.

96. Jancarik, J.; Pufan, R.; Hong, C.; Kim, S.-H.; Kim, R., Optimum solubility (OS) screening: an efficient method to optimize buffer conditions for homogeneity and crystallization of proteins. *Acta Crystallographica Section D* **2004,** *60* (9), 1670-1673.

97. Fusari, C.; Demonte, A. M.; Figueroa, C. M.; Aleanzi, M.; Iglesias, A. A., A colorimetric method for the assay of ADP-glucose pyrophosphorylase. *Analytical Biochemistry* **2006,** *352* (1), 145-147.

VITA

Natalie Gumataotao was born and raised in Anigua, Guam. She received her Bachelor of Science in Chemistry at the University of San Francisco in 2005. She worked for Gilead Sciences in Analytical Development for four years following her graduation from college. In 2009, she began the PhD program in Chemistry at Loyola University Chicago.